Composite

Materials and Structures Program

Rensselaer Polytechnic Institute
Troy, N.Y. 12180-3590

NASA-CR-174077
19850004658

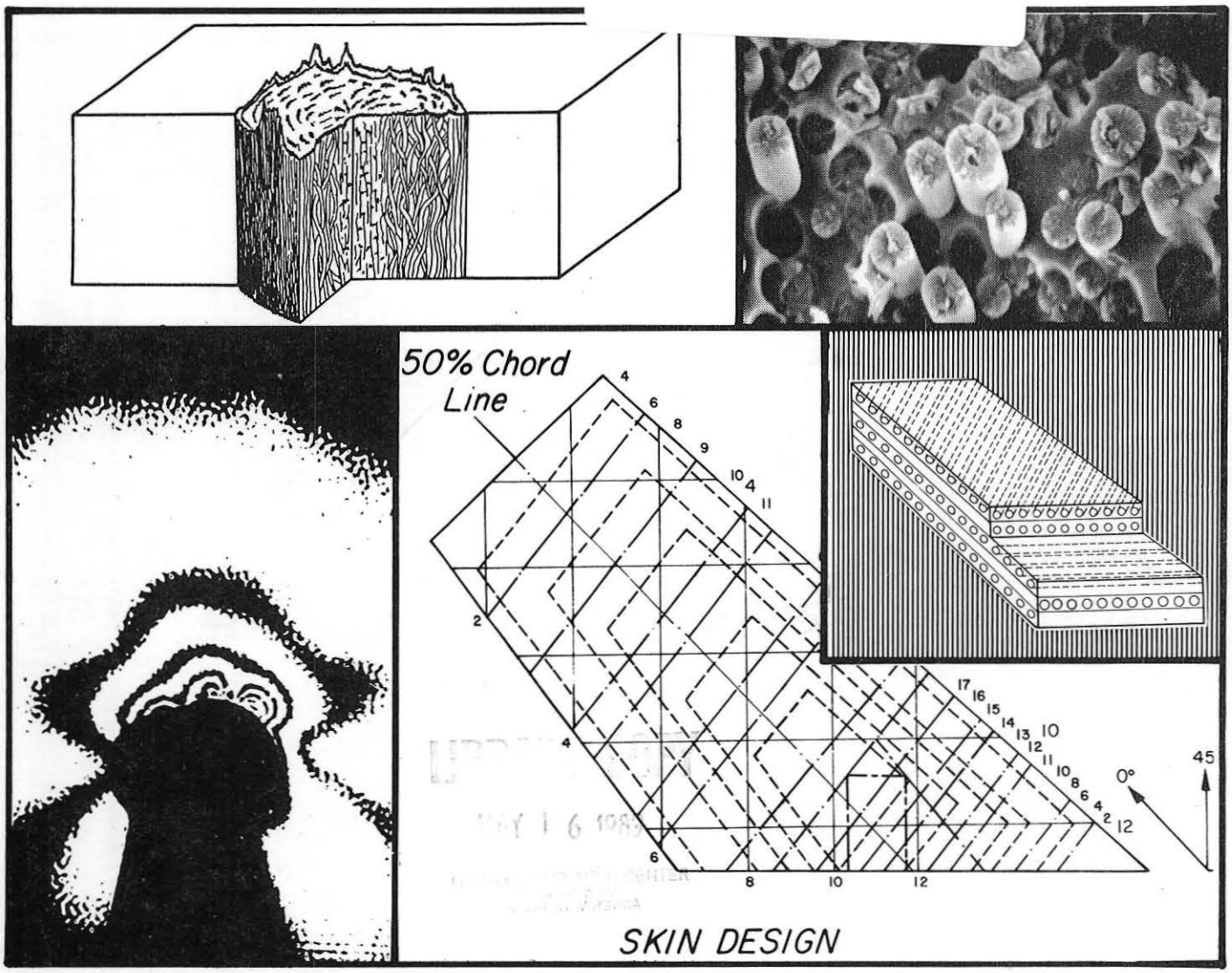

Sponsored by

NASA/AFOSR

DISPLAY 85N12966/2
85N12966*# ISSUE 4 PAGE 467 CATEGORY 24 RPT#: NASA-CR-174077 NAS 1.26:174077 SAPR-46 CNT#: NGL-33-018-003 84/08/00 174 PAGES
UNCLASSIFIED DOCUMENT
UTTL: Composite structural materials TLSP: Semiannual Progress Report, 30 Sep. 1983 - 30 Apr. 1984
AUTH: A/ANSELL, G. S.; B/LOEWY, R. G.; C/WIBERLY, S. E.
CORP: Rensselaer Polytechnic Inst., Troy, NY. CSS: (School of Engineering.)
AVAIL.NTIS
SAP: HC A08/MF A01
CIO: UNITED STATES Sponsored in cooperation with AFOSR
MAJS: /*AIRCRAFT STRUCTURES/*CARBON FIBERS/*FATIGUE (MATERIALS)/*FIBER COMPOSITES/*GRAPHITE-EPOXY COMPOSITES/*METAL MATRIX COMPOSITES
MINS: / COMPOSITE MATERIALS/ MECHANICAL PROPERTIES/ SPACECRAFT STRUCTURES/ TECHNOLOGY ASSESSMENT/ TEMPERATURE EFFECTS
ANN: The development and application of filamentary composite materials, is considered. Such interest is based on the possibility of using relatively brittle materials with high modulus, high strength, but low density in composites with good durability and high tolerance to damage. Fiber reinforced composite materials of this kind offer substantially improved performance and potentially lower costs for aerospace hardware. Much progress has been made since the initial developments in the mid 1960's. There were only limited applied to the primary structure of operational
MORE ENTER:

P

DISPLAY 85N12966/2
vehicles, mainly as aircrafts. For individual titles see N85-12967 through N85-12977.
ENTER:

Semi-Annual Progress Report
September 30, 1983 through April 30, 1984

COMPOSITE STRUCTURAL MATERIALS

Air Force Office of Scientific Research
and
National Aeronautics and Space Administration
Grant No. NGL 33-018-003

Co-Principal Investigators:

George S. Ansell
Dean, School of Engineering

Robert G. Loewy
Institute Professor

and

Stephen E. Wiberley
Professor of Chemistry

Rensselaer Polytechnic Institute
Troy, New York 12181

NASA Technical Officer

Michael A. Greenfield
Materials and Structures Division
NASA Headquarters

46th Semi-Annual Report August 1984

CONTENTS

	Page
LIST OF TABLES	v
LIST OF FIGURES	vi
PART I. INTRODUCTION	1
PART II. CONSTITUENT MATERIALS	9
II-A CHEMICAL MODIFICATION OF THE SURFACE OF HIGH MODULUS CARBON FIBERS (R. J. Diefendorf)	11
1. Introduction	11
2. Status	12
3. Progress During Report Period	13
4. Plans for Upcoming Period	23
5. References	23
6. Current Publications or Presentations by Professor Diefendorf on this Subject	24
PART III. COMPOSITE MATERIALS	27
III-A FATIGUE IN COMPOSITE MATERIALS (E. Krempl)	29
1. Introduction	29
2. Status	29
3. Progress During Report Period	29
4. Plans for Upcoming Period	32
5. References	33
6. Current Publications or Presentations by Professor Krempl on this Subject	33
III-B EXPERIMENTAL AND THEORETICAL STUDIES OF MOISTURE AND TEMPERATURE EFFECTS ON THE MECHANICAL PROPERTIES OF GRAPHITE/EPOXY LAMINATES AND NEAT RESINS (S. S. Sternstein)	35
1. Introduction	35
2. Status	35
3. Progress During Report Period	36
4. Plans for Upcoming Period	38
5. Current Publications or Presentations by Professor Sternstein on this Subject	38

Page

III-C NUMERICAL INVESTIGATION OF THE MICROMECHANICS OF COMPOSITE FRACTURE (M. S. Shephard) 39
1. Introduction 39
2. Status 39
3. Progress During Report Period 40
a. Modified T-Criterion 40
b. Singular Element Size Effect 41
c. Automatic Crack Tracking System 47
4. Plans for Upcoming Period 55
5. References 61
6. Current Publications or Presentations by Professor Shephard on this Subject 62

III-D FREE-EDGE FAILURES OF COMPOSITE LAMINATES (T. L. Sham) 63
1. Introduction 63
2. Status 63
3. Progress During Report Period 63
4. Plans for Upcoming Period 64

PART IV. GENERIC STRUCTURAL ELEMENTS 65

IV-A QUANTIFICATION OF SAINT-VENANT'S PRINCIPLE FOR A GENERAL PRISMATIC MEMBER (D. B. Goetschel) .. 67
1. Introduction 67
2. Status 69
3. Progress During Report Period 72
4. Plans for Upcoming Period 84
5. References 84

IV-B IMPROVED BEAM THEORY FOR ANISOTROPIC MATERIALS (O. Bauchau) 89
1. Introduction 89
2. Status 90
3. Progress During Report Period 91
4. Plans for Upcoming Period 96
5. References 99
6. Current Publications or Presentations by Professor Bauchau on this Subject 99

Page

PART V. PROCESSING SCIENCE AND TECHNOLOGY 101

V-A VARIATION OF RESIN PROPERTIES THROUGH THE THICKNESS OF CURED SAMPLES (B. Wunderlich) 103

1. Introduction 103

a. Resin Systems and Reactions 103

b. Mobility in the Epoxy Matrices 105

c. Glass Transition and the Hysteresis Phenomenon 109

2. Status 114

3. Progress During Report Period 115

4. Plans for Upcoming Period 124

5. References 125

V-B ACCURATE MEASUREMENT OF HEAT CAPACITY BY DIFFERENTIAL SCANNING CALORIMETRY (B. Wunderlich) 127

1. Introduction 127

2. Status 127

3. Progress During Report Period 129

a. Instrumentation 129

b. Results 131

c. Conclusions 138

4. Plans for Upcoming Period 144

5. References 144

6. Current Publications or Presentations by Professor Wunderlich on this Subject 145

V-C INITIAL SAILPLANE PROJECT: THE RP-1 (F. P. Bundy, R. J. Diefendorf, H. Hagerup) 147

V-D SECOND SAILPLANE PROJECT: THE RP-2 (F. P. Bundy, R. J. Diefendorf, H. Hagerup) 149

1. Status 149

2. Progress During Report Period 149

3. Plans for Upcoming Period 153

4. Current Publications or Presentations by Professor Bundy on this Subject 154

Page

PART VI. TECHNICAL INTERCHANGE 155

PART VII. PERSONNEL, AUTHOR INDEX 171

PERSONNEL 173

AUTHOR INDEX 177

LIST OF TABLES

Number		Page
IV-A-1	AMPLITUDE COEFFICIENTS FOR MODAL SUPERPOSITION USING THE END CONDITION IN FIGURE IV-A-5b	82
IV-A-2	AMPLITUDE COEFFICIENTS FOR MODAL SUPERPOSITION USING THE END CONDITION IN FIGURE IV-A-5c	85
IV-B-1	NUMERICAL RESULTS FOR THE DIFFERENT APPROACHES	95
V-A-1	CHEMICAL FORMULAE	104
V-A-2	REACTION EQUATIONS FOR THE POLYMERIZATION WITH ACID	106
V-A-3	REACTION EQUATIONS FOR THE POLYMERIZATION WITH BASE	107
V-A-4	CURE REACTION WITH DIAMINE	108
V-B-1	COMPUTER READINGS OF PEN AMPLITUDES IN RUNS SHOWN IN FIGURE V-B-1	136
V-B-2	COMPUTER READINGS OF THE ISOTHERM AMPLITUDES OF THE RUNS SHOWN IN FIGURE V-B-5	142
VI-1	CALENDAR OF COMPOSITES-RELATED MEETINGS	158
VI-2	COMPOSITES-RELATED TECHNICAL MEETINGS ATTENDED OFF-CAMPUS	159
VI-3	COMPOSITES-RELATED MEETINGS/TALKS HELD AT RPI	161
VI-4	COMPOSITES RELATED VISITS TO RELEVANT ORGANIZATIONS	162
VI-5	COMPOSITE MATERIALS AND STRUCTURES PROGRAM BROWN BAG LUNCH (BBL) SCHEDULE	164
VI-6	NASA/AFOSR COMPOSITE MATERIALS AND STRUCTURES PROGRAM ON-SITE VISIT: AGENDA	167
VI-7	NASA/AFOSR COMPOSITE MATERIALS AND STRUCTURES PROGRAM ON-SITE VISIT: ATTENDEES	169

LIST OF FIGURES

Number		Page
II-A-1	Schematic of Events Occurring on the Fiber During Deposition in a Reactive Medium	14
II-A-2	Deposition of Amide as a Function of Effective Bath Concentration of Amine [B] and Anhydride [A]	18
II-A-3a	Surface of High Modulus Carbon Fibers After Scouring with a Solution of Chloroform and Chlorobenzene (1000x)	19
II-A-3b	SEM Surface of HM Fibers After Treatment with DTA	19
II-A-3c	HM Fiber Surface, Preoxidized in Thirty Percent Hydrogen Peroxide Before the Deposition of DTA	20
II-A-3d	Fiber Surface After Deposition of DTA and DDSA	21
II-A-3e	Fiber Surface After Deposition of DTA and DDSA with DDSA Deposition in Ultrasonic Bath	22
III-C-1	Fracture Load for a Slant Crack Under Remote Tension Normalized with Mode I ($\beta = 90°$) Fracture Load	42
III-C-2	Fracture Loci for a Slant Crack Under Remote Tension Normalized with Mode I ($\beta = 90°$) Fracture	43
III-C-3	Error in Evaluating the Stress Intensity Factors in Slant Crack Problems, with ($\beta = 40°$) Versus the Ratio of Singular Element Side Length, ℓ, to Half Crack Length, a	44
III-C-4	Error in Crack Propagation Angle, θ, Versus the Ratio of l/a for the Plane Strain, Slant Crack Problem, with $\beta = 40°$, Under Remote Tension	45
III-C-5	Error in Propagation Increment Versus the Ratio of l/a for the Plane Strain, Slant Crack Problem, with $\beta = 40°$, Under Remote Tension ..	46

Number		Page
III-C-6	Geometry Modification Operations	50
III-C-7	Forty-Five Degree Slant Crack Problem	51
III-C-8	Starting Mesh for the Slant Crack Problem	52
III-C-9	Crack Propagation Path and Corresponding Fracture Load (P) Predictions	53
III-C-10	The Automatically Generated Mesh for the Geometry of Figure III-C-9	56
III-C-11	Plate with Pressurized Hole	57
III-C-12	Starting Mesh for Plate with Pressurized Hole	58
III-C-13	Geometry for Plate with Pressurized Hole After Four Crack Propagation Increments	59
III-C-14	Mesh for Plate with Pressurized Hole After Four Crack Propagation Increments	60
IV-A-1	Geometry for Homogeneous Graphite/Epoxy Plate	73
IV-A-2	Deformed Shapes of Graphite/Epoxy Plate for Several Decay Rates	74
IV-A-3	Deformed Shapes of Graphite/Epoxy Beam for Several Decay Rates	76
IV-A-4	Geometry and Boundary Conditions for T-Section Used for Modal Superposition	78
IV-A-5	Some of the Symmetric Modes Used in the Modal Superposition Analysis of the T-Section Beam .	80
IV-A-6	Some of the Antisymmetric Modes Used in the Modal Superposition Analysis of the T-Section Beam	81
IV-A-7	Results of Modal Superposition for the Boundary Condition in Figure IV-A-4b	83
IV-A-8	Results of Modal Superposition for the Boundary Condition in Figure IV-A-4c	86
IV-B-1	The Thin-Walled, Rectangular Cross-Sectional Beam Analyzed in the Numerical Example	93
IV-B-2	A Few Eigenwarpings of the Rectangular Section	94

Number		Page
IV-B-3	Stress Distributions in the Upper Skin of the Beam (Root Section) Under Uniform Transverse Load p_o	97
IV-B-4	Stress Distributions in the Upper Skin of the Beam (Root Section) Under Uniform torque m_o	98
V-A-1	Exothermic Hysteresis (schematic)	111
V-A-2	Endothermic Hysteresis (schematic)	112
V-A-3	Characteristic Temperatures in the Glass Transition Region	113
V-A-4	Glass Transition Temperatures as a Function of Hardener Concentration	116
V-A-5	Cure-Time Dependence of T_g of TGDDM (MY 720) Without Hardener at 473° K	117
V-A-6	Change of the Glass Transition Hysteresis Peak Area, ΔH_h, and the Breadth of the Glass Transition, ΔT, as a Function of Glass Transition, T_g, for Cross-Linked Polystyrene	119
V-A-7	Change of the Glass Transition Hysteresis Peak Area, ΔH_h, and the Breadth of the Glass Transition Region, ΔT, as a Function of Glass Transition, T_g, for the Sample Described in Figure V-A-5 (MY 720)	120
V-A-8	Breadth of the Glass Transition, ΔT, Versus Hysteresis Peak Area (cross-linked polystyrenes, see Figure V-A-6)	121
V-A-9	Breadth of the Glass Transition, ΔT, Versus Hysteresis Peak Area (TGDDM [MY 720], see Figures V-A-5 and 7)	122
V-A-10	Glass Transition Temperatures, T_g, Versus Degree of Cross-Linking	123
V-B-1	Heat Capacity of Polyoxymethylene as a Function of Temperature	130
V-B-2	Heat Flow Curves of Sample Runs A and B Described in Figure V-B-1	133
V-B-3	Heat Flow Curves Observed on a Sapphire Reference	134

Number		Page
V-B-4	Plot of Heat Flow Versus Temperature	119
V-B-5	Heat Capacity of Polyoxymethylene Melt as a Function of Temperature	143

PART I

INTRODUCTION

INTRODUCTION

The promise of filamentary composite materials, whose development may be considered as entering its second generation, continues to generate intense interest and applications activity. Such interest and activity are well-founded, since they are based on the possibility of using relatively brittle materials with high modulus, high strength, but low density in composites with good durability and high tolerance to damage and which, when they do fail, do so in a non-catastrophic manner. Fiber reinforced composite materials of this kind offer substantially improved performance and potentially lower costs for aerospace hardware.

Much progress has been achieved since the initial developments in the mid 1960's. Rather limited applications to primary structure have been made on operational vehicles, however, mainly in a material-substitution mode on military aircraft. More extensive experiments are currently underway on large passenger airplanes in commercial operation as part of NASA's influential ACEE program and in a few military developments, such as the AV-8B and X-29 which have not seen service use.

To fulfill the promise of composite materials completely requires a strong technology base. NASA and AFOSR recognize the present state of the art to be such that to fully exploit composites in sophisticated aerospace structures, the technology base must be improved. This, in turn, calls for

expanding fundamental knowledge and the means by which it can be successfully applied in design and manufacture.

As the technology of composite materials and structures moves toward fuller adoption into aerospace structures, some of the problems of an earlier era are being solved, others which seemed important are being put into perspective as relatively minor, and still others unanticipated or put aside are emerging as of high priority. The purpose of the RPI program as funded by NASA and AFOSR has been to develop critical advanced technology in the areas of physical properties, structural concepts and analysis, manufacturing, reliability and life prediction.

Our approach to accomplishing these goals is through an interdisciplinary program, unusual in at least two important aspects for a university. First, the nature of the research is comprehensive - from fiber and matrix constituent properties research, through the integration of constituents into composite materials and their characterization, the behavior of composites as they are used in generic structural components, their non-destructive and proof testing and, where the state of the art will be advanced by doing so, extending the research effort into simulated service use so that the composite structure's long-term integrity under conditions pertinent to such use can be assessed. Inherent in the RPI program is the motivation which basic research into the structural aspects provides for research at the materials level, and vice versa.

Second, interactions among faculty contributing to program objectives - which is a group wider than that supported under the project - is on a day to day basis, regardless of organizational lines. Program management is largely at the working level, and administrative, scientific and technical decisions are made, for the most part, independent of considerations normally associated with academic departments. Involvement of this kind includes - depending on the flow of the research - faculty, staff and students from chemistry, civil engineering, materials engineering and the department of mechanical engineering, aeronautical engineering and mechanics.

Both of these characteristics of the NASA/AFOSR program of research in composite materials and structures foster the kinds of fundamental advances which are triggered by insights into aspects beyond the narrow confines of an individual discipline. This is a program characteristic often sought in many fields at a university, but seldom achieved.

A third aspect is a newly instituted initiative to increase involvement of NASA's Research Center scientists and engineers in the program at RPI and vice versa. This will require, first, identification of individual researchers within NASA centers whose areas of interest, specialization and active investigation are in some way related to those of RPI faculty supported under the subject grant. Second, means to bring about their interaction will be sought and a program

of active interchange encouraged. Important benefits foreseen for this increased communication include a clearer window to directions in academia for NASA researchers; opportunities to profit from NASA experience, expertise and facilities for the faculty so involved; and an additional channel for cross-fertilization across NASA Research Center missions through the campus program.

Overall program emphasis is on basic, long-term research in the following categories: (a) constituent materials, (b) composite materials, (c) generic structural elements, (d) processing science technology and (e) maintaining long-term structural integrity. Emphasis has shifted, and can be expected to continue to shift from one time period to another, among these areas depending on the states of composite materials and structures. Progress in the program will be reported in the following pages under these headings. Those computer methodology developments are also undertaken which both support Rensselaer projects in composite materials and structures research in the areas listed above and which also represent research with the potential of widely useful results in their own right.

In short, the NASA/AFOSR Composites Aircraft Program is a multi-faceted program planned and managed so that scientists and engineers in a number of pertinent disciplines at RPI will interact, both among themselves and with counterpart NASA Center researchers, to achieve its goals. Research in the basic composition, characteristics and processing science

of composite materials and their constituents is balanced against the mechanics, conceptual design, fabrication and testing of generic structural elements typical of aerospace vehicles so as to encourage the discovery of unusual solutions to present and future problems. In the following sections, more detailed descriptions of the progress achieved in the various component parts of this comprehensive program are presented.

PART II

CONSTITUENT MATERIALS

II-A CHEMICAL MODIFICATION OF THE SURFACE OF HIGH MODULUS CARBON FIBERS

II-A CHEMICAL MODIFICATION OF THE SURFACE OF HIGH MODULUS CARBON FIBERS

Senior Investigator: R. J. Diefendorf

1. Introduction

Over the last two decades, there has been great demand for engineering materials with very high specific strength and stiffness. Extensive research led to the emergence of the families of kevlar, boron, carbon fibers and others. Unfortunately, carbon fibers with higher specific modulus (>450 GPa) usually have a graphitic surface and are poorly bonded by most polymeric matrices[1]*. The interface between high modulus fibers and epoxy matrices accounts for the low interfacial shear strength observed in composites comprised of these constituents. Consequently, one of the central challenges in the development and application of high modulus and ultra-high modulus carbon fibers is how to improve their composite interlaminar shear strength, while at least maintaining composite toughness[2,3,4]. Several approaches to modifying either the matrix resin, fiber surface or both have met with varying degrees of success, in that real improvements may incur high cost, longer processing times or are at the expense of composite toughness[5,6,7].

In the past, considerable effort at RPI has been expended to study the surface of high modulus fibers, matrix

*Numbers in brackets in this section refer to the references which are listed on page 23.

resins and epoxy curing agents and to observe how much their interfaces differ. In cases where differences do exist, investigations were made to try to match these differences and to design a more predictable or controlled fiber-matrix interface.

The aim of the present sub-study is to describe the deposition of selected monomers on the surface of high modulus carbon fibers. This research, being conducted by graduate student Cyprian Uzoh, is part of a continuing effort to understand and define the fundamental principles which provide the basis for the design of a predictable interfacial bond between carbon fibers and polymeric matrices.

2. Status

The surface energy of anhydride cured epoxies had been characterized and the dominant role of the curing agents and meaning of the critical surface energy defined, at the beginning of this reporting period.

It was learned in our earlier studies[8,9] that amines preferentially adsorb (or react) on the basal planes of graphite and dictate the effective value of the surface energy. From this work, it became apparent that an effective method for the design of a controlled fiber-matrix interface is to incorporate or graft to the fiber surface those chemical species that could interact with the matrix, with the expectation that the shear strengths and toughness of the resulting

composite could be related to fiber surface chemistry.

3. Progress During Report Period

Based on the earlier observations, various chemical methods were used to graft functional groups (amine, anhydride, amide etc.) and monomers on the surface of high modulus carbon. (Before grafting, the fibers were scoured in a 50/50 solution of chloroform and chlorobenzene, then with chloroform, acetone and, finally, with anhydrous ether, then dried at 150° C for 12 hours.)

The reactivity of the various surface grafts with epoxy resins was probed with differential scanning calorimetry (DSC). The type of functional groups on the fiber surface was determined with infra-red spectroscopy. The nitrogen and hydrogen assay of the various treatments was obtained with an elemental analyzer, and, finally, the surface morphology of the modified fibers was examined with scanning electron spectroscopy (SEM).

a. Results and Discussion

Pure graphite is hydrophobic in nature, but this hydrophobicity is decreased if oxygen is present on the surface of graphite. Oxidative treatment of carbon fiber surface introduces several different polar groups on the fiber surface. The most abundant species are carboxyl (RCOOH), phenolic hydroxy (R-OH) and carbonyl ($\rangle C=O$), which are largely acidic[10,11,12]. The other functional groups known to be

present, but not always firmly established, include hydroperoxide, quinones, hydroquinones and lactones.

Oxygen enrichment of the carbon fiber surface due to oxidation for brief periods in hydrogen peroxide renders the fiber surface hydrophilic. Dramatic increases in fiber reactivity were observed when a peroxide-treated fiber was reacted with diethylenetriamine, in an ultrasonic bath. However, the observed weight gains were quite in excess of what would have been expected from amine adsorption or reaction with the basal and graphitic edge sites on the fiber. The results are illustrated in Figure III-A-1 and can be explained by several factors, namely:

a) a small amount of residual peroxide being trapped between the filaments after it had been partially dried,

b) the wetting of the fiber by the reaction medium and

c) the concentrations of amine in the bath, bath temperature and agitation and, to some extent, the duration of treatments.

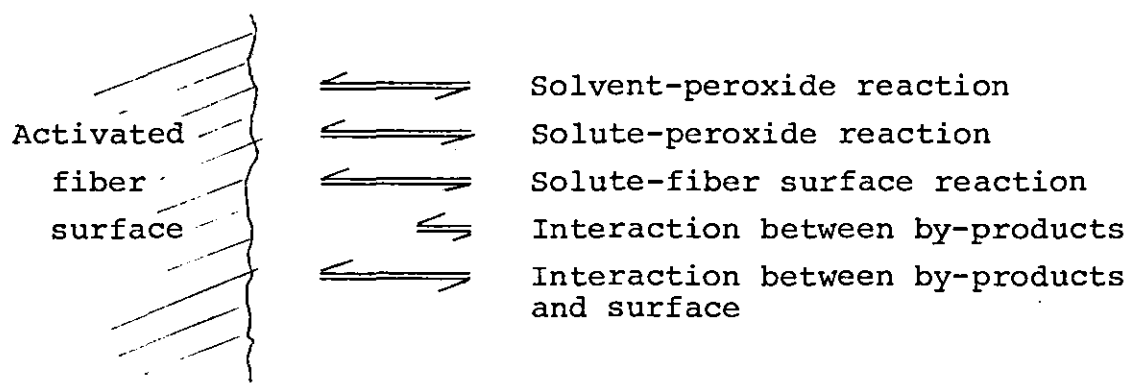

Figure II-A-1. Schematic of Events Occurring on the Fiber During Deposition in a Reactive Medium

While the reaction medium, diethyl ether, is known to be an inert medium for amines, it is not inert to the residual hydrogen peroxide (H_2O_2) on the filament's surface. The primary product of the oxidation of aliphatic ether under mild conditions (30°C-70°C) is hydroperoxide[13]. The primary products of hydroperoxide decomposition are esters, alcohols, acids and aldehydes[13,14,15]. Apart from the possible reactions between the solvent and the peroxide, the nitrogen in an amine is in its lowest oxidation state and can be easily oxidized by residual peroxide on the fiber surface. Diethylenetriamine, though a mixed amine, will most likely react with peroxides to form nitroso compounds, via initially formed hydroxylamine[16]. A third variation of various feasible reactions in the vicinity of the oxygen-enriched fiber surface is the reaction of amine with some pendant carbonyl group at the edges of graphite planes to form imines[17].

$$\geq C = O + RNH_2 \rightleftharpoons \geq C = NR + H_2O$$

The shift of the equilibrium in this reversible reaction can be shifted to favor imine formation by the selective removal of water. However, the carbonyl group, like other bond groups, is hindered on the surface and will only react if an amine specie diffuses close enough for them to interact with. At lower concentrations of amine, the pickup of amine by the fiber is small and not affected by peroxide concentration. With increasing amine concentration (>0.25 eg/L), rapid

build-up of oily, gel-like material occurs. Studebaker, in a similar experiment using Philblack-0 and Spheron 9[18,19], concluded that the fixation of nitrogen depends on the oxygen-containing groups initially present on the surface. The nitrogen was so firmly bonded that only a small fraction could be recovered on heating with concentrated sodium hydroxide or hydrochloric acid at 300° C, which showed great stability of the surface complex formed.

The presence of ammonium ions in the acidic fiber surface oxide, for our fiber, is discounted by infrared spectroscopy of surface functional groups. There are sharp reductions in the peaks of the starting diethylene triamine, particularly, N-H stretch and bend (at 2.97μ-3.05μ and 6.27μ) and CH stretch and bend (at 3.4μ-3.56μ and 6.85μ), respectively. Of particular interest is the emergence of a pronounced peak around 6μ. Preliminary wet analysis of fiber surface deposit may indicate that the peak is due to the carbonyl group. Even though a comparatively thick deposit is not a requirement for the development of a good-coupling between modified fibers and matrix, or for the formation of a tenacious film, it will be of interest to compare the behavior of composite interface resulting from the reaction of amine on a hydrophobic fiber surface to that of an oxygen enriched surface.

The polymerization of diethylene triamine with Nadic methyl anhydride (NMA) or with Dodecenylsuccinic anhydride (DDSA) to form their corresponding N,N-Disubstituted amide

on the fiber surface under differenct conditions is shown in Figure II-A-2. Fiber weight gain increased with the effective concentration [A][B] of the amine, a base [B] and the acid anhydride [A]. However, yields were not as high as when anhydrides were absent. As in the case of the deposition of amine, rendering the fiber surface hydrophilic, by scouring in hydrogen peroxide, increases yield. Performing the final deposition (anhydride) in the ultrasonic bath reduces fiber weight gain. Finally, the comparatively low yield observed for Nadic methyl anhydride on an oxygen-enriched fiber surface, is consistent with other results; namely, that scouring the fiber surface with hydrogen peroxide renders the surface more acidic.

Examination of the various treated fibers in a scanning electron microscope reveals (as shown in Figures II-A-3a to -3e) that, in all instances, lower concentrations of amine and anhydride produce fairly uniform deposits. At higher concentrations of monomers or weight gains, nonuniform deposits prevail, as represented by the clumps on the fibers in Figure II-A-3d. However, when the final deposition is performed in an ultrasonic bath, these clumps are dispersed (see Figure II-A-3e). Additional work has been done to relate conditions of treatment to the structure and morphology of coating.

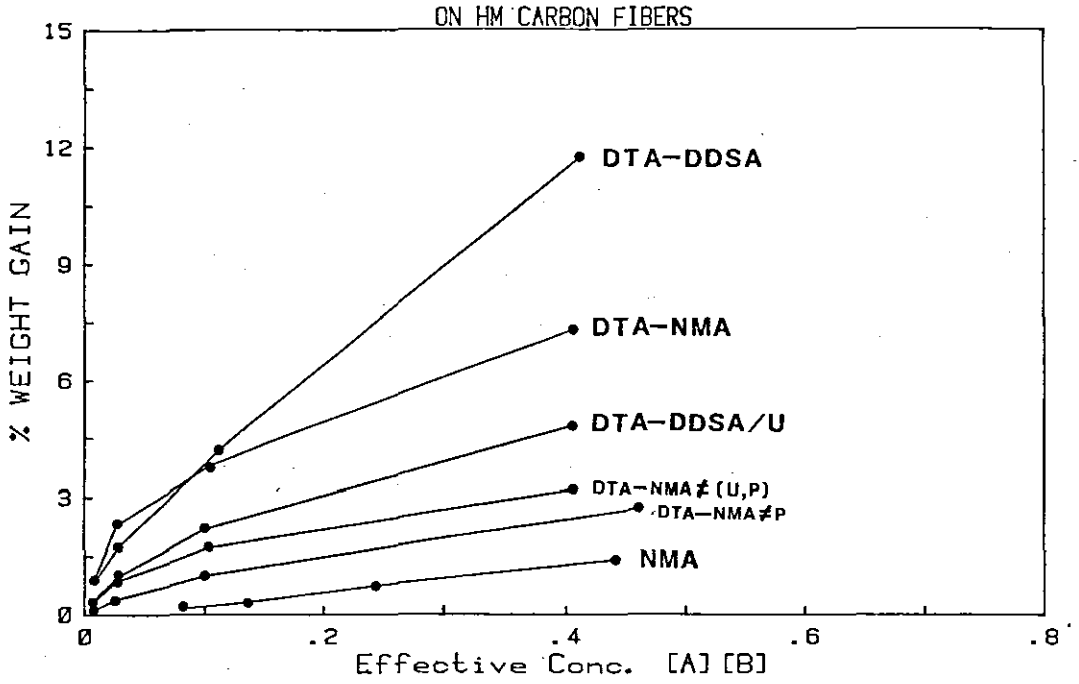

NOTE:
1) DTA-DDSA; DTA-NMA; dodecenyl succinic anhydride and nadic methyl anhydride deposition on diethylene amine, respectively
2) DTA-DDSA/u; anhydride deposition per formed in ultrasonic bath
3) DTA-NMAH(u,p); room temperature deposition without ultrasonic bath or peroxide oxidation
4) DTA-NMA≠P; no fiber peroxide oxidation
5) Deposition of only nadic methyl anhydride on fibers

Figure II-A-2. Deposition of Amide as a Function of Effective Bath Concentration of Amine [B] and Anhydride [A]

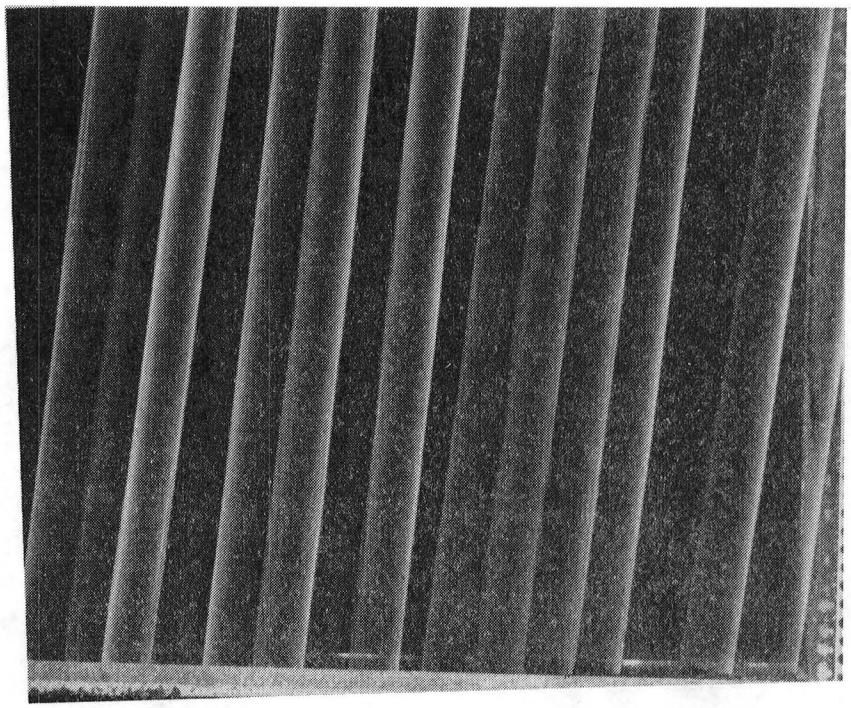

Figure II-A-3a. Surface of High Modulus Carbon Fibers After Scouring with a Solution of Chloroform and Chlorobenzene (1000x)

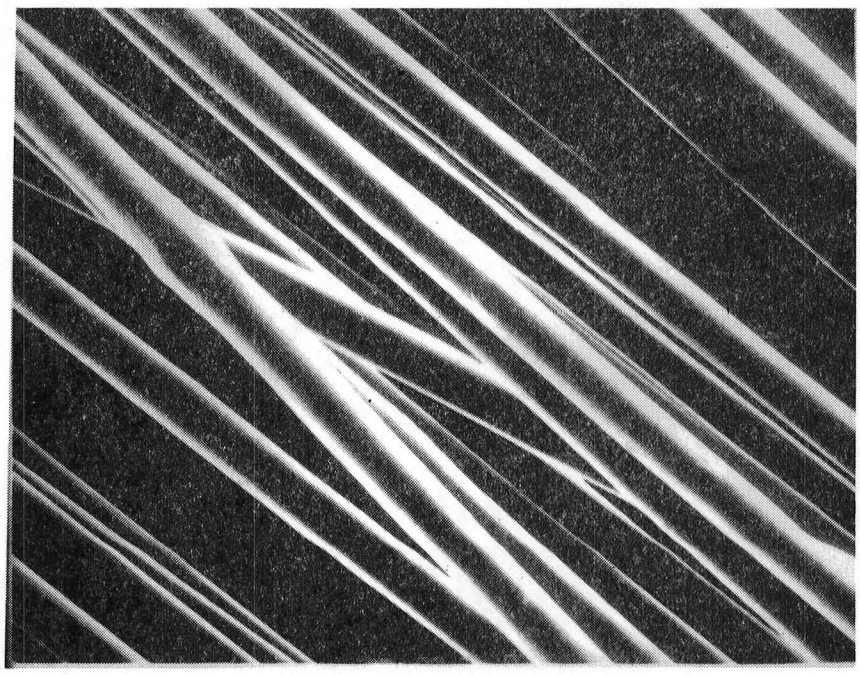

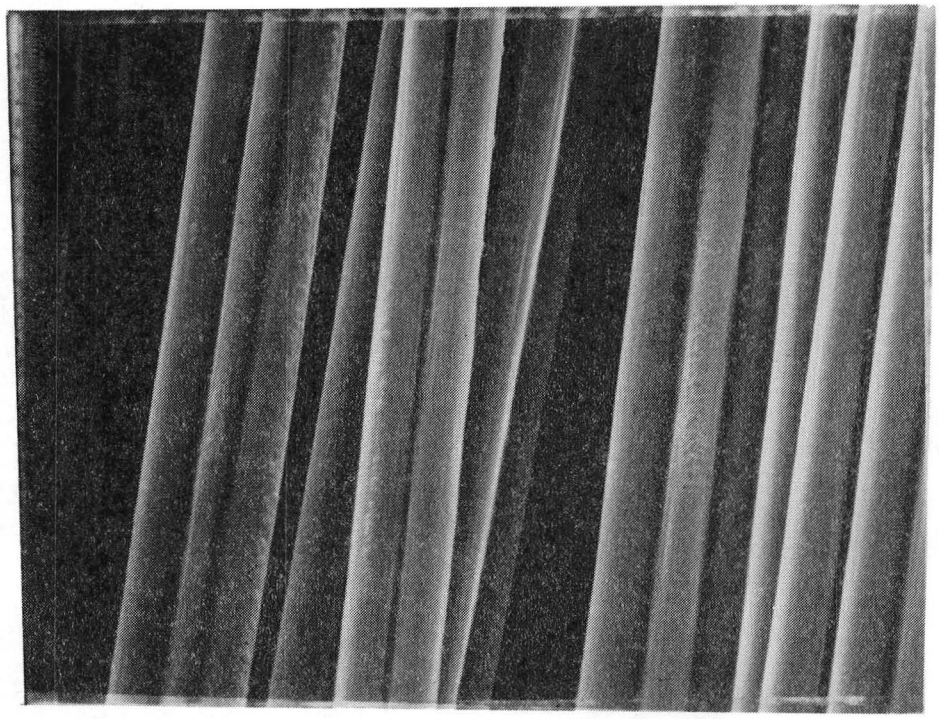

Figure II-A-3c. HM Fiber Surface, Preoxidized in Thirty Percent Hydrogen Peroxide Before the Deposition of DTA (34.6% gain gel formation)

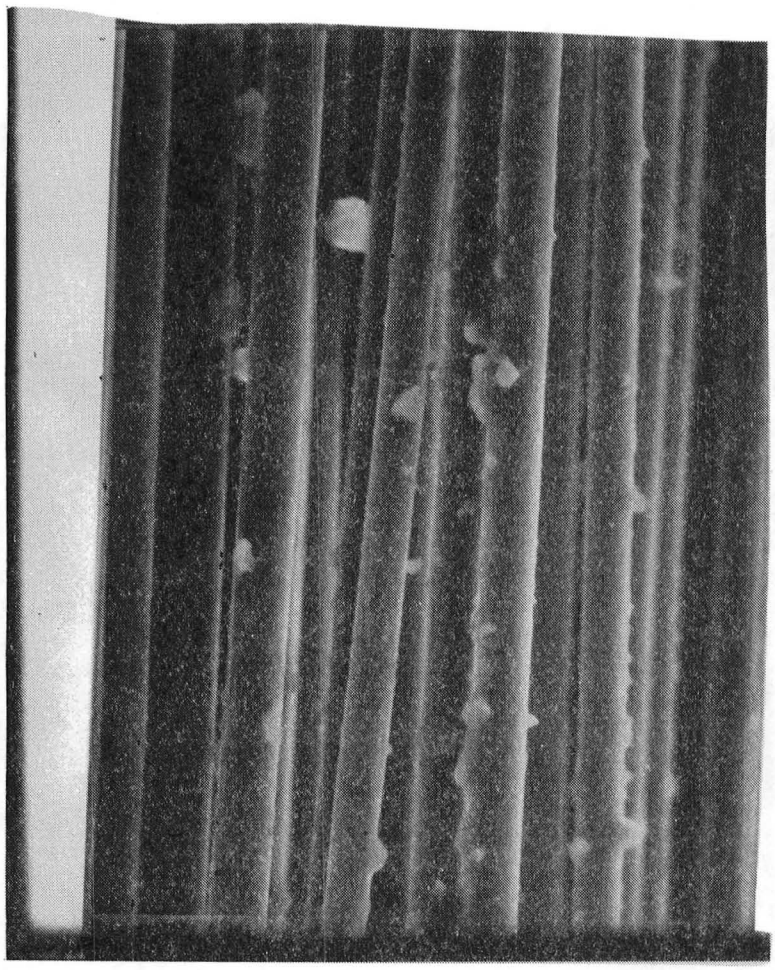

Figure II-A-3d. Fiber Surface After Deposition of DTA and DDSA. (fiber weight gain 11.7%)

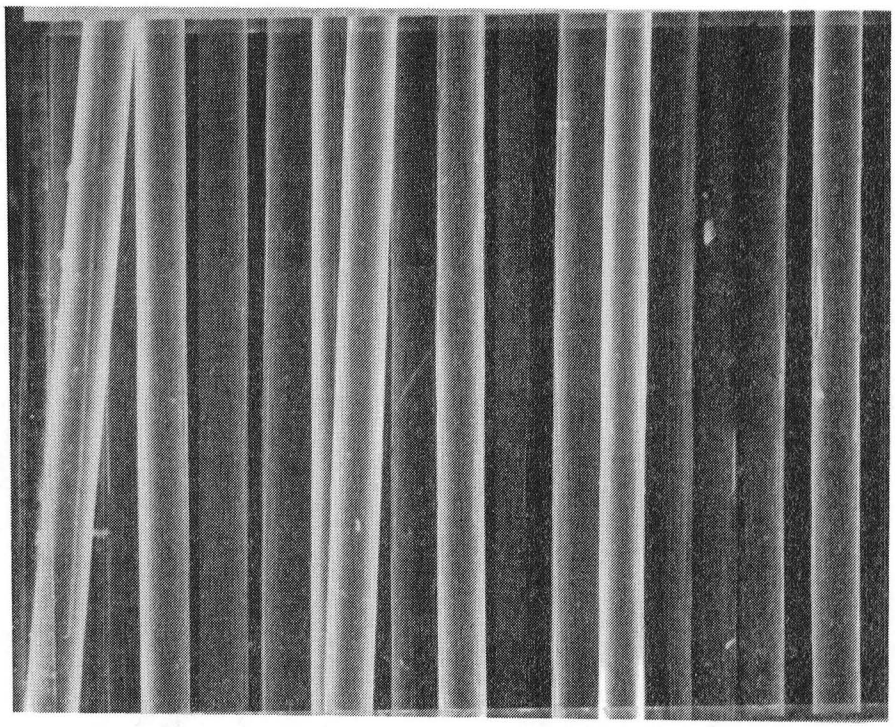

Figure II-A-3e. Fiber Surface After Deposition of DTA and DDSA with DDSA Deposition in Ultrasonic Bath. (4.8% weight gain)

4. Plans for Upcoming Period

Considerable effort will be devoted to studying the influence of various deposited monomers on the modification of fiber-matrix interfacial strength, in high modulus carbon fiber-epoxy composites. In particular, the effect of the interface on crack propagation is to be studied with single fibers embedded in a matrix film.

5. References

1. Goan, J. C. and S. P. Prosen, ASTM-STP 452, 1968, pp. 3-26.
2. Milewski, J. V., R. G. Shaver and S. H. Morgen, Proceedings Society Plastic Engr., Montreal, Canada, March 1966.
3. Shaver, R. G., "Silicon Carbide Whiskered Graphite Fiber", American Institute of Chem. Engr. Materials Conference, Philadelphia, PA, April 1978.
4. Diefendorf, R. J. and E. Tokarsky, AFML-TR-72-33, Part 1, October 1971.
5. Donnet et al., "Their Place in Modern Technology", Paper 9, Proceedings Intl. Conference on Carbon Fiber, London, UK, 1974.
6. Papirer et al., Carbon, Vol. 16, No. 2, 1974, pp. 124-131.
7. Fitzer et al., Carbon, Vol. 18, 1980, pp. 389-393.
8. Diefendorf, R. J., "High Modulus graphite Fiber Surface Modification for Improved Interaction with Matrices", RPI/NASA/AFOSR Composite Structural Materials, 39th Semi-Annual Report, January 1981, pp. 124-155.
9. Diefendorf, R. J., "The Surface Energy of Anhydride-Cured Epoxy Resins", RPI/NASA/AFOSR Composite Structural Materials, 43rd Semi-Annual Report, December 1982, pp. 9-18.
10. McKee, D. W. and V. J. Mimeault, "Surface Properties of Carbon Fibers", Chemistry and Physics of Carbon, P. L. Walker and P. A.Thrower, eds., Vol. 8, Marcel Dekker, 1973, pp. 152-240.

11. Boehm, H. P., "Advanced Catalysis", Vol. 16, 1966, p. 179.

12. Ryoichi, H., R. G. Scott and R. E. Winans, "Oxidation of Coal", Oxidation in Organic Chemistry Part 5D, W. S. Trahanovsky, ed., Academic Press, 1982, pp. 279-354.

13. Dehisov, E. T., "The Oxidation of Alcolols, Ketones, Ethers, Esters and Acids in Solution", Comprehensive Chemical Kinetics, Vol. 16 - Liquid Phase Oxidation, C. H. Bamford and C. F. H. Tipper, eds., Elsevier Sci. Publishing Co., pp. 125-191.

14. Ogata, Y., K. Tomizawa and K. Furuta, "Photochemistry and Radiation Chemistry of Peroxides", The Chemistry of Peroxides, S. Patai, ed., John Wiley and Sons, 1983, pp. 711-760.

15. Božo Plesničar, "Oxidations with Peroxy Acids and Other Peroxides", Oxidation in Organic Chemistry, Vol. 5C, W. S. Trahanovsky, ed., Academic Press, 1978, pp. 2110280.

16. Božo Plesničar, "Polar Reaction Mechanism Involving Peroxides in Solution", The Chemistry of Peroxides, S. Patai, ed., John Wiley and Sons, 1983, pp. 521-580.

17. Kemp, D. S. and F. Vellaccio, "Organic Chemistry", Worth Publishing Inc., 1980, pp. 1224-1231.

18. Studebaker, M. L., "Rubber Age", New York, Vol. 80, 1957, p. 661.

19. Puri, B. R., "Surface Complexes on Carbons", Chemistry and Physics of Carbon, Walker, ed., Vol. 6, Marcel Dekker, 1970, pp. 191-275.

20. "Interfacial Synthesis", Vols. I and II., Millich and Carraher, eds., Marcel Dekker Inc., NY, 1977.

6. Current Publications or Presentations by Professor Diefendorf on this Subject

"Forchung in den USA", with G. Helwig, V. Paedelt and C. Verpoort

Published in Luftfahrt International, pp. 156-157, February 1984.

"Mesophase Formation in Polynuclear Aromatic Compounds: A Route to Low Cost Carbon Fibers"
"Molecular Weight and Molecular Weight Distributions in Pitches", with S. H. Chen
"Pitch Solvent Interactions and Their Effects on Mesophase Formation", with J. G. Venner

To be published in Polymers for Fibers, E. Dall and R. J. Diefendorf et al., eds., ACS, June 1984.

"Composite Structures for Army Applications"

Presented to AMMRC at Fort Lewis, Fort Lewis, WA, October 20, 1983.

"Composite Materials"

Presented at GE Modern Engineering Course, Saratoga Springs, NY, November 5, 1983.

"Transverse Fiber Properties"
"Consumer Applications of Carbon Fiber Composites"

Presented at the 4th International Conference on Metal Matrix Composite Materials, Bratislava, Czechoslovakia, November 8-10, 1983.

"A Comparison of High Modulus Fibers"

Presented at the International Conference on Carbon Fiber Applications", San José dos Campos, Brazil, December 5-7, 1983.

"Carbon Fibers"

Presented at American Chemical Society Meeting, St. Louis, MO, April 17, 1984.

"RP Sailplane Project"

Presented at GE Research and Development Center, Schenectady, NY, April 17, 1984.

"Carbon Fiber Structures and Properties"

Presented at Aluminum/Carbon Composite Workshop, Naval Surface Weapons Center, White Oaks, CA, April 24-25, 1984.

PART III

COMPOSITE MATERIALS

III-A FATIGUE IN COMPOSITE MATERIALS

III-B EXPERIMENTAL AND THEORETICAL STUDIES OF MOISTURE AND TEMPERATURE EFFECTS ON THE MECHANICAL PROPERTIES OF GRAPHITE/EPOXY LAMINATES AND NEAT RESINS

III-C NUMERICAL INVESTIGATION OF THE MICROMECHANICS OF COMPOSITE FRACTURE

III-D FREE-EDGE FAILURES OF COMPOSITE LAMINATES

III-A FATIGUE IN COMPOSITE MATERIALS

Senior Investigator: E. Krempl

1. Introduction

The deformation and failure behavior of graphite/epoxy tubes under biaxial (axial and torsion) loading is being investigated. The aim of this research is to increase basic understanding of and provide design information for the biaxial response of graphite/epoxy composites to fatigue loads.

2. Status

The research activities up to the beginning of this reporting period consisted predominantly of experimental investigations of the biaxial fatigue and fracture behavior of graphite/epoxy thin-walled tubes. These studies continued with tests on $[0,\pm 45]_s$ graphite/epoxy tubes. We have now started literature studies on phenomenological damage accumulation laws in composites. Based on these studies, a tentative plan was formulated to study the progression of damage by residual strength measurements of prefatigued specimens and to establish a multiaxial damage accumulation law.

3. Progress During Report Period

It is well-known that the Palmgren/Miner[1,2]* approach to block loadings (one stress or strain amplitude followed by

*Numbers in brackets in this section refer to the references which are listed on page 33.

a higher - or lower - amplitude) does not predict a sequence effect. In this approach the sequence (high/low or low/high) of block loadings has no effect on the predicted life.

The few results of tests on composites which are available indicate that the low/high sequence is more damaging than the high/low block loading[3,4].

In establishing phenomenological theories of damage accumulation, either residual lifetime[5-8] or residual strength[4,9] are adopted. It was tentatively decided to use residual strength as a measure of damage in future studies.

Guided by the Paris law of crack growth and previous studies[7,10], it is proposed to use

$$\frac{dD}{dN} = g(D)\,f(S) \tag{1}$$

as an evolution equation for damage. In the above,

N is the cycle number,

D is the dimensionless damage,

S is the dimensionless amplitude and

g( ) and f( ) are positive functions which are only zero when their argument is zero.

It is postulated that

$$D = 0 \qquad \text{for } \bar{\sigma}_r = \frac{\sigma_f}{\sigma_{uts}} = 1 \tag{2}$$

and

$$D \to \infty \qquad \text{for } \bar{\sigma} \to 0. \tag{3}$$

where

σ_f denotes the fracture strength at any time,

σ_{uts} is the ultimate tensile strength and

$\bar{\sigma}_r$ is the dimensionless residual strength.

For working purposes, it is assumed that the relationship between $\bar{\sigma}_r$ and D is given by

$$\bar{\sigma}_r = \exp[-h(D)] \tag{4}$$

where

h(D) is a monotonic increasing function of argument.

When special forms for h( ) and g( ) are chosen, the relationships proposed in References 3 and 4 can be recovered.

As an example, the fatigue curve for completely reversed loading is expressed as

$$S = 1 + \Gamma \log N \tag{5}$$

with Γ a constant < 0. Further, h(D) = D, and $g(D) = D^a$ where a is a value to be chosen and is > than 0. Then the residual strength is given by

$$\bar{\sigma} = \exp\left[\left(10^{\frac{1-S}{\Gamma}\frac{1}{1-a}} N^{\frac{1}{1-a}}\right) \ln S\right] \tag{6}$$

It can also be shown that Equation (1) predicts block sequence independence up to the final stage. In a two-block loading sequence the behavior of composites is reproduced by (1) together with (2) and (3).

A simple extension of Equation (1) to multiaxial loading is

$$\frac{dD}{dt} = g(D)f(\bar{S}) \tag{7}$$

with

$$\bar{S} = F_{ij}S_iS_j + G_iS_i \tag{8}$$

where

summation from 1 to 6 is implied over repeated indices,

F_{ij} and S_i are matrices (vectors) which represent the appropriate material anisotropies and

symbol t denotes time.

For proportional loading with common period T_c the cycle dependence proposed in Equation (1) can be recovered.

Preliminary studies were made using Equations (7) and (8) together with results obtained previously[11]. Initial correlation is encouraging, and the approach outlined briefly here will be pursued further.

4. Plans for Upcoming Period

The theory described above will continue to be developed and checked against data. A test program will be outlined, aimed specifically at verifying the above approach and at its further development. In addition, biaxial fatigue tests with $[0,\pm45]_s$ graphite/epoxy specimens under proportional loading will be performed.

5. References

1. Palmgren, A., "Die Lebensdauer von Kugellagern", ZVDI, 68, 1924, pp. 339-341.
2. Miner, M. A., "Cumulative Damage in Fatigue", ASME Journal of Applied Mechanics, 67, 1945, pp. A159-A164.
3. Broutman, L. J. and S. Sahu, "A New Theory to Predict Cumulative Fatigue Damage in Fiberglass Reinforced Plastics", ASTM STP 497, 1972, pp. 170-188.
4. Yang, J. N. and D. L. Jones, "Effect of Load Sequence on the Statistical Fatigue of Composites", AIAA, 18, No. 12, pp. 1525-1531.
5. Subramanyan, S., "A Cumulative Damage Rule Based on the Knee Point of the S-N Curve", ASME Journal of Engineering Materials and Technology, 98, 1976, pp. 316-321.
6. Hashin, Z. and A. Rotem, "A Cumulative Damage Theory of Fatigue Failure", Materials Science and Engineering, 34, 1978, pp. 147-160.
7. Ostergren, W. J. and E. Krempl, "A Uniaxial Accumulation Law for Time-Varying Loading Including Creep-Fatigue Interaction", ASME Journal Pressure Vessel Technology, 101, pp. 118-124.
8. Chaboche, J. L., "Life Prediction and Cumulative Damage Under High-Temperature Conditions", ASTM STP 770, 1982, pp. 81-104.
9. Yang, J. N. and M. D. Liu, "Residual Strength Degradation Model and Theory of Periodic Proof Tests for Graphite/Epoxy Laminates", Journal of Composite Materials, 11, pp. 176-203.
10. Cernocky, E. and E. Krempl, "A Coupled, Isotropic Theory of Thermoviscoplasticity and Its Prediction for Stress and Strain Controlled Loading in Torsion", Thermal Stresses in Severe Environments, D. P. H. Hasselman and R. A. Heller, eds., Plenum Press, 1980, pp. 47-60.
11. Niu, T.-M., Dr. Engr. Thesis, Rensselaer Polytechnic Institute, Troy, NY, May 1983.

6. Current Publications or Presentations by Professor Krempl on this Subject

"Time-Dependent Deformation and Fatigue Behavior of $[\pm 45]_s$ Graphite/Epoxy Tubes under Combined Loading" with T.-M. Niu.

To be presented at the ASTM Symposium on Composite Materials: Fatigue and Fracture, Dallas/Ft.Worth, TX, October 24-25, 1984.

"Biaxial Fatigue and Damage Accumulation in Thin-Walled Graphite/Epoxy Tubes:, with D. An.

To be presented at the IUTAM Symposium on the Mechanics of Damage and Fatigue, July 1-4, 1985, Technion-Israel Institute of Technology and Tel Aviv University.

III-B EXPERIMENTAL AND THEORETICAL STUDIES OF MOISTURE AND TEMPERATURE EFFECTS ON THE MECHANICAL PROPERTIES OF GRAPHITE/EPOXY LAMINATES AND NEAT RESINS

Senior Investigator: S. S. Sternstein

1. Introduction

This project is concerned with those properties of high performance composites which are strongly dependent on the physical properties of the matrix resin.

Moisture is known to adversely affect the properties of both neat epoxy resin and epoxy matrix composites. Inhomogeneous swelling makes a major contribution to the moisture degradation of mechanical properties, both in the neat resin and the composite. It is postulated that the postcuring process can change structure-moisture interactions and partially alleviate its adverse effects. Both analytical and experimental studies have been directed toward understanding the physical-mechanical-thermodynamic aspects of this problem.

2. Status

Relevant experimental and theoretical findings have been summarized in the previous progress report (No. 45, page 35). Work reported here has been performed by graduate students P. Yang and S. Singh under the direction of Dr. Sternstein.

3. Progress During Report Period

Studies on the effects of moisture and temperature histories on the mechanical properties of graphite/epoxy composite laminates have been concluded during the report period. Two theses, one doctoral and one master's, are in the process of being completed. Several journal publications are being prepared and will be submitted shortly. A brief summary of our findings during the last two years, as generalized in the report periods, follows.

Experimental studies on the effects of postcuring history on the sensitivity of moisture uptake and the damage resulting therefrom have shown that void formation, delamination cracks and fiber-matrix interfacial failure are strongly dependent on the prior thermal and moisture histories of the laminate. A properly postcured laminate displays little or no reduction in out-of-plane bending stiffness (hereafter referred to as stiffness) when subjected to modest moisture uptake. Conversely, an as-cured laminate (no postcure) shows dramatic reduction in stiffness, which is highly nonlinear with moisture uptake, suggesting internal damage. Microscopic observations bear out the damage hypothesis and corroborate our previous observation that the out-of-phase dynamic mechanical loss modulus (a measure of dissipative work of deformation) increases substantially, when moisture is absorbed in an as-cured sample.

Recognizing the complexity of the curing process and the gradients of cure which must exist in any finite size laminate,

it is clear that it may be difficult or highly impractical to properly postcure real (not laboratory sized) engineering structures.

The results of detailed observations on the effects of moisture uptake, glass transition reduction and reversibility, and dynamic loss modulus increase in postcured and as-cured laminates will be the subject of the papers to be submitted for publication in the near future.

Our theoretical studies have centered on the application of inhomogeneous swelling theory to the moisture induced swelling and stress field in epoxy matrix materials. A most important result has been obtained in that we have shown that a gradient in cross-link density can produce a hydrostatic tension field sufficient to cause cavitation, namely, $\sigma_1 = \sigma_2 = \sigma_3 = 16{,}000$ psi. Contrary to what might be expected, a gradient in cross-link density is more severe than a spherical hard particle (a box gradient) and produces much higher tensile stresses. Since gel particles and cross-link gradients are generally believed to occur in all thermosets, these theoretical findings are very promising, in that they form a basis by which environmentally induced (solvent) failure due to cavitation can be explained.

The analysis shows that the stress field resulting from an inhomogeneous material structure depends not only on the cross-link density at a point but also on the cross-link density gradient. Therefore, correlations of solvent uptake,

cavitation resistance, dimensional changes (e.g., swelling) etc., with average cross-link density, are invalid. A missing internal variable is the cross-link density distribution. The chemical and materials characterization of a thermoset, which does not evaluate the distribution, can lead to numerous errors in the evaluation of resin resistance to moisture related damage.

4. Plans for Upcoming Period

A new apparatus is being designed for the measurement of stress and stress state effects on equilibrium swelling and absorption phenomena in multiphase systems including composites. Such data are virtually nonexistant in the literature and are crucial to the further development of the theory. Applications include solvent induced cracking, crazing, fatigue and delamination.

5. Current Publications or Presentations by Professor Sternstein on this Subject

"Mechanical Characterizations of Composites"

Presented at the Society of Rheology Meeting, Knoxville, TE, February 20-22, 1983.

"Overview of Composites Research"

Presented at the Ninth Annual Mechanics of Composites Review, Dayton, OH, October 24-26, 1983.

"Viscoelastic Characterization of Neat Resins and Composites"

Presented at the Gordon Conference on Composites, Santa Barbara, CA, January 16-20, 1984.

"Mechanical Properties of Composites"

Presented at the Asilomar Conference on Polymers, Asilomar, CA, February 20-22, 1984.

III-C NUMERICAL INVESTIGATION OF THE MICROMECHANICS OF COMPOSITE FRACTURE

Senior Investigator: M. S. Shephard

1. Introduction

To understand mechanisms of failure in composites it is necessary to develop insight into their micromechanical behavior, including interactions between matrix and fibers as the load is increased from zero to that corresponding to failure. Investigations of these phenomena, either experimental or numerical, pose serious problems. The purpose of this project, being carried out by graduate student Nabil Yehia, is to develop a nonlinear finite element analysis methodology capable of performing numerical investigations into two-dimensional micromechanical failure of composites.

2. Status

A generalized program for the two-dimensional analysis of static crack growth problems has been developed and is being tested. In addition to a detailed examination and development of fracture criteria needed to track cracks in composites at the micromechanical level, the program employs fully automatic finite element mesh generation. This is an entirely new approach in program structure that is being taken to allow for the automatic tracking of discrete crack growth. We found that no existing form of the maximum strain

energy density criterion (i.e., T-criterion) could be directly used for crack propagation tracking, and a modified T-criterion was postulated.

3. Progress During Report Period

During the last reporting period, our effort concentrated on (a) completion of the modified T-criterion, (b) investigation of the effect of the singular element size of fracture criteria and (c) integration of the component parts of the automatic crack propagation system. The system combines finite element analysis techniques, fully automatic mesh generation and crack propagation criteria into a single program capable of analyzing general two-dimensional crack propagation.

The modifications of the geometry data base required to account for different crack initiation and propagation situations have been developed. Final testing of the system is being carried out.

a. Modified T-Criterion

The maximum strain energy density criterion, T-criterion[1]*, has been found to be a good alternative to the minimum strain energy density criterion, S-criterion[2], for predicting crack propagation history. As outlined in the last progress report, investigation of the T-criterion has led to the modified T-criterion. During this reporting period,

*Numbers in brackets in this section refer to the references which are listed on page 61.

formulation of the modified T-criterion has been completed, including a complete comparison between the S-criterion and the modified T-criterion[3]. For a slant crack problem under remote unidirectional load, comparison of the normalized fracture loads predicted by the two criterion are shown in Figure III-C-1, while the fracture loci are given in Figure III-C-2. Note that the modified T-criterion is denoted by R in these figures. The S and R criteria yield results which are quite close for plane stress problems, while the differences are much larger in the case of plane strain. These differences arise primarily from the changes in size of plastic zone associated with plane stress, in one case, and plane strain, in the other[3].

b. Singular Element Size Effect

While the singular element size has been shown to affect the numerical evaluation of stress intensity factors, such errors appear to be within acceptable engineering accuracy, e.g., within 10%, for most cases[4,5]. Errors in stress intensity factors and in crack propagation angle, obtained in a numerical study of the slant crack problem[7] for practical ranges of ℓ/a values, are shown in Figures III-C-3 and 4. Here too, errors are shown to be within ±10%. On the other hand, errors in predicting crack propagation increment for this problem go beyond acceptable engineering accuracy for small ℓ/a, and the error decreases as ℓ/a increases (Figure III-C-5). In the absence of information as to which criterion

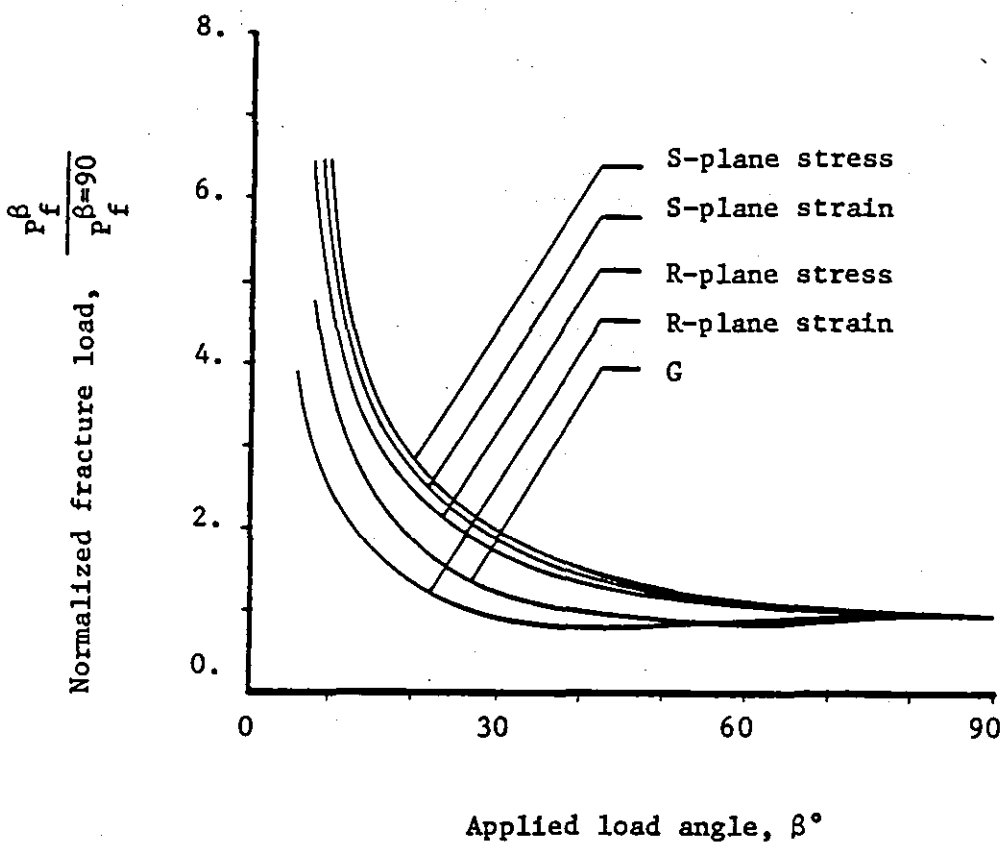

Figure III-C-1. Fracture Load for a Slant Crack Under Remote Tension Normalized with Mode I ($\beta = 90°$) Fracture Load. (G is the energy release rate criterion.)

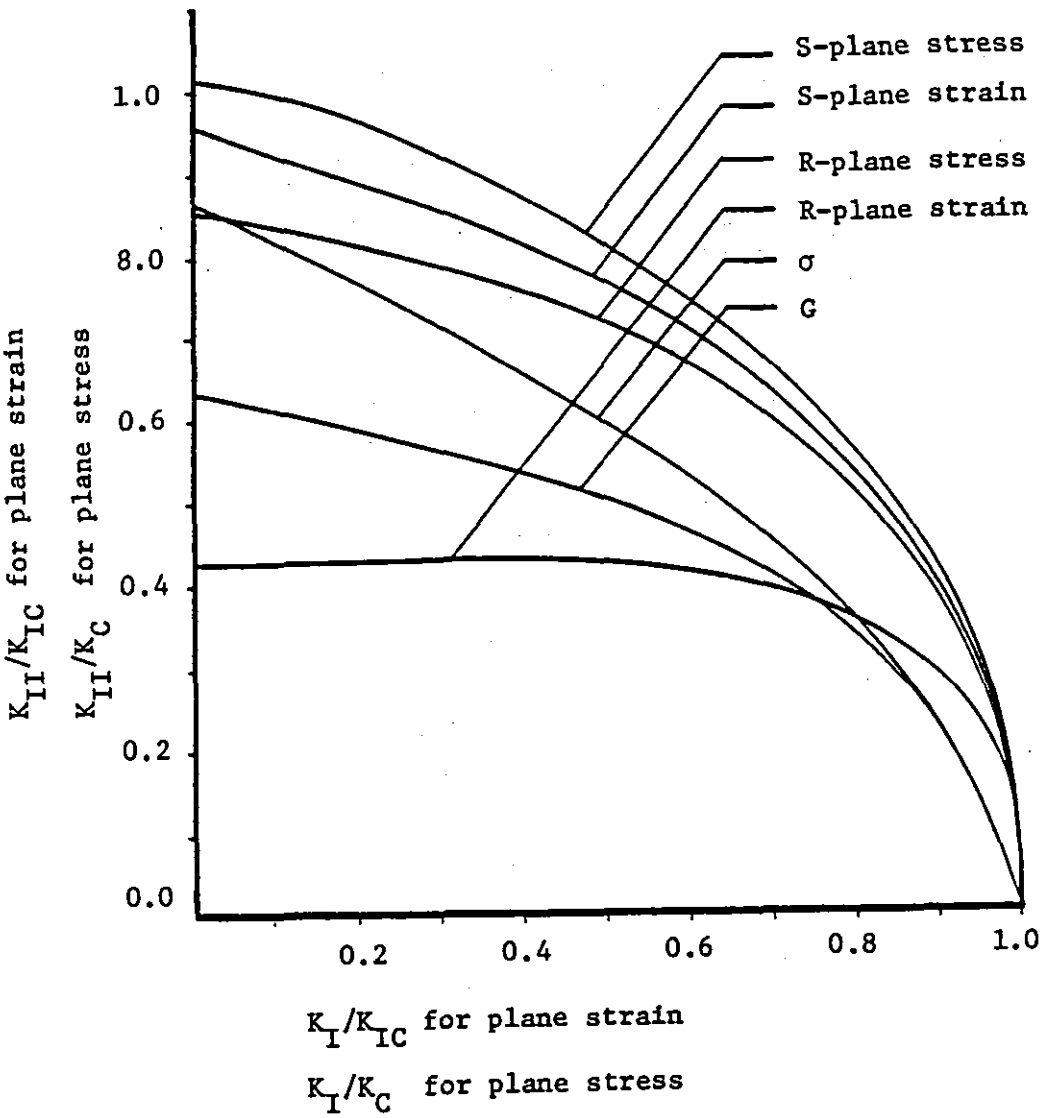

Figure III-C-2. Fracture Loci for a Slant Crack Under Remote Tension Normalized with Mode I ($\beta = 90°$) Fracture (G is the energy release rate criterion and σ is maximum tangential stress criterion.)

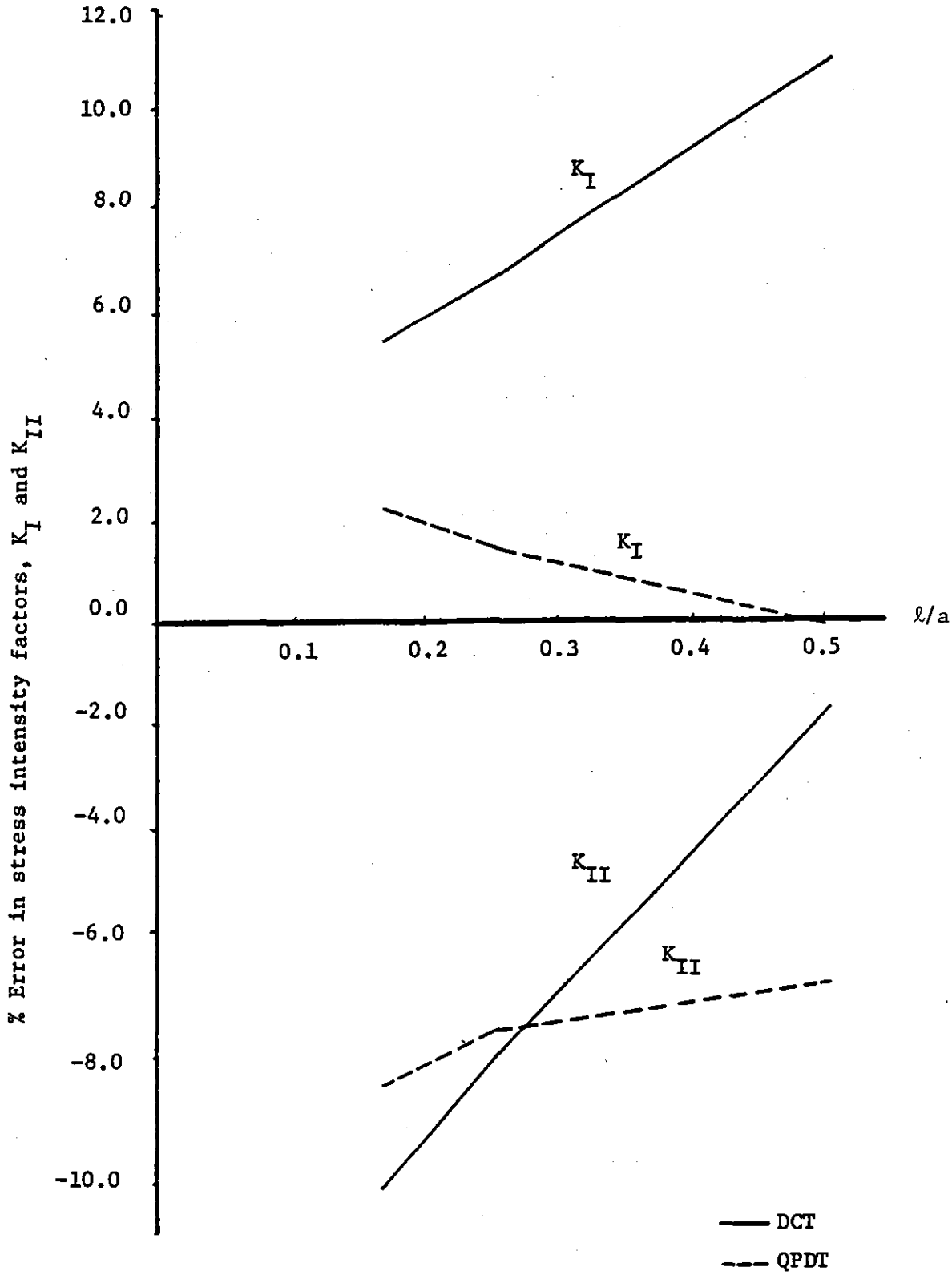

Figure III-C-3. Error in Evaluating the Stress Intensity Factors in Slant Crack Problems, with ($\beta = 40°$) Versus the Ratio of Singular Element Side Length, ℓ, to Half Crack Length, a.

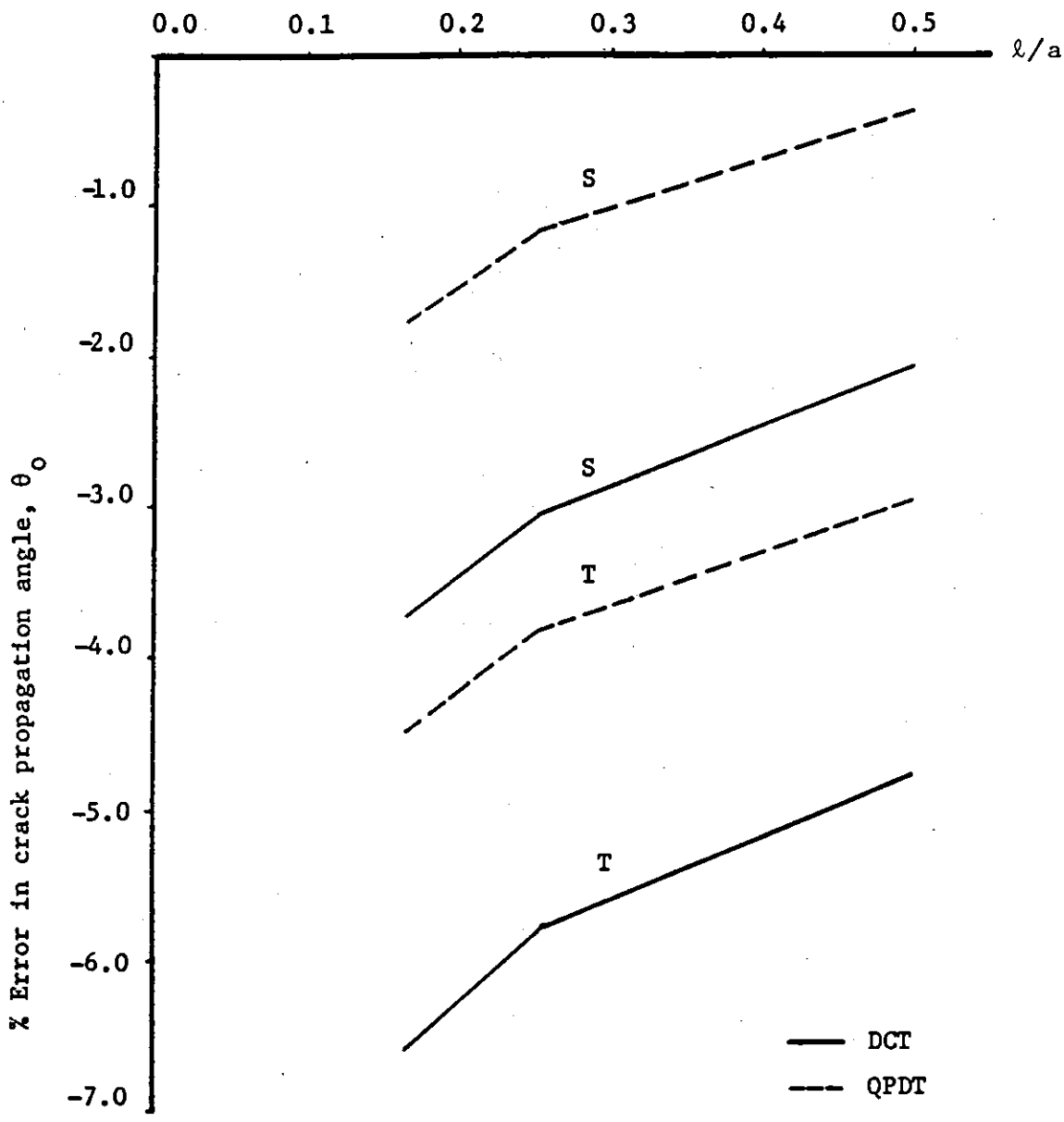

Figure III-C-4. Error in Crack Propagation Angle, θ, Versus the Ratio of ℓ/a for the Plane Strain, Slant Crack Problem, with $\beta = 40°$, Under Remote Tension

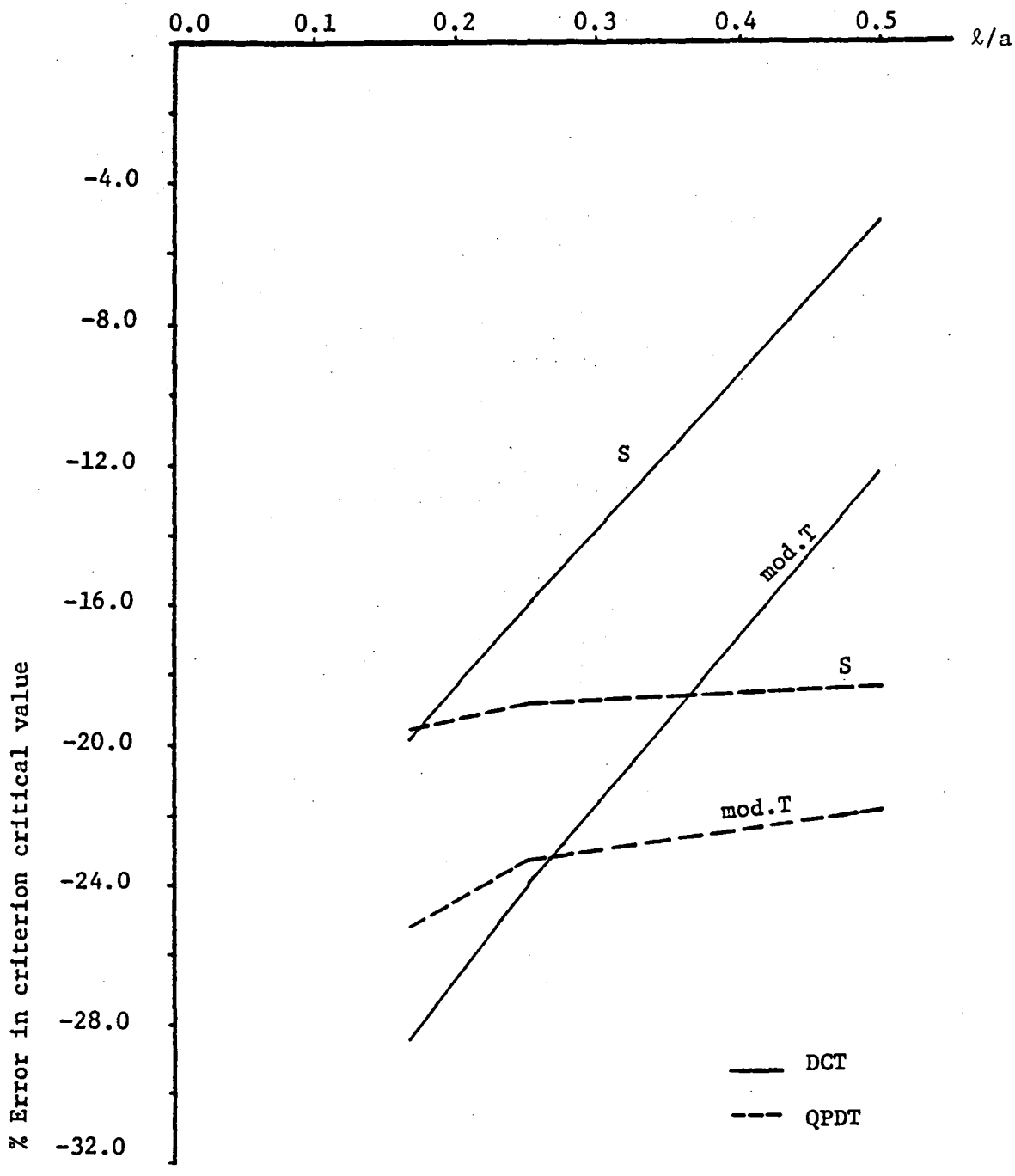

Figure III-C-5. Error in Propagation Increment Versus the Ratio of ℓ/a for the Plane Strain, Slant Crack Problem, with $\beta = 40°$, Under Remote Tension.

leads to exact results, and since the prediction of crack propagation angles and increments are criterion-dependent, it is assumed that when the exact stress intensity factors are used, the error in predicting crack propagation increment and angle is zero. It is noted, therefore, that Figure III-C-5 indicates only those errors introduced into the crack propagation criteria due to inaccuracies in the stress intensity factors. A complete study of the ℓ/a effect is given in References [6] and [7]. In Figures III-C-3, 4 and 5, QPDT and DCT stand for quarter point displacement techniques[6] and displacement correlation techniques[4] which are two techniques used in this study to evaluate the crack tip intensity factors.

c. Automatic Crack Tracking System

The crack propagation system is comprised of two separate computer programs. The first is an interactive graphics program used to define the problem to be analyzed. The second is the crack propagation analysis program[8] which combines all aspects of finite element mesh generation[9,10] and finite element analyses. In the problem definition program[11], the geometry of the object and the problem attributes of loads, material properties and boundary conditions are defined. In addition, fracture-oriented attributes, including the existence of crack tips and the values of bond strengths at material interfaces, are defined.

There is no finite element mesh generated during the problem definition phase, only the problem geometry in terms of material region boundary curves. All the problem attributes

are assigned to that geometry.

The second analysis program automatically carries out all facets of the numerical analysis process including:

1) generating a finite element mesh specifically accounting for all crack tips and the application of the problem attributes to that mesh[9],
2) carrying out the finite element analysis,
3) predicting any crack propagation occurring during that load increment and
4) updating the geometry to account for any crack growth.

Since this program accepts a geometric input definition and combines mesh generation with the finite element fracture analysis procedures, its overall operation and data structures are different from those employed in standard finite element codes. For example, the combination of the component parts of this program is complicated by the fact that different types of algorithms and data interchanges are required for each. The modified-quadtree mesh generator[9,10] makes extensive use of recursive algorithms and tree data structures, while the finite element and crack propagation portions require high precision computation and a large library of mathematical functions. To address both these issues, a hybrid programming technique is used. The majority of the mesh generation process is written in PASCAL, a language that allows recursion and the straightforward definition of complex data structures, while the majority of the analysis portions are written in FORTRAN.

The data used by the crack tracking program can be broken into three segments, namely;

1) geometry data: consisting of that information that defines the problem geometry and all the problem attributes of loads, material properties and boundary conditions,
2) mesh data: consisting of the modified-quadtree and the finite element mesh tied to it and
3) analysis data: consisting of all the finite element matrices and fracture criterion information.

Although separate, there are a number of specific ties between the three groups of data. The mesh data is created by the mesh generator directly from the geometry data, while the finite element data is constructed from the mesh data. Finally, the geometry data is modified based on the results of the finite element analysis and fracture criterion evaluation.

All program data generation and program operations are controlled by the geometry data. During the fracture process the model must be repeatedly updated to account for crack propagation. These changes are represented in the geometry data only, and since all subsequent information is generated from that data, all crack initiation and propagation is reflected directly in it, and it is the only data that must be updated. A detailed description of the data structure of the program can be found in References [8] and [9].

Depending on the location of the crack, different modifications are made to the geometry data base. Cracks initiating

Modification	Before Modification	After Modification	Operation Number	Explanation
Initiate crack on interior of a region	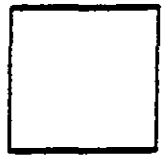	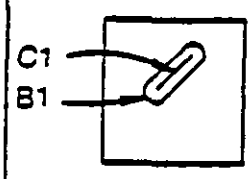	1	Create curve C1 (crack flank)
			2	Create boundary B1
Propagate a crack on the interior of a region	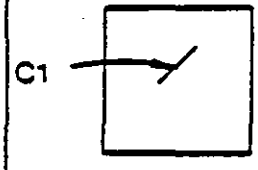	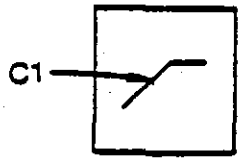	3	Extend curve C1 (crack flank)
Initiate a crack on a material interface	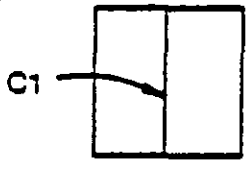	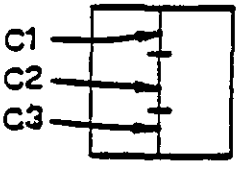	4	Divide curve C1 into curves C1, C2 (crack flank) and C3
Propagate crack along material interface	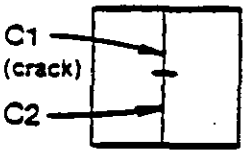	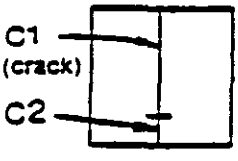	4	Divide curve C2 into curve C2 and a section to be merged with crack flank
			5	Merge section of C2 with C1
Propagate crack to an existing curve	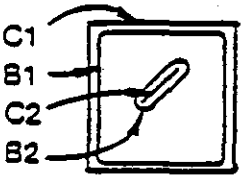	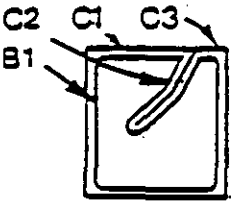	4	Divide curve C1 into curves C1 and C3
			3	Extend curve C2
			6	Merge boundary B2 into B1

Figure III-C-6. Geometry Modification Operations

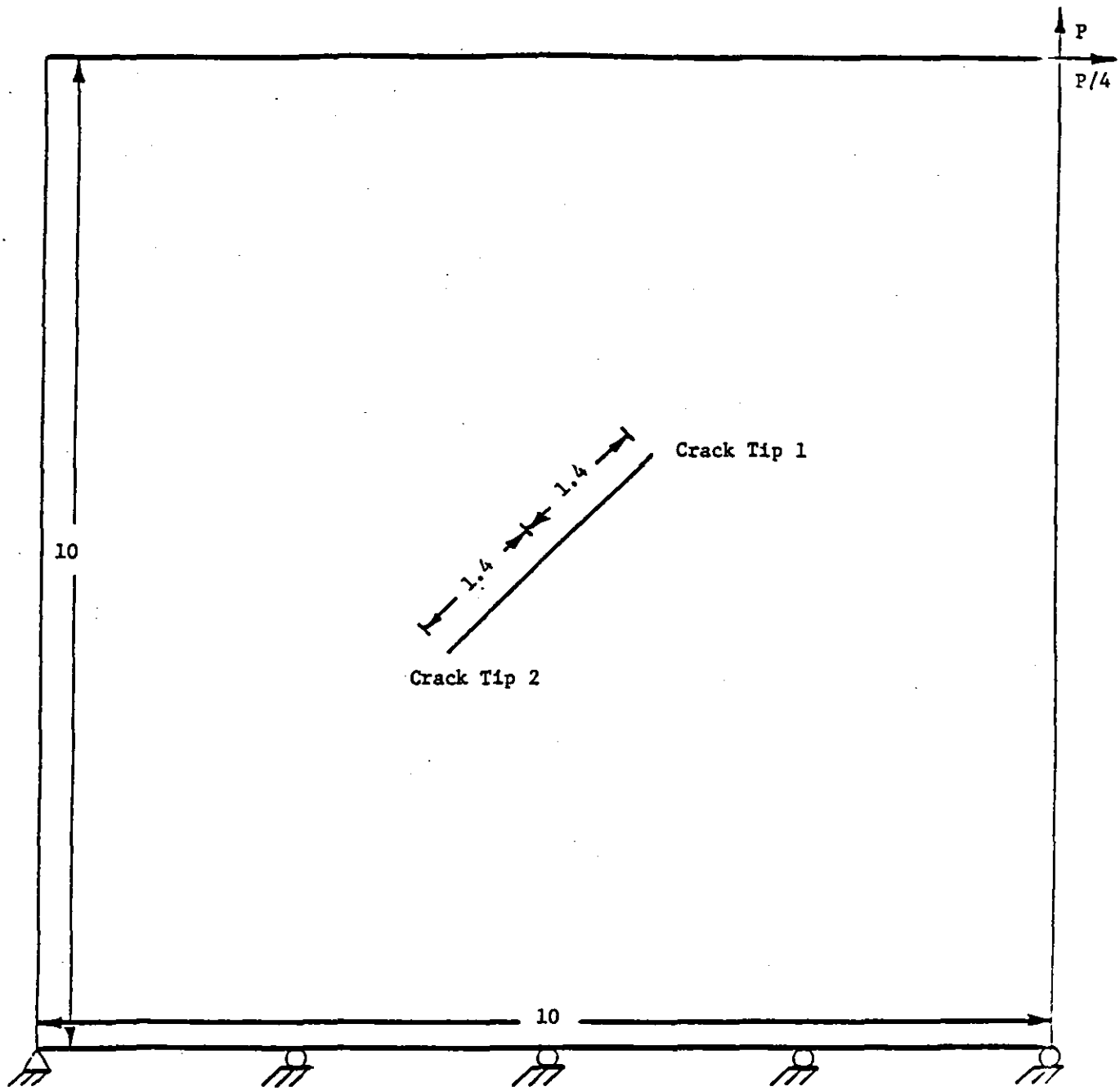

Figure III-C-7. Forty-Five Degree Slant Crack Problem (Young's Modulus, fracture toughness, thickness and yield stress equal to 1.0, Poissons Ratio equal to 0.3.)

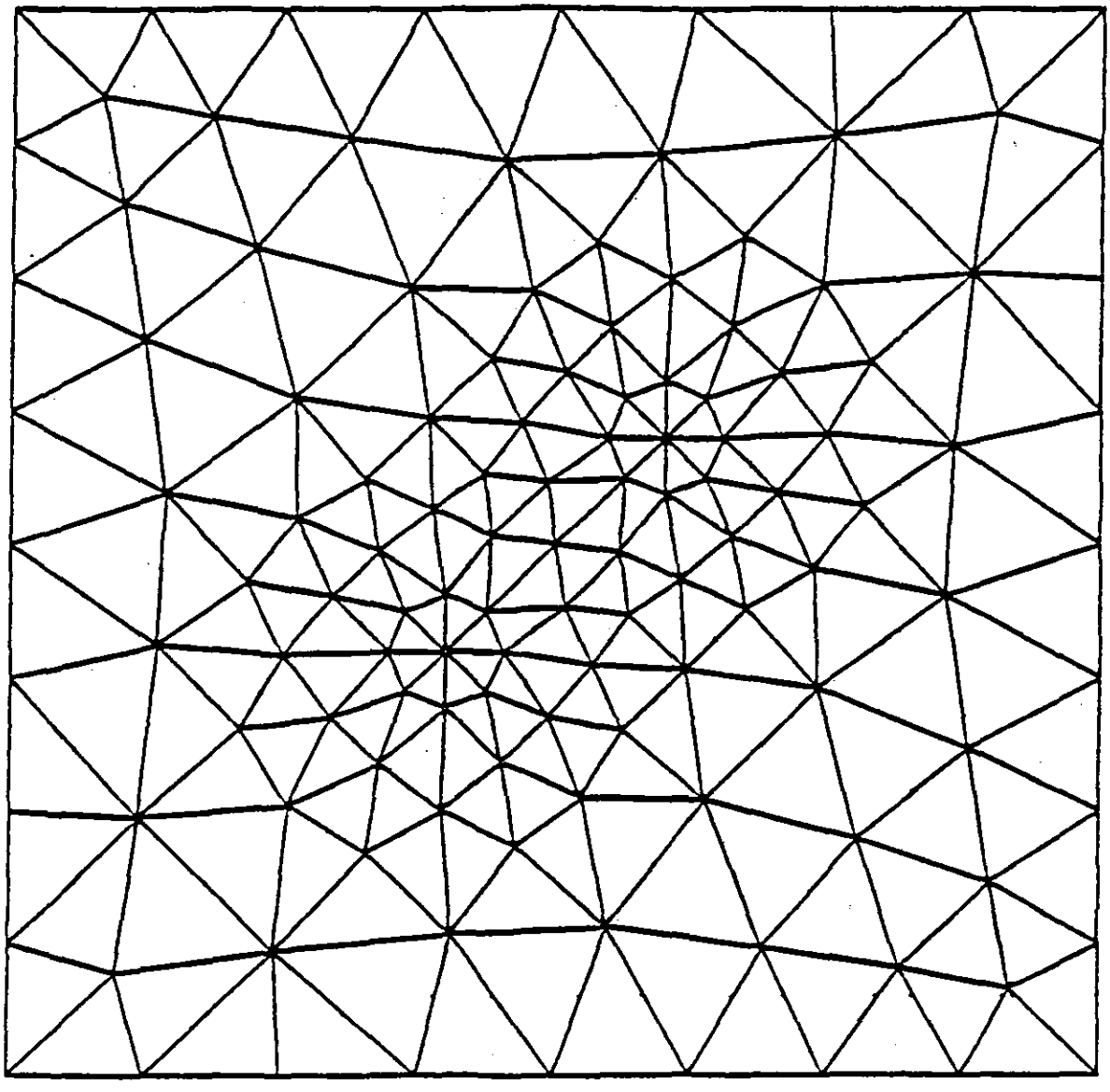

Figure III-C-8. Starting Mesh for the Slant Crack Problem

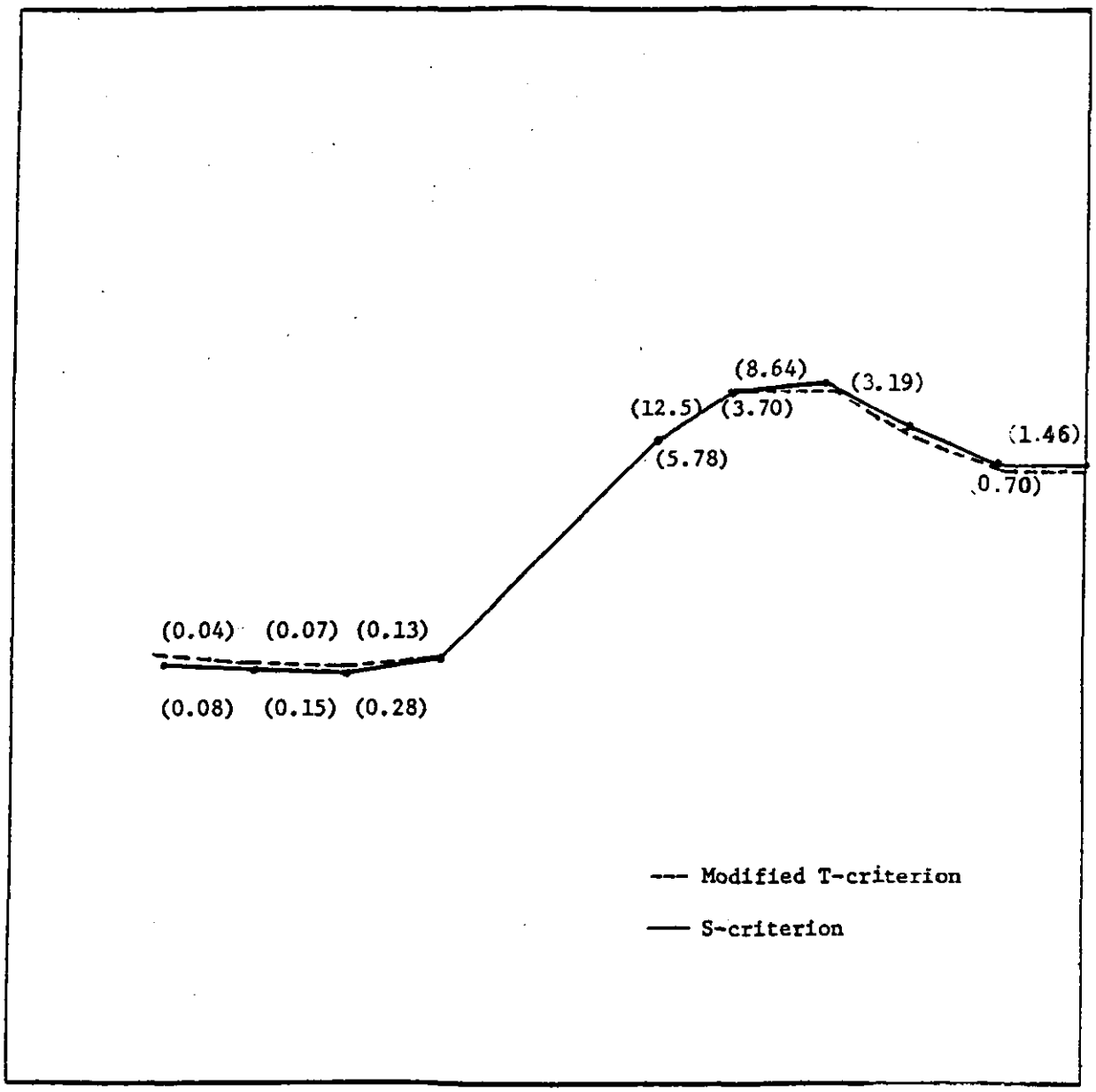

Figure III-C-9. Crack Propagation Path and Corresponding Fracture Load (P) Predictions

on the interior of a region require the creation of curves and boundaries, while cracks initiating at material interfaces require the division of existing curves. Similarly, propagation of cracks on the interior of a region require extending the curves representing the crack flanks, while propagation of cracks along material interfaces requires dividing the existing curves and merging a part of the divided curves with the curve that represents the crack flank.

The various modifications to the geometry data base can be broken down into the following basic operations:

1) create a curve,
2) create a boundary,
3) extend a curve,
4) divide a curve,
5) merge two curves and
6) merge two boundaries.

Figure III-C-6 illustrates how these operations are combined to handle the various situations that arise as cracks initiate and propagate. Creation of curves and boundaries are straightforward additions to the geometry data base. The other operations require more complex considerations, but are efficiently handled in the hierarchial geometry data structure and link lists used to store that information[6,9].

As a preliminary application of the developed system, the 45-degree slant crack problem shown in Figure III-C-7 has been considered. Figure III-C-8 shows the mesh automatically generated for this problem. The crack growth for this problem is unstable, as indicated by the negative load increments listed in Figure III-C-9, which are predicted as required for subsequent propagation using either the modified T-criterion[3]

or the S-criterion[2]. The upper crack tip is the first to propagate. It hits the exterior boundary, and further propagation is thus eliminated. The lower left crack tip then propagates until complete separation occurs. The mesh of the geometry of Figure III-C-9 is shown following crack propagation in Figure III-C-10 as established by the automatic mesh generator; note that the upper crack tip has been eliminated from the mesh.

As a second example, the plate with two holes, shown in Figure III-C-11, was considered. The starting mesh for this case is shown in Figure III-C-12. As indicated in this figure, one hole is under pressure and the other has a crack emanating from it. The crack begins to propagate when the pressure, p, equals 2.36. In this case, too, the crack is unstable, and the load levels required to cause the next two crack propagation increments are only 1.83 and 1.50, respectively. The crack geometry after four crack propagation increments is shown in Figure III-C-13, while the associated element mesh is shown in Figure III-C-14.

4. Plans for Upcoming Period

During the next reporting period, effort will concentrate on final debugging and testing of the fully automatic meshing algorithms integrated with the analysis procedures. In addition, attempts will be made to improve the criterion for treating cracks on material interfaces, and further micromechanics analyses will be carried out.

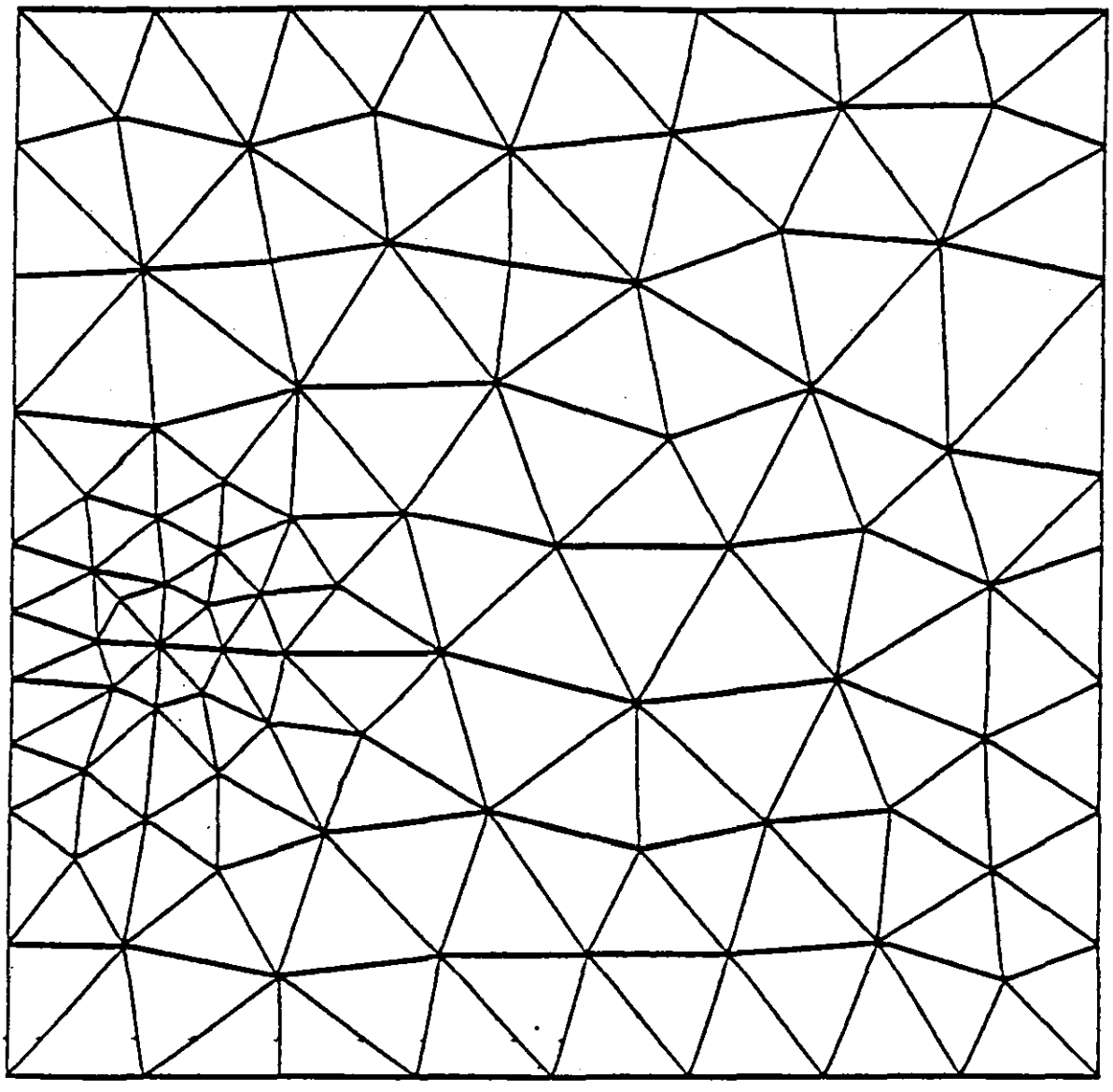

Figure III-C-10. The Automatically Generated Mesh for the Geometry of Figure III-C-9

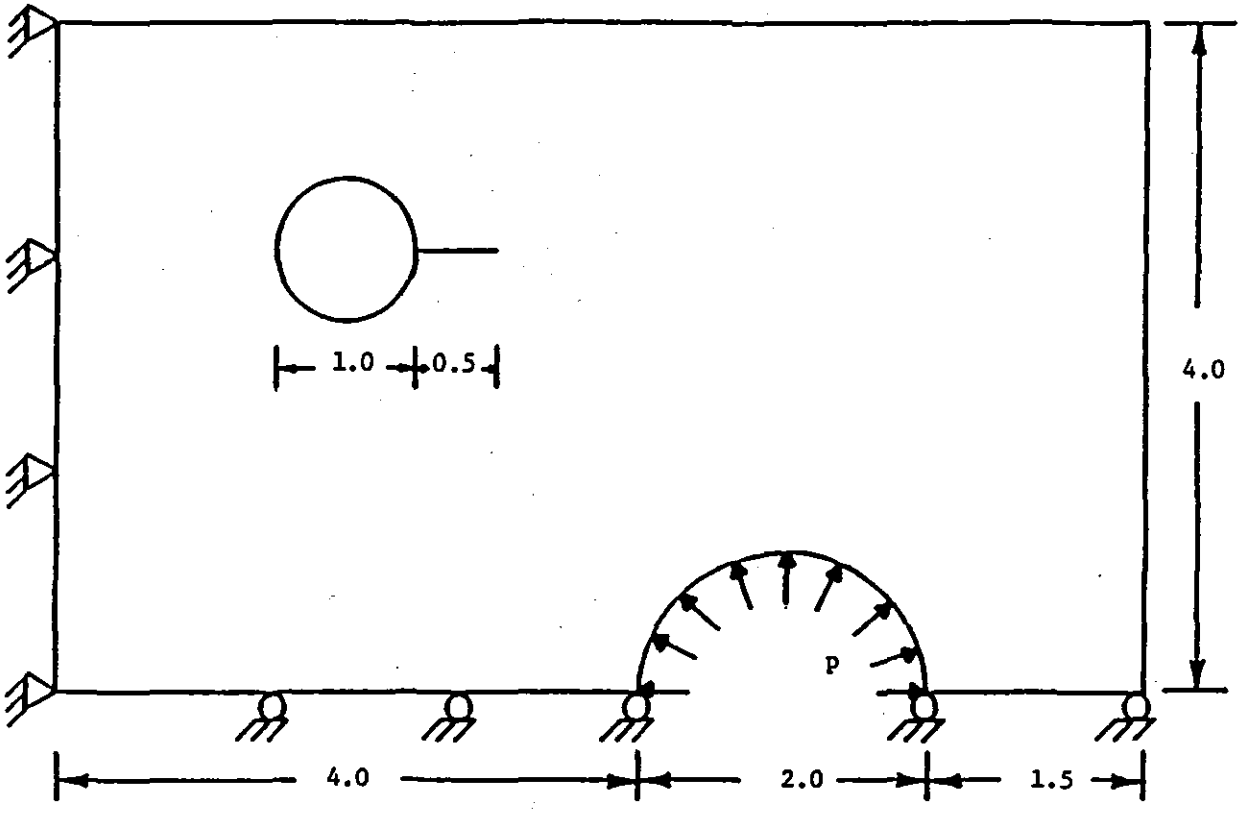

Figure III-C-11. Plate with Pressurized Hole (Youngs Modulus, fracture toughness, thickness and yield stress equal to 1.0, Poissons Ratio equal to 0.3.)

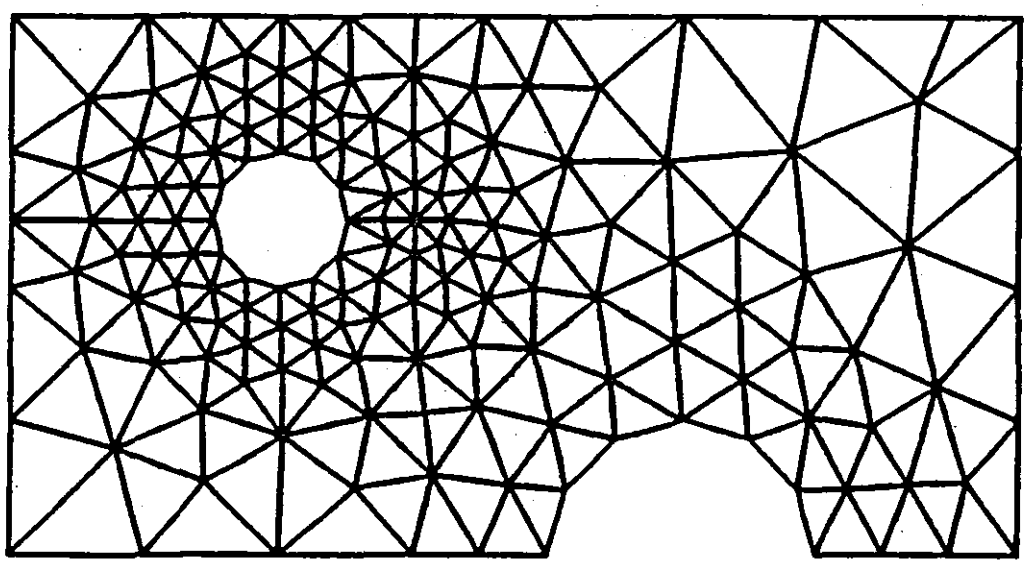

Figure III-C-12. Starting Mesh for Plate with Pressurized Hole

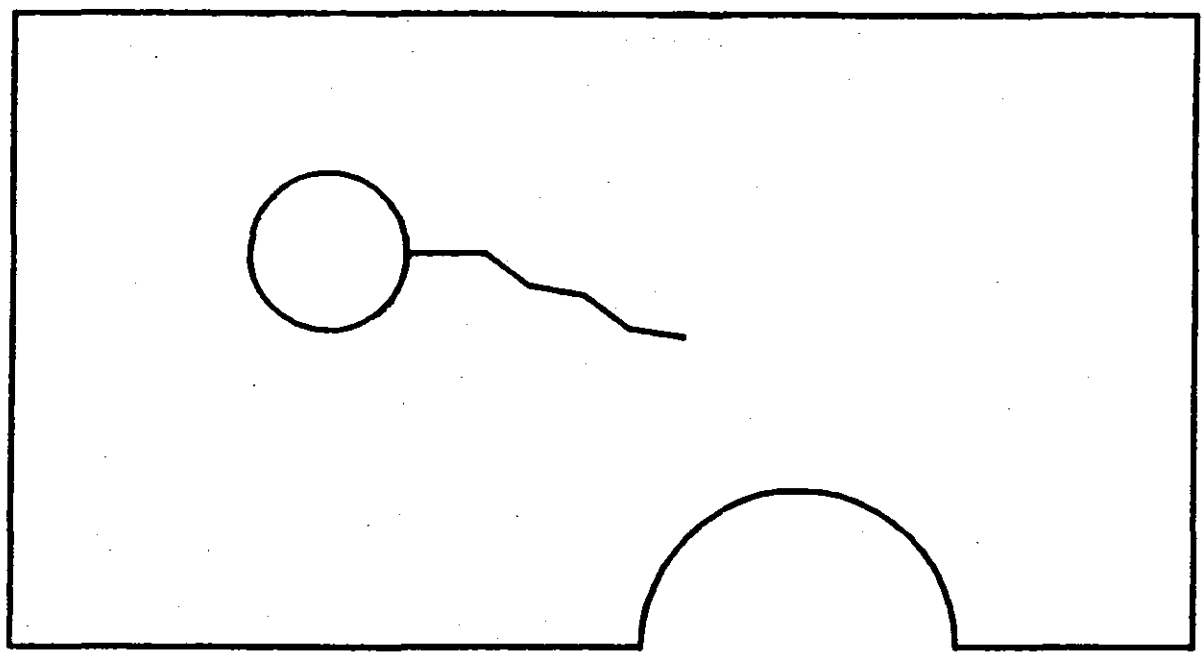

Figure III-C-13. Geometry for Plate with Pressurized Hole After Four Crack Propagation Increments

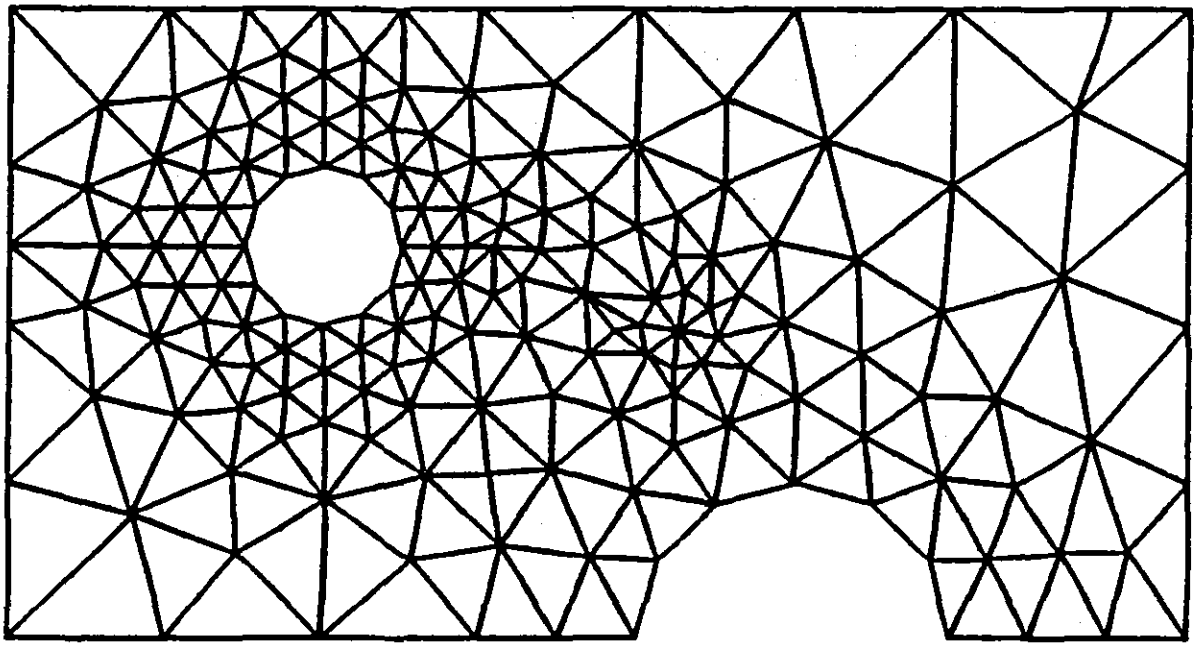

Figure III-C-14. Mesh for Plate with Pressurized Hole After Four Crack Propagation Increments

5. References

1. Theocaris, P. S., G. A. Kardomateas and N. P. Andrianepoulos, "Experimental Study of the T-criterion in Ductile Fractures", Eng. Fract. Mech., Vol. 17, No. 5, 1982, pp. 439-447.

2. Sih, G. C., "Strain-Energy Density Factor Applied to Mixed Mode Crack Problems", Int. J. Fracture, Vol. 20, No. 3, September 1974, pp. 305-321.

3. Yehia, N. A. B., "On the Use of the T-criterion in Fracture Mechanics", to appear Engrg. Fract. Mechanics.

4. Ingraffea, R. A. and C. Manu, "Stress-Intensity Factor Computation in Three Dimensions with Quarter-Point Element", Int. J. Num. Meth. Engrg., Vol. 15, 1980, pp. 1426-1445.

5. Saouma, V. E. and D. Schwemmer, "Numerical Evaluation of the Quarter-Point Crack Tip Element", Department of Civil Engineering, University of Pittsburgh, Pittsburgh, PA 15261, personal communication.

6. Yehia, N. A. B., "Automatic Tracking of Micromechanical Cracking Via Finite Elements", Ph.D. Thesis, Department of Civil Engineering, Rensselaer Polytechnic Institute, Troy, NY 12181, August 1984.

7. Yehia, N. A. B. and M. S. Shephard, "On the Effect of Quarter-Point Elements on Fracture Criteria", accepted for publication in Int. J. Num. Meth. Engrg.

8. Shephard, M. S., N. A. B. Yehia, G. S. Burd and T. J. Weidner, "Automatic Crack Propagation Tracking", Proceedings of Symposium on Advances and Trends in Structures and Dynamics, 1984, Arlington, VA and to appear in Computers and Structures.

9. Burd, G. S., "An Automatic Finite Element Mesh Generator and Adaptive Geometry Data Base for Tracking General Two-Dimensional Crack Growth", Masters Thesis, Department of Mechanical Engineering, Rensselaer Polytechnic Institute, Troy, NY 12181, 1984.

10. Yerry, M. A. and M. S. Shephard, "A Modified Quadtreee Approach to Finite Element Mesh Generation", IEEE Computer Graphics and Application, Vol. 3, No. 1, 1983, pp.39-46.

11. Shephard, M. S., C. N. Tonias and T. J. Weidner, "Attribute Specification for Finite Element Models", Computers and Graphics, Vol. 6, No. 2, 1982, pp. 83-91.

6. Current Publications or Presentations by Professor Shephard on this Subject

"Finite Element Modeling Developments at RPI"

Published in Proceedings of 3rd International Conf. on Computing in Civil Engineering, ASCE, 1984, pp. 203-212.

Presented at 3rd Intl. Conference on Computing in Civil Engrg., San Diego, CA, April 6, 1984.

"Nonlinear Finite Element Analysis of an ITR Flexure Under Limit Loading", with M. H. Ackroyd, R. G. Loewy and M. A. Yerry.

Published as RTC Report S-84-1, Rensselaer Polytechnic Institute, Troy, NY, 1984.

"Automatic Crack Propagation Tracking", with N. A. Yehia, G. S. Burd and T. J. Weidner.

To be published in Computers and Structures.

"On the Use of the T-Criterion in Fracture Mechanics", with N. A. Yehia.

To be published in Engrg. Fracture Mechanics.

"Combined Finite Element-Transfer Matrix Method Based on a Mixed Method", with E. E. Degen and R. G. Loewy.

To be published in Computers and Structures.

"Automatic Mesh Generation for Three-Dimensional Solids", with M. S. Yerry.

To be published in Computers and Structures.

III-D FREE-EDGE FAILURES OF COMPOSITE LAMINATES

Senior Investigator: T. L. Sham

1. Introduction

Analytical study on the free-edge delamination of graphite/epoxy laminates under static loading is being conducted. The objective of this research is to obtain fundamental understanding of the mechanics involved, from the continuum mechanics point of view, in the process of free-edge delamination of composite laminates. Such understanding could serve as a basis for control of and design against free-edge delamination.

2. Status

The initiation of delamination at free edges has been examined using the principles of continuum mechanics. The analyses are conducted by idealizing the material response of each ply in the laminate as homogeneous, linear elastic and anisotropic. A generalized plane strain elastic boundary value problem has been formulated to investigate the energy variation of such a body.

3. Progress During Report Period

Based on the boundary value problem formulated earlier and described in the December 1983 progress report, candidate global parameters that could serve to characterize the initiation of free-edge delamination have been investigated. A

generalized plane strain finite element program, having the capability of analyzing orthotropic layers and oriented at arbitrary angles with respect to the loading axis, has been developed. The finite element program will be used to assess the suitability of the candidate parameters (when used in conjunction with a critical-value type of criterion) for characterizing the initiation of free-edge delaminations. The capability of predicting the effects of stacking sequence, thickness effects, etc., on free-edge delamination will be the basis for assessing the suitability of these candidate characterizing parameters.

4. Plans for Upcoming Period

Finite element calculations, using the developed program, will be conducted as described in Section 3, above.

PART IV

GENERIC STRUCTURAL ELEMENTS

IV-A QUANTIFICATION OF SAINT-VENANT'S PRINCIPLE FOR A GENERAL PRISMATIC MEMBER

IV-B IMPROVED BEAM THEORY FOR ANISOTROPIC MATERIALS

IV-A QUANTIFICATION OF SAINT-VENANT'S PRINCIPLE FOR A GENERAL PRISMATIC MEMBER

Senior Investigator: D. B. Goetschel

1. Introduction

Saint-Venant's principle states that statically equivalent systems of load on a body will produce nearly identical stress fields in regions of the body which are remote from the loaded area. Recently, investigators[1-6]* have developed more precise, mathematical statements of this principle to the effect that the difference between the stress fields resulting from two statically equivalent load systems shows an exponential decay with distance from the loaded area. The rate of this decay may be calculated[5-13] and is of critical importance in determining the significance of edge effects in structural members.

Numerous investigators[14-16] have used finite element and finite difference techniques to examine edge and end effects for composite structural elements, but these have been standard static analyses for particular loadings or boundary conditions. Dong and Goetschel[7] have developed a semianalytic finite element method for finding the decay rates of edge effects in anisotropic layered plates. The purpose of the present work is to extend that method to the treatment of prismatic members of an arbitrary cross section composed of any number of anisotropic elements. This analysis may be

*Numbers in brackets in this section refer to the references which are listed on page 84.

used to find general solutions to end-effect problems for any loading.

In order to accomplish this, we use the method discussed in Reference [7] but perform a two-dimensional analysis rather than the one-dimensional analysis used there. We adopt the displacement components at the end of the prismatic member as the dependent variables. Two-dimensional finite element polynomial interpolation functions are used to model the behavior through the cross section of the member, and exponential behavior is assumed in the direction along the axis of the prismatic member. As in Reference [7], a second-order eigenvalue problem results in which the eigenvalues are the decay rates and the eigenvectors are the nodal displacements. Each eigensolution represents one possible mode of deformation corresponding to a specific self-equilibrating load system which must be determined from the displacement field.

If we use N degrees of freedom (d.o.f.) in the finite element scheme, then we have an N x N system of equations with N eigensolutions. Having found a number of such solutions, we may perform a modal superposition analysis to construct approximate solutions corresponding to any self-equilibrating load system. This is analogous to the modal superposition analyses used in structural dynamics problems, whereas, the methods in References [14-16] are analogous in the same way to time-step analyses.

2. Status

Previous to this reporting period, the method described had been developed, the governing equations formulated and the Finite Element Method computer program written and used to find decay rates for several different geometries.

As we discussed in some detail in the previous report, we choose to formulate the governing equations by assuming a displacement field of the form

$$u_i(x,y,z) = P_i \exp(-\gamma x) \tag{1}$$

where

u_1, u_2 and u_3 are the x, y and z components of the displacement vector at the point (x,y,z),

P_i are polynomial interpolation functions in the cross section and

γ is the characteristic decay rate.

When these displacement functions are substituted into the stress equations of equilibrium

$$T_{ji,j} + f_i = 0 \tag{2}$$

where

T_{ji} and f_i are the components of the stress tensor and the body force vector, respectively, a repeated index implies summation over 1, 2 and 3, and a comma followed by an index denotes partial differentiation with respect to the corresponding coordinate.

Finite element discretization leads to a system of equations of the form

$$[K]\{U\} = \{F\} \tag{3}$$

where, if we use N degrees of freedom,

[K] is the N x N stiffness matrix and

{U} and {F} are N-element column vectors representing the displacement d.o.f and the corresponding force d.o.f., respectively.

The stiffness matrix arises from integration of the surface tractions over the end and sides of each element and of the body force over the volume of each element. It is therefore natural to express the stiffness matrix as

$$[K] = [K_e] + [K_s] + [K_v] \tag{4}$$

where

e, s and v denote end, side and volume.

Since we will only be considering problems in which there is no body force in the interior of the elements and there are no tractions on the sides, we may write Equation (3) as two equations:

$$[K_e]\{U\} = \{F\} \tag{5}$$

$$([K_s] + [K_v])\{U\} = \{0\} \tag{6}$$

If we expand Equation (6) and gather like powers of γ, we obtain an equation of the form

$$(\gamma^2[K_2] + \gamma[K_1] + [K_0])\{U\} = \{0\} \tag{7}$$

which is the second-order eigenproblem we must solve. Since the matrices $[K_2]$ and $[K_0]$ are symmetric and $[K_1]$ is antisymmetric, the eigenvalues, γ, and the eigenvectors, {U}, are in

general complex. Note that, from Equation (1), if γ is real and positive or complex with positive real part then the solution decays with distance from the end, whereas, if γ has negative real part the solution grows exponentially with distance from the end. Since we require bounded solutions in the semi-infinite prismatic member, solutions with $Re\gamma < 0$ are not of interest. If γ and $\{U\}$ are complex, then the complex conjugates γ^* and $\{U\}^*$ also provide a solution and both must be included in order that the displacement field in the member be real.

Decay rates were calculated for isotropic and homogeneous graphite-epoxy composite plates and the results compared with exact solutions[5] which exist for these cases. Agreement was found to be excellent. Decay rates have also been calculated for isotropic and composite-laminate I-beams, box-beams and rectangular-beams, and for a skin-stringer arrangement. As one would expect, end effects in thin-walled, open cross sections decay much more slowly than those in solid cross sections; for example, the slowest decay rates (smallest $Re\gamma$'s, corresponding to the most troublesome end effects) were up to thirteen times slower for isotropic I-beams than for isotropic rectangular beams. It was also found that anisotropy can lower the decay rate by a factor of three or four for identical cross sections.

3. Progress During Report Period

Since the computer program has been developed and debugged by the start of this reporting period, recent effort has been directed towards extending the postprocessing capabilities of the program to calculate the displacement and stress fields in the prismatic member from the nodal displacement vectors (eigenvectors) and decay rates (eigenvalues) and to perform modal superposition analyses to construct solutions to problems with specific applied forcing functions using the calculated eigensolutions.

The displacement fields corresponding to the decay rates with positive real part have been determined for a homogeneous graphite/epoxy plate two units thick. Four elements were used, with three nodes per side in the vertical (z) direction and two nodes per side in the horizontal (y) direction, as shown in Figure IV-A-1. Although the geometry shown appears to be that of a beam, in this case the plane strain behavior of a plate has been enforced by requiring the y-displacements of the nodes to be zero and the x and z displacements for nodes with the same y-coordinate to be the same. Thus, for eighteen nodes we have 18 d.o.f., and we can determine eighteen different modes of deformation. The deformed shapes have been plotted and are shown in Figure IV-A-2 for the lowest several decay rates. Note that the displacement fields are either symmetric or antisymmetric in z and that as $Re\gamma$ increases the deformation becomes increasingly complicated.

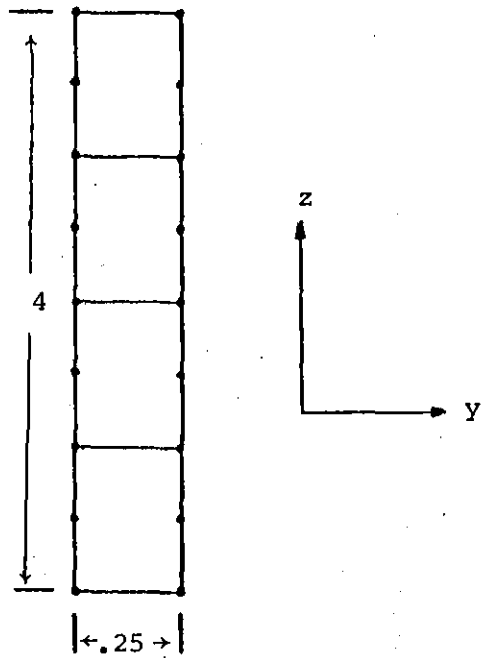

Figure IV-A-1. Geometry for Homogeneous Graphite/Epoxy Plate

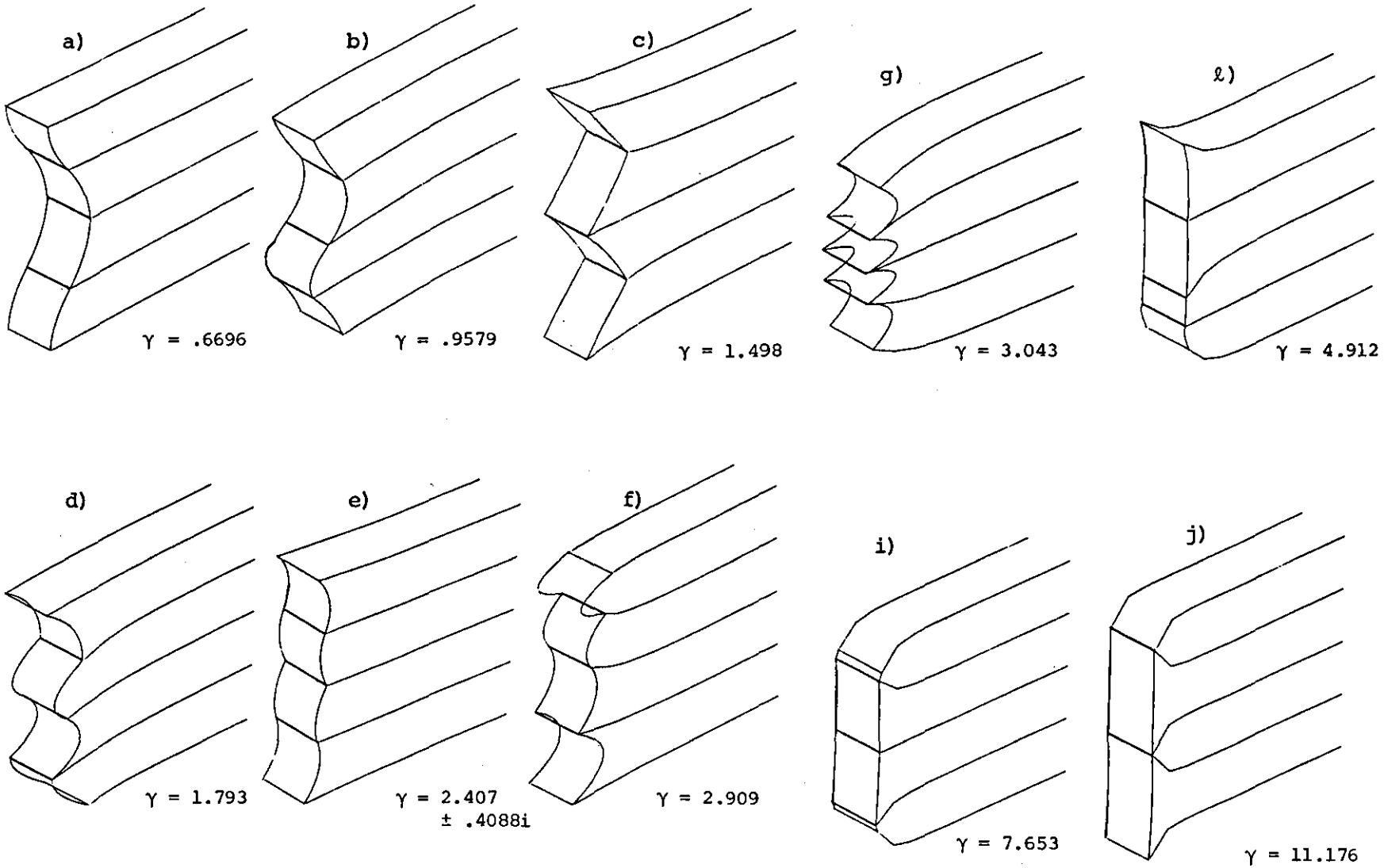

Figure IV-A-2. Deformed Shapes of Graphite/Epoxy Plate for Several Decay Rates

Since γ is small for the first few modes and the displacement is predominantly in the x-direction, it is difficult to see the decay of the deformation with x. However, it is clearly visible for the higher modes.

By using the same geometry shown in Figure IV-A-1 but allowing all the modes to move freely in any direction, we have the behavior of a rectangular beam two units high by one-half unit thick. In this case the eighteen nodes give us fifty-four different modes of deformation. The corresponding deformed shapes of the member have been plotted and are shown in Figure IV-A-3 for the lowest several decay rates. Note that, included in the possible modes of deformation for the beam are those for the plate which are shown in Figure IV-A-2. However, the geometry of the beam also permits displacement in the y-direction; note, for example, the bending behavior shown in Figure IV-A-3c.

We have performed modal superposition analyses for specific displacement boundary conditions in the following manner. Suppose we have an end condition of the displacement field

$$u_i(0,y,z) = u_i^{(bc)}(y,z) \tag{8}$$

We must first evaluate $u_i^{(bc)}$ at the coordinates of each node in order to construct a nodal boundary condition vector $\{U^{bc}\}$, and then superpose an appropriate number of the eigensolutions to form an approximation to $\{U^{bc}\}$. In general we need not consider all possible modes of deformation (i.e., all N eigensolutions), since the highest-order modes (largest γ's)

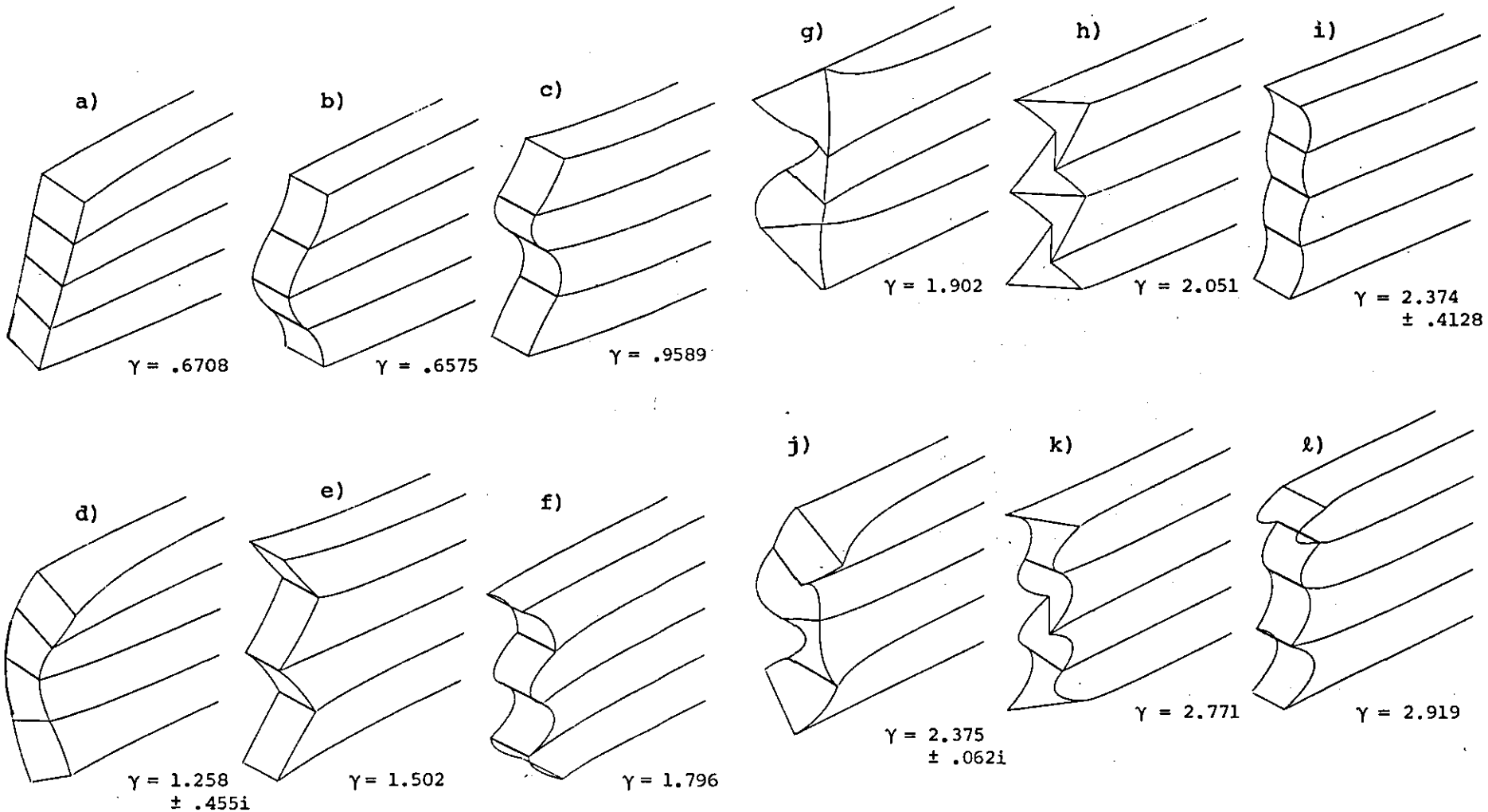

Figure IV-A-3. Deformed Shapes of Graphite/Epoxy Beam for Several Decay Rates

do not contribute significantly to the solution for most end conditions of practical interest; however, determining what number of modes is "appropriate" in a given situation must be based to some extent on experience, which is scarce at this time. Thus, if we choose n eigensolutions, we can superpose them as follows:

$$\{U^{bc}\} = [\{U^{(1)}\}|\{U^{(2)}\}|\ldots|\{U^{(n)}\}]\{a\} \tag{9}$$

where $\{U^{(i)}\}$ are the nodal displacement vectors of the i-th eigensolution, here constituting the columns of a rectangular matrix, and $\{a\}$ is a column vector of undetermined amplitude coefficients. $\{U^{bc}\}$ is a column vector of dimension N (where N is the number of d.o.f. at one station, x = 0), $[\{U^{(i)}\}]$ is a matrix of dimension N x n, and $\{a\}$ is a column vector of dimension n, so that Equation (9) cannot be solved exactly for $\{a\}$ unless N = n; however, in accordance with the discussion above, this is rarely necessary. We can obtain a best R.M.S. fit[17] by operating on both sides of Equation (9) with

$$[\{U^{(1)}\}\{U^{(2)}\}\ldots\{U^{(n)}\}]^T \equiv [B]^T \tag{10}$$

where superscript T denotes the transpose. Then we have

$$\{B^T U^{bc}\} = [B^T B]\{a\} \tag{11}$$

which may readily be solved for $\{a\}$.

Such a modal superposition has been performed for two different boundary conditions for the T-section shown in Figure IV-A-4a. There are twenty nodes in the isotropic,

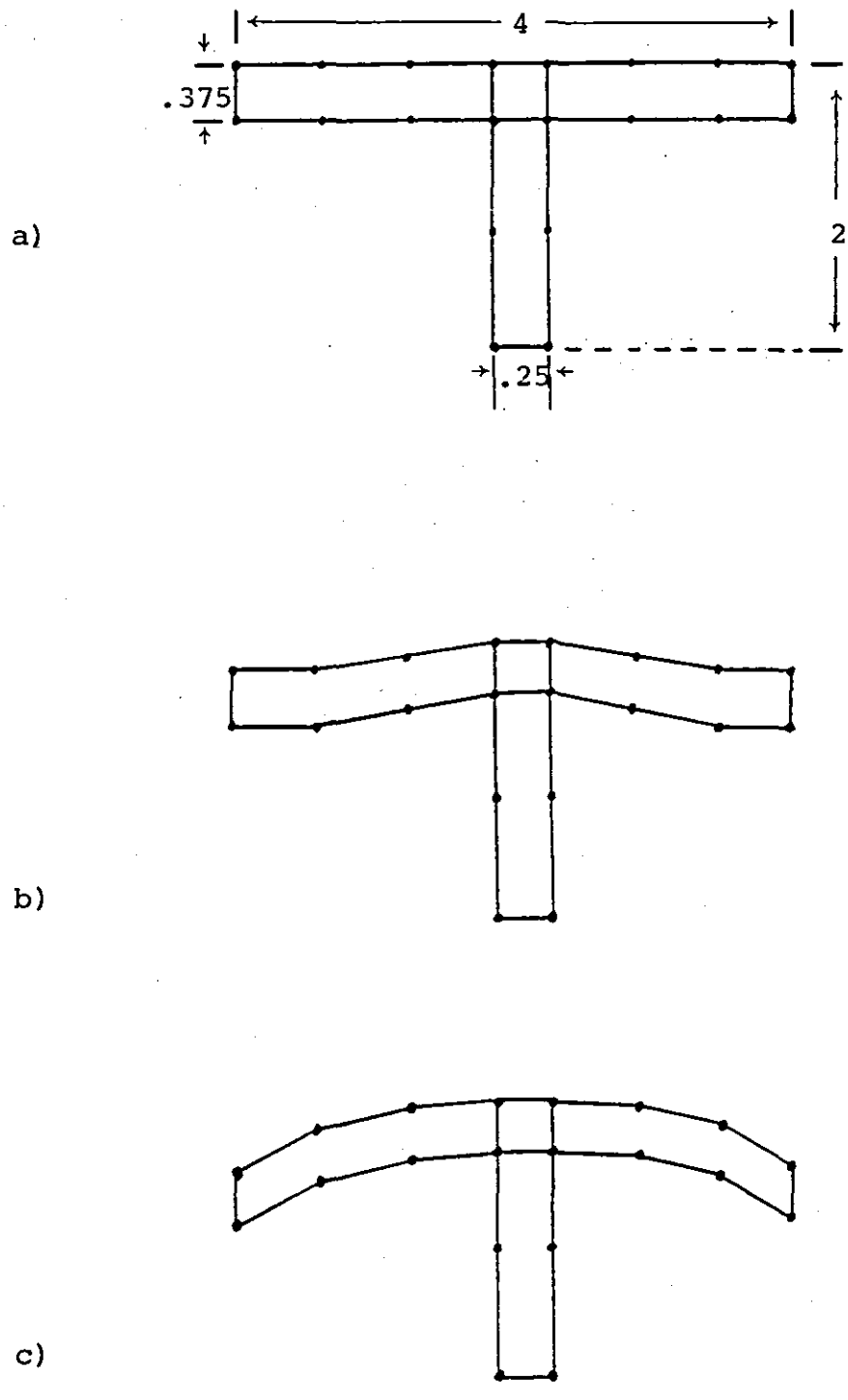

Figure IV-A-4. Geometry and Boundary Conditions for T-Section Used for Modal Superposition

four-element member, and the bottom two nodes are fixed, so that this situation could be thought of as representing the symmetric modes of deformation in an I-beam, as well. There are 54 degrees-of-freedom. Figures IV-A-4b and 4c show the displacement boundary conditions imposed in two cases. In both cases, the u_1-displacement (the x-direction) is zero. In Figure IV-A-4b, the flange has been deformed to follow a parabolic curve, and the web has been compressed slightly. This is a somewhat simpler situation than that shown in Figure IV-A-4c, in which the edges of the flange have been clamped to form a compound bend, so we would expect to see higher-order (larger γ) modes play a more important role for 4c than 4b.

Some of the modes of deformation we have used in the modal superposition analysis are shown in Figures IV-A-5 and 6. Note that since both deformations are symmetric about the plane $y = 0$, the modes shown in Figure IV-A-6, which are antisymmetric about this plane, should not contribute to the solutions. In Table IV-A-1 we list the superposition coefficients [the a's in Eq. (11)] calculated for the modal superposition for the simpler boundary condition in Figure IV-A-4b using - successively - nineteen modes, thirteen modes, nine modes and three modes. Note that the first important mode is the fourth. The results of these superpositions plotted along with the applied boundary condition are shown in Figure IV-A-7. It can be seen that with three modes the agreement

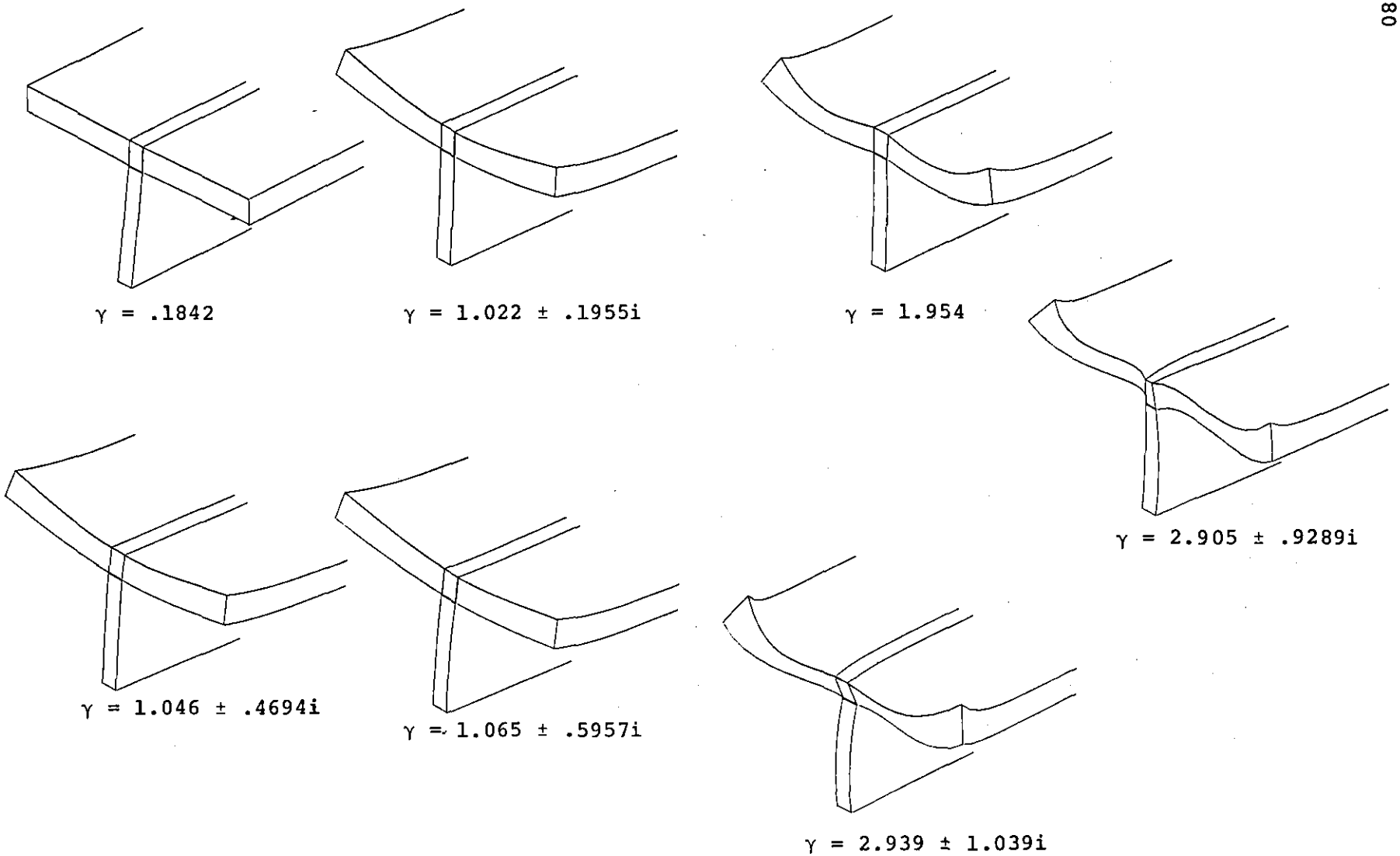

Figure IV-A-5. Some of the Symmetric Modes Used in the Modal Superposition Analysis of the T-Section Beam

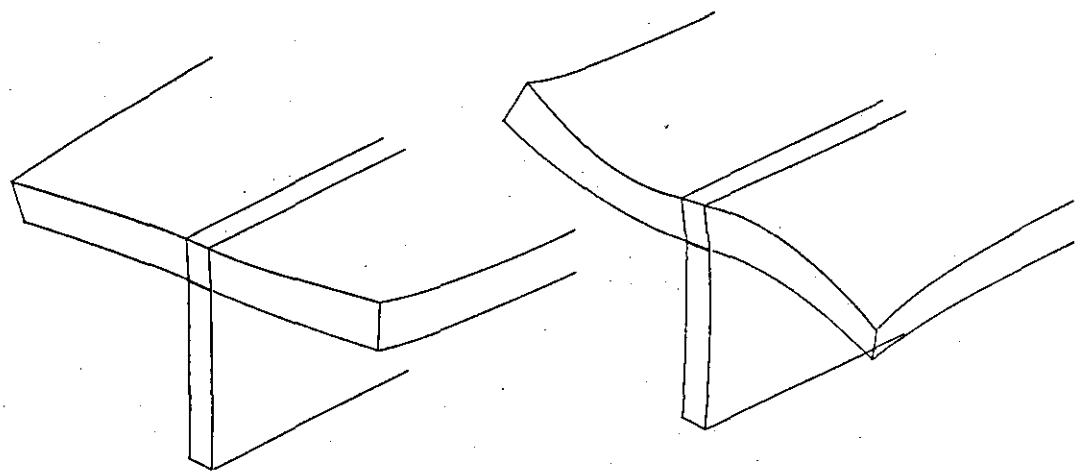

$\gamma = .9466$ $\gamma = 1.440$

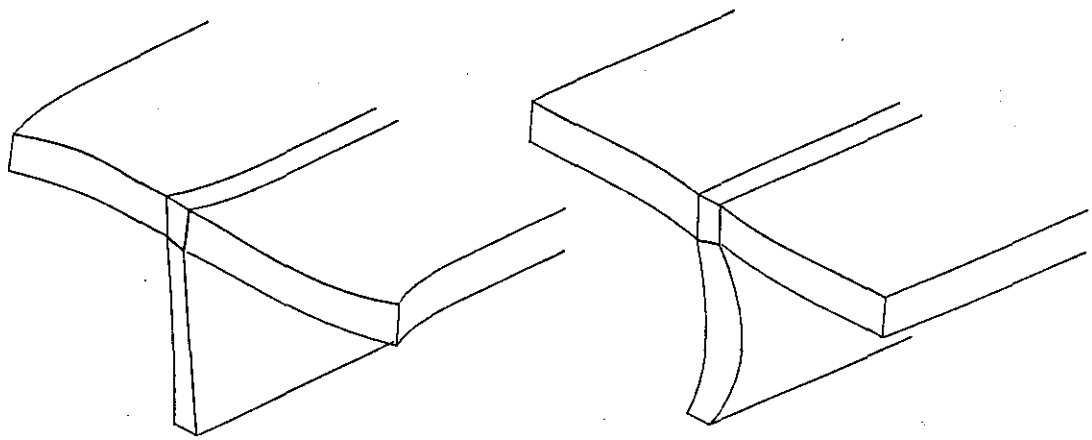

$\gamma = 1.896 \pm .7713i$ $\gamma = 2.964 \pm 2.276i$

Figure IV-A-6. Some of the Antisymmetric Modes Used in the Modal Superposition Analysis of the T-Section Beam

TABLE IV-A-1

AMPLITUDE COEFFICIENTS FOR MODAL SUPERPOSITION USING THE END CONDITION IN FIGURE IV-A-5b

No.	γ	19 Modes	13 Modes	9 Modes	3 Modes
1.	.18421	-.00593	-.00104	-.000397	.0224
2.	.5850	------	------	------	------
3.	.9466	------	------	------	------
4.	1.0215 + .1955i	-1.0989 - 1.0501i	-1.0557 - .9981i	-1.008 - 1.211i	
5.	1.0215 - .1955i	-1.0989 + 1.0501i	-1.0557 + .9981i	-1.008 + 1.211i	
6.	1.0461 + .4694i	.3046 - 1.1625i	.2596 - 1.0591i	.2937 - 1.112i	
7.	1.0461 - .4694i	.3046 + 1.1625i	.2596 + 1.0591i	.2937 + 1.112i	
8.	1.0649 + .5957i	.2613 + .3724i	.2258 + .3222i	.1872 + .3274i	
9.	1.0649 - .5957i	.2613 - .3724i	.2258 - .3222i	.1872 - .3274i	
10.	1.4398	------	------	------	
11.	1.8960 - .7713i	------	------	------	
12.	1.8960 + .7713i	------	------		
13.	1.9539	-.003848	.2711		
14.	2.9046 - .9289i	.0735 - .0103i	------		
15.	2.9046 + .9289i	.0735 + .0103i	------		
16.	2.9389 - 1.039i	-.00401 + .0798i			
17.	2.9389 + 1.039i	-.00401 - .0798i			
18.	2.9640 + 2.276i	------			
19.	2.9640 - 2.276i	------			

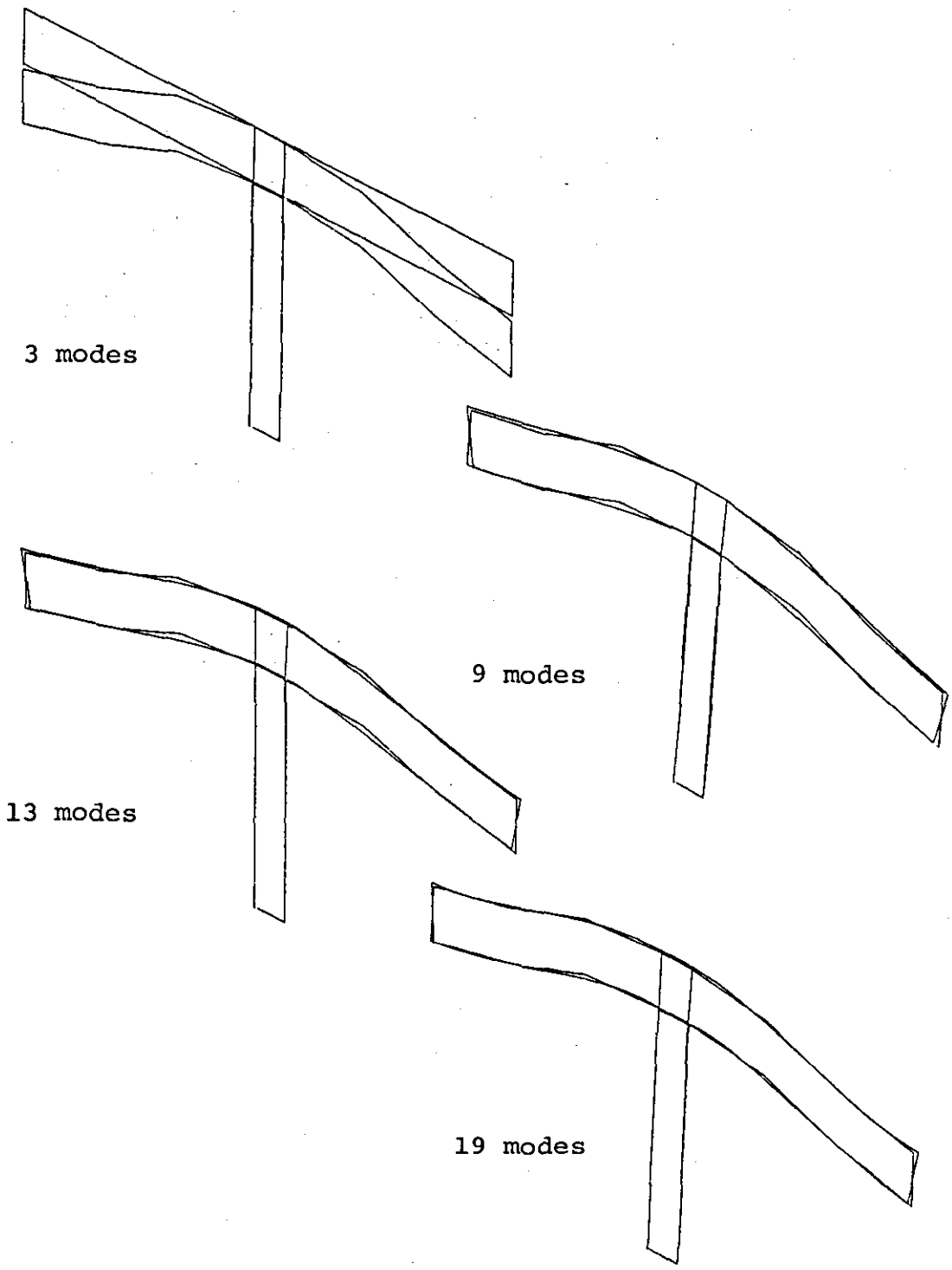

Figure IV-A-7. Results of Modal Superposition for the Boundary Condition in Figure IV-A-4b.

is poor and with nine modes the agreement is substantially improved. With both thirteen and nineteen modes the agreement is excellent, and the two are virtually indistinguishable. This is because the thirteenth mode is the last important one; the amplitudes for the fourteenth through seventeenth modes are several orders of magnitude smaller than the thirteenth. Thus, in this case, the "appropriate number" of modes we spoke of above is thirteen.

In Table IV-A-2 are listed the amplitudes for the more complicated boundary condition of Figure IV-A-4c. Since the boundary conditions are not drastically different from one another, this table shows the same trends as Table IV-A-1, but it can be seen that the higher-order modes play a somewhat more significant role in this case. In Figure IV-A-8 are shown the results of these superpositions along with the applied boundary condition. The same remarks made about Figure IV-A-7 apply as well to Figure IV-A-8.

4. Plans for Upcoming Period

The program will be extended so that traction boundary conditions may be specified for modal superposition, as well as the displacement boundary conditions considered here.

5. References

1. Toupin, R. A., "Saint-Venant's Principle", Archive for Rational Mechanics and Analysis, Vol. 18, 1965, pp. 83-96.

TABLE IV-A-2

AMPLITUDE COEFFICIENTS FOR MODAL SUPERPOSITION USING THE END CONDITION IN FIGURE IV-A-5c

No.	γ	19 Modes	13 Modes	9 Modes	3 Modes
1.	.18421	.001875	-.001214	.00174	.0302
2.	.5850	------	------	------	------
3.	.9466	------	------	------	------
4.	1.0215 + .1955i	-1.032 - .7451i	-1.114 - .8058i	-.8919 - 1.787i	
5.	1.0215 - .1955i	-1.032 + .7451i	-1.114 + .8058i	-.8919 + 1.787i	
6.	1.0461 + .4694i	-.2498 - 1.327i	-.1342 - 1.335i	.0233 - 1.580i	
7.	1.0461 - .4694i	-.2498 + 1.327i	-.1342 + 1.335i	.0233 + 1.580i	
8.	1.0649 + .5957i	.4865 + 1.892i	.4575 + .2282i	.2789 + .2521i	
9.	1.0649 - .5957i	.4865 - 1.892i	.4575 - .2282i	.2789 - .2521i	
10.	1.4398	------	------	------	
11.	1.8960 - .7713i	------	------	------	
12.	1.8960 + .7713i	------	------		
13.	1.9539	1.494	1.2520		
14.	2.9046 - .9289i	-.00094 + .0449i	------		
15.	2.9046 + .9289i	-.00094 - .0449i	------		
16.	2.9389 - 1.039i	-.0526 - .0539i			
17.	2.9389 + 1.039i	-.0526 + .0539i			
18.	2.9640 + 2.276i	------			
19.	2.9640 - 2.276i	------			

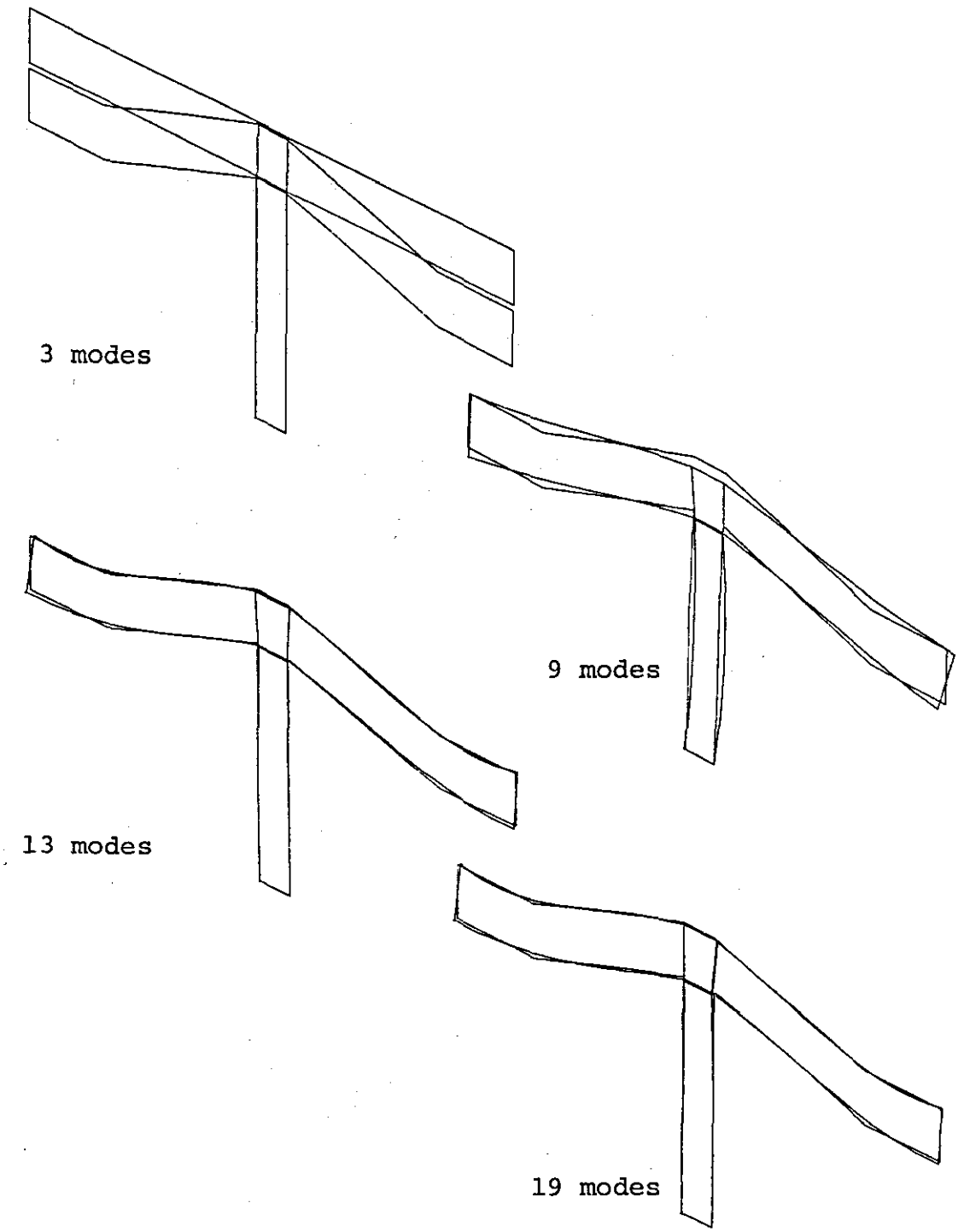

Figure IV-A-8. Results of Modal Superposition for the Boundary Condition in Figure IV-A-4c

2. Knowles, J. K., "On Saint-Venant's Principle in the Two-Dimensional Linear Theory of Elasticity", Archive for Rational Mechanics and Analysis, Vol. 21, 1966, pp. 1-22.

3. Horgan, C. O., "On Saint-Venant's Principle in Plane Anisotropic Elasticity", Journal of Elasticity, Vol. 2, 1972, pp. 169-180.

4. Horgan, C. O., "Some Remarks on Saint-Venant's Principle for Transversely Isotropic Composites, Journal of Elasticity, Vol. 2, 1972, pp. 335-339.

5. Choi, I. and C. O. Horgan, "Saint-Venant's Principle and End Effects in Anisotropic Elasticity", ASME Journal of Applied Mechanics, Vol. 44, No. 3, 1977, pp. 424-430.

6. Choi, I. and C. O. Horgan, "Saint-Venant's End Effects for Plane Deformation of Sandwich Strips", International Journal of Solids and Structures, Vol. 14, No. 3, 1978, pp. 187-195.

7. Dong, S. B. and D. B. Goetschel, "Edge Effects in Laminated Composite Plates", ASME Journal of Applied Mechanics, Vol. 49, March 1982, pp. 129-135.

8. Klemm, J. L. and R. W. Little, "The Semi-Infinite Elastic Cylinder Under Self-Equilibrated End Loading", SIAM J. of Applied Mathematics, Vol. 19, 1970, pp. 241-255.

9. Power, L. D. and S. B. Childs, "Axisymmetric Stresses and Displacements in a Finite Circular Bar", International J. of Engineering Science, Vol. 9, 1971, pp. 241-255.

10. Duncan Fama, M. E., "Radial Eigenfunctions for the Elastic Circular Cylinder", Quarterly Journal of Mechanics and Applied Mathematics, Vol. 25, 1972, pp. 479-495.

11. Mitra, D. N., "On Axisymmetric Deformations of a Transversely Isotropic Elastic Cylinder of Finite Length", Archiwum Mechaniki Stodowanej, Vol. 17, 1965, pp. 739-747.

12. Warren, W. E., A. L. Roark and W. B. Bickford, "End Effect in Semi-Infinite Transversely Isotropic Cylinders", AIAA Journal, Vol. 5, 1967, pp. 1448-1455.

13. Horgan, C. O., "The Axisymmetric End Problem for Transversely Isotropic Circular Cylinders", International J. of Solids and Structures, Vol. 10, 1974, pp. 837-852.

14. Spilker, R. L. and S. C. Chou, "Edge Effects in Symmetric Composite Laminates: Importance of Satisfying the Traction-Free-Edge Condition", Journal of Composite Materials, Vol. 14, 1980, pp. 2-20.

15. Altus, E., A. Rotem and M. Shmueli, "Free Edge Effect in Angle Ply Laminates - A New Three-Dimensional Finite Difference Solution", Journal of Composite Materials, Vol. 14, 1980, pp. 21-30.

16. Sandorff, P. E., "Saint-Venant's Effects in an Orthotropic Beam", Journal of Composite Materials, Vol. 14, July 1980, pp. 199-212.

17. Lancaster, P., "Theory of Matrices", Academic Press, New York, 1969, p. 303.

IV-B IMPROVED BEAM THEORY FOR ANISOTROPIC MATERIALS

Senior Investigator: O. Bauchau

1. Introduction

Timoshenko beam theory is widely used by structural designers as a first approximation in numerous structural applications. For solid cross-sectional beams made out of isotropic material, this theory gives accurate predictions for aspect ratios $L/h \gtrsim 5$ (L is the span of the beam and h its height). Because it is based on the assumption that cross sections remain plane after deformation, the theory predicts a linear distribution of axial strains. However, additional axial strains are induced by warping incompatibilities generated either by specific loading or boundary conditions, or by the occurrence of nonuniform torsion or bending. According to Saint-Venant's Principle these additional strains tend to decay away from the perturbation that created them. The decay length, δ, is defined as the distance it takes for these strains to decay to a negligible value. For solid cross-sectional beams made out of isotropic materials, this decay length is of the order of the height of the beam, i.e., $\delta \simeq h$. A physical meaning of the validity range of the theory is found by rewriting it as $L/\delta \gtrsim 5$, stating that the span of the beam must be large compared to the perturbed zone, δ.

In the case of thin-walled box beams, it was recognized early that beam theory provides only a poor representation because warping and shear lag effects are significant for those structures. More recently, with the increasing use of composite materials, Saint-Venant's principle has been investigated theoretically for anisotropic elasticity[1,2]*. The decay length, δ, was found to be proportional to $\sqrt{E/G}$ (E is the longitudinal Young's modulus, and G is the shear modulus). This means that for highly anisotropic materials the decay length can be much larger than for isotropic materials. Goetschel[3] calculated these decay lengths for different beam configurations made of unidirectional graphite/epoxy. For a thin-walled rectangular cross section, δ was found to be 7h, and for an I cross section, δ = 15h. Beam theory can still be applied if $L/\delta \gtrsim 5$, i.e. $L/h \gtrsim 35$ and 75, respectively. Needless to say, however, such a restriction makes beam theory inapplicable to a great many practical structures.

The purpose of this work is to investigate a more appropriate representation of the behavior of beams made of anisotropic material.

2. Status

This work was initiated at the beginning of the reporting period, and concentrated on the analysis of thin-walled, closed cross-sectional beams made of anisotropic material.

---

*Numbers in brackets in this section refer to the references which are listed on page 99.

The analysis is based on the sole assumption that each cross section is infinitely rigid in its own plane, but free to warp out-of-plane. This assumption has two important implications: 1) The in-plane displacements of the cross section are fully represented by three rigid body modes, respectively, i.e. two translations and the rotation of the section. 2) Any applied transverse load only induces membrane stresses in the structure, specifically an axial stress flow, n, and a shear stress flow, q. For thin-walled beams, these two stress flows are uniform across the thickness and the other stress components are assumed negligible.

Based on these assumptions, a set of orthonormal eigenwarping functions can be derived from the principle of minimum potential energy. The solution of the problem can then be obtained by expanding the axial displacement or axial stress distributions as a series of these eigenwarpings.

3. Progress During Report Period

During the report period two tasks were completed:

1) Closed form solutions of the problem have been derived using two alternative approaches. In the first approach (the "Improved Bernoulli"), the axial displacements are expanded as a series of eigenwarpings, and the principle of minimum potential energy is used to derive the governing equations. This solution is an assumed displacement approach and yields a lower bound of the strain energy. In the second approach (the "Improved St.-Venant"), the axial stresses are

expanded as a series of eigenwarpings and the Reissener energy principle is used to find the solution. Since an equilibrating stress field is assumed, the solution yields an upper bound of the strain energy.

2) A finite element solution was also derived using the same displacement field as in the "Improved Bernoulli" approach. The 4-segment beam model has the following degrees of freedom at each node; 3 displacements, 3 rotations and 1 degree of freedom per eigenwarping to be considered.

A specific example will be described here to illustrate these different approaches. Figure IV-B-1 depicts the thin-walled, rectangular cross-sectional beam to be analyzed, and Figure IV-B-2 shows the few first eigenwarpings for this section. The transverse displacement, v, of the beam under a uniform transverse load, p_o, and the twist, θ, under a uniform torque, m_o, have been calculated using the different approaches. Values of the tip deflection, $\frac{v_{tip}}{p_o L^4}$, and the tip twist, $\frac{\theta tip}{m_o L^4}$, listed in Table IV-B-1, call for the following remarks:

-warping effects can be very significant, specially in the torsional analysis;

-all methods have an excellent convergence rate; An accurate solution in bending can be obtained with 2 eigenwarpings in the Bernoulli approach and only 1 eigenwarping in the St.-Venant approach. In torsion, convergence requires 3 and 2 eigenwarpings, respectively.

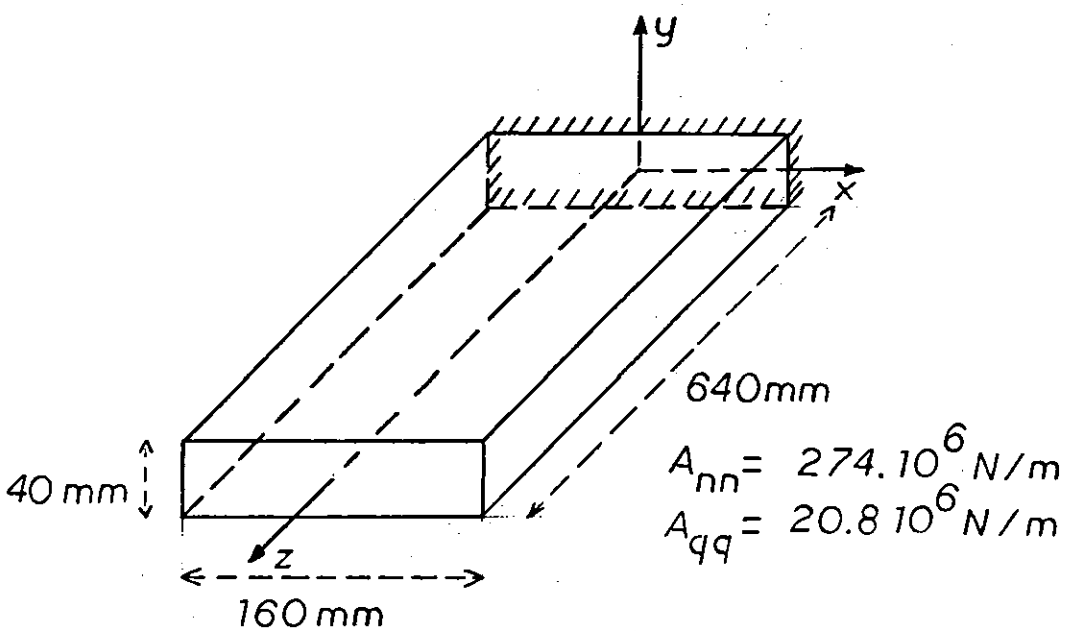

Figure IV-B-1. The Thin-Walled, Rectangular Cross-Sectional Beam Analyzed in the Numerical Example

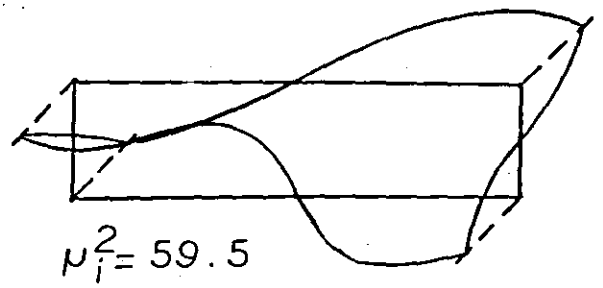

$\mu_i^2 = 59.5$

$U_i = 0.\quad V_i = 0.\quad \Theta_i = 3.86\ 10^{-2}$

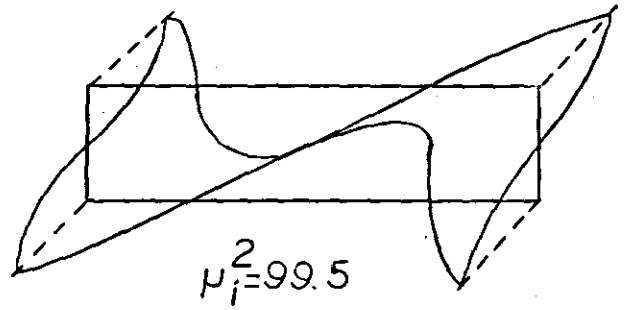

$\mu_i^2 = 99.5$

$U_i = 0.\quad V_i = 7.03\ 10^{-3}\quad \Theta_i = 0.$

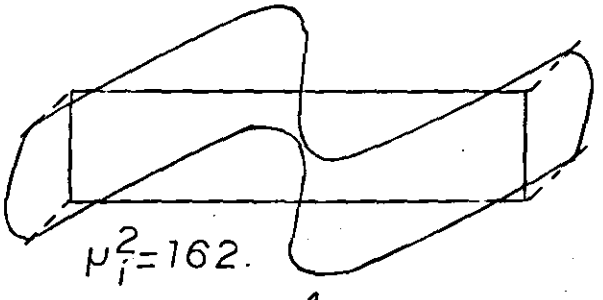

$\mu_i^2 = 162.$

$U_i = 9.25\ 10^{-4} V_i = 0.\quad \Theta_i = 0.$

Figure IV-B-2. A Few Eigenwarpings of the Rectangular Section

TABLE IV-B-1

NUMERICAL RESULTS FOR THE DIFFERENT APPROACHES

	Tip Deflection = $\frac{v_{tip}}{P_o L^4}[10^{-6}m]$			Tip Twist = $\frac{\theta_{tip}}{m_o L^4}[10^{-6}m]$		
	Bernoulli	St.-Venant	F.E.M.	Bernoulli	St.-Venant	F.E.M.
Basic Solution	4.024	4.860	4.02	91.7	143.3	91.7
1st Term	0.446	-0.160	NA	20.7	-9.9	NA
2nd Term	0.104	-0.018	NA	10.1	-2.1	NA
3rd Term	0.028	-0.003	NA	3.6	-0.5	NA
4th Term	0.002	-0.000	NA	0.7	-0.1	NA
TOTAL	4.604	4.667	4.597	126.7	130.8	126.3

-as expected, the Bernoulli solution and the finite element approach give similar results, since they are based on the same assumed displacement field.

Figure IV-B-3 shows the distribution of axial stress, $\frac{n}{p_o L^2}$, and shear stress, $\frac{q}{p_o L^2}$, in the upper face of the beam under a uniform loading, p_o. Instead of the uniform axial stress distribution predicted by the basic theory, a large shear lag effect is observed. Figure IV-B-4 depicts the stress distribution when the loading is a uniformly distributed torque, m_o. Here the uniform shear stress distribution predicted by the basic theory is significantly altered and large axial stresses are generated near the corners of the section.

4. Plans for Upcoming Period

The main task to be completed in the upcoming period is an experimental verification of the improved beam theory presented here. Test specimens will be made of two rectangular graphite/epoxy facings joined by two aluminum channels to fabricate a box beam. Displacements and strains will be monitored during a standard static test. A comparison with calculated values should provide insights into the accuracy and limitations of the different methods.

Specimens presenting bending-twisting coupling terms will be tested, too, to assess the influence of these couplings on the behavior of the beam. The analytical model will be updated to allow these coupling effects to be accounted for.

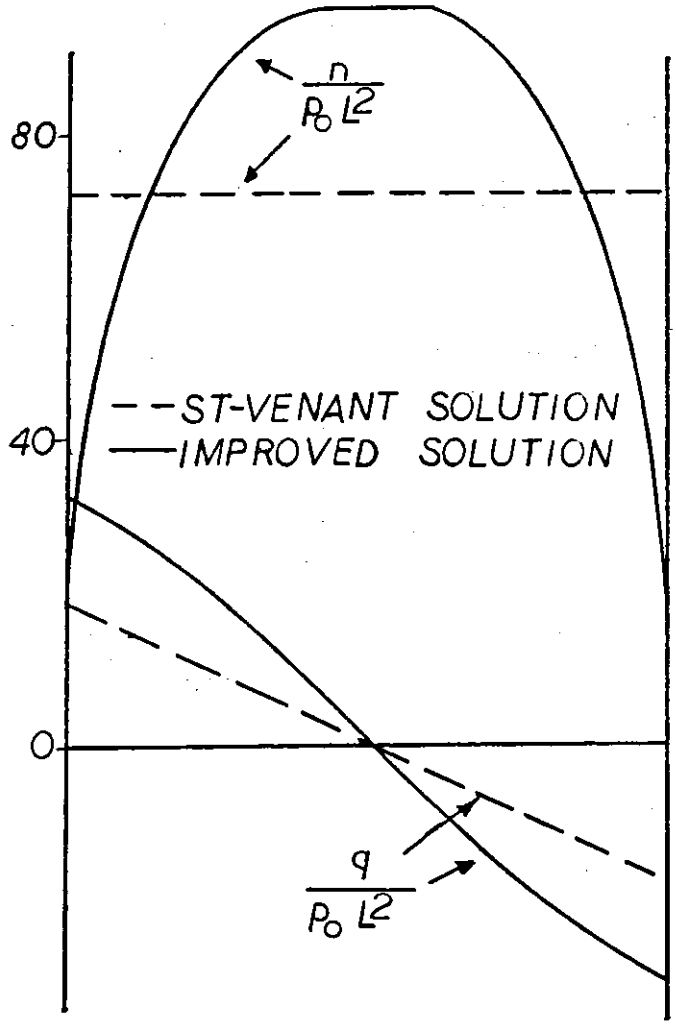

Figure IV-B-3. Stress Distributions in the Upper Skin of the Beam (Root Section) Under Uniform Transverse Load p_o

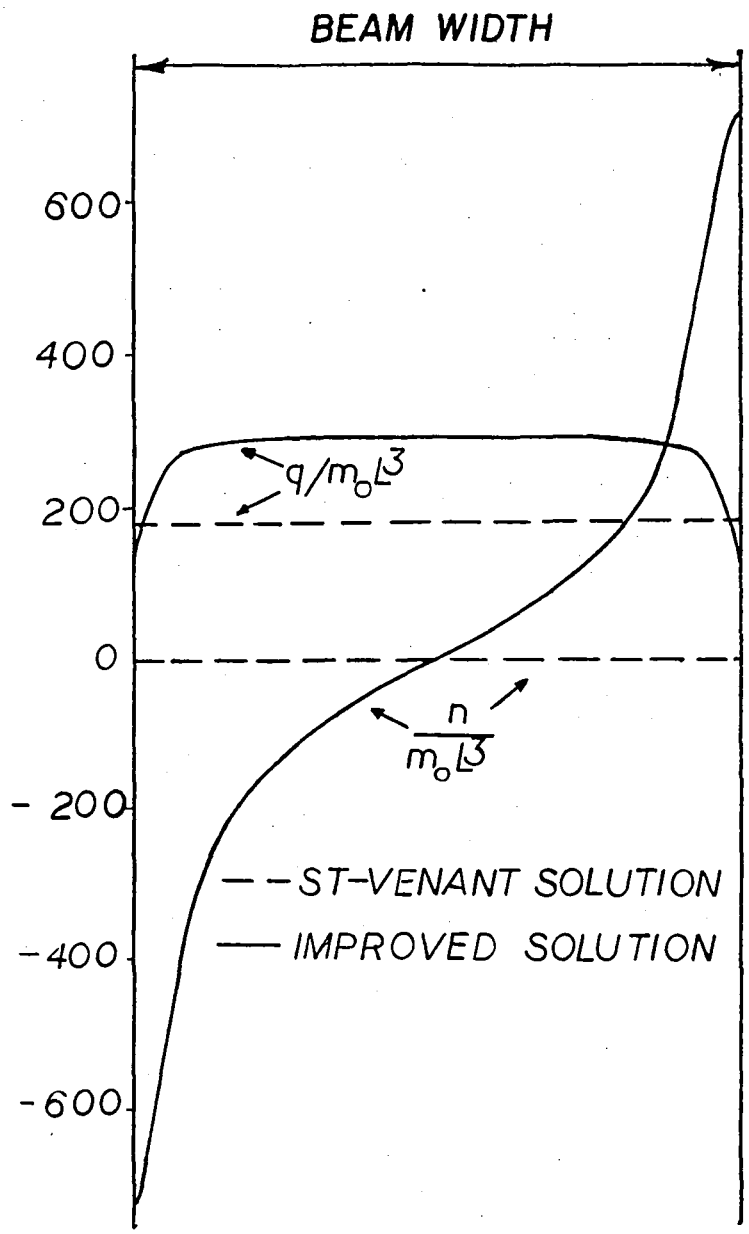

Figure IV-B-4. Stress Distributions in the Upper Skin of the Beam (Root Section) Under Uniform torque m_o

5. References

1. Horgan, C. O., "On St.-Venant's Principle in Plane Anisotropic Elasticity", J. of Elasticity, Vol. 2, 1972, pp. 169-180.

2. Choi, I. and C. O. Horgan, "St.-Venant's Principle and End Effects in Anisotropic Elasticity", J. Appl. Mech., Vol. 44, No. 3, 1977, pp. 424-430.

3. Goetschel, D. B. and T. H. Hu, "Quantification of St.-Venant's Principle for a General Prismatic Member", to appear in J. Appl. Mech.

6. Current Publications or Presentations by Professor Bauchau on this Subject

"A Beam Theory for Anisotropic Materials"

To be published in the Journal of Applied Mechanics.

PART V

PROCESSING SCIENCE AND TECHNOLOGY

V-A VARIATION OF RESIN PROPERTIES THROUGH THE THICKNESS OF CURED SAMPLES

V-B ACCURATE MEASUREMENT OF HEAT CAPACITY BY DIFFERENTIAL SCANNING CALORIMETRY

V-C INITIAL SAILPLANE PROJECT: THE RP-1

V-D SECOND SAILPLANE PROJECT: THE RP-2

V-A VARIATION OF RESIN PROPERTIES THROUGH THE THICKNESS OF CURED SAMPLES

Senior Investigator: B. Wunderlich

1. Introduction

a. Resin Systems and Reactions

A commonly used aerospace epoxy matrix is N,N,N',N'-tetraglycidyl-4,4'-diaminodiphenylmethane (TGDDM). This is also called N,N,N',N'-tetraglycidyl-4,4'-methylenebisbenzeneamine. It is cured with 4,4'-diaminodiphenylsulphone (DDS). TGDDM, an amorphous, tetrafunctional epoxide monomer, is liquid at room temperature, whereas, DDS has a melting temperature of 178°C[1]*. The structures of both components are given in Table V-A-1.

Narmco 5208, Fiberite 934 and Hercules 3501-6 are commercially available TGDDM/DDS resin systems, available as prepregs, with the latter two also containing a boron trifluoride-ethylamine catalyst[2,3]. Commercial TGDDM is sold as Araldite MY-720. The major impurity found in MY-720 is the trifunctional (instead of the tetrafunctional) epoxide monomer[4]. The reported formulation for Fiberite 934 is 64 percent by weight TGDDM (MY-720), 25 percent DDS (Eporal, Ciba-Geigy), 11 percent diglycidyl orthophthalate epoxide (DGOP) (GLY-Cel-A-100, Celanese) and 0.4 percent boron trifluoride/ethylamine (Harshaw)[5]. Ciba-Geigy recommends a formulation of 69.4 percent-by-weight MY 720 to 30.6 percent DDS[6].

*Numbers in brackets in this section refer to the references which are listed on page 125.

TABLE V-A-1

CHEMICAL FORMULAE

N,N,N',N'-Tetraglycidyl-4,4'-Diaminodiphenyl Methane (TGDDM)

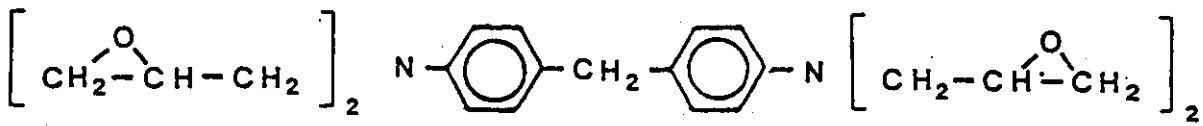

4,4'-Diaminodiphenylsulphone (DDS)

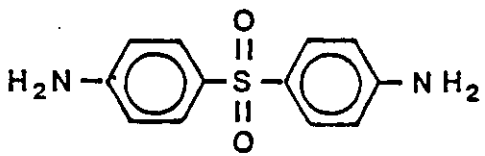

Curing of TGDDM/DDS systems involves two types of cross-linking reactions: epoxide-epoxide and epoxide-amine. Though an amine hardener (DDS) is present, epoxide groups will react with each other[4,7]. The epoxide-epoxide reaction is probably similar to the polymerization of polyethylene oxide. In the presence of small amounts of water, epoxides will hydrolyze to glycols. Other active-hydrogen compounds, such as amines, will react similarly[8,9]. Both acid and base catalyzed reactions are listed in Tables V-A-2 and 3. The epoxide-amine reaction is given in Table V-A-4[14].

b. Mobility in the Epoxy Matrices

It is believed that the epoxy cross-linked networks form into a more or less heterogeneous structure. That is, particles of high cross-link density form and grow in the matrix of uncross-linked or sparsely cross-linked material. As the cross-linking reaction advances, these gel particles become interconnected into a global network, but the intrinsic heterogeneity may remain. Further, the gradual decrease in mobility of reacting molecules causes the network built at the end of the reaction to be considered lower in cross-link density than that which was formed initially.

The two different cross-link densities should have two glass transition temperatures.

Using differential scanning calorimetry (DSC), measurements of heat capacity can be made to provide a basis for study of the glass transition region. Such heat capacity

TABLE V-A-2

REACTION EQUATIONS FOR THE POLYMERIZATION WITH ACID

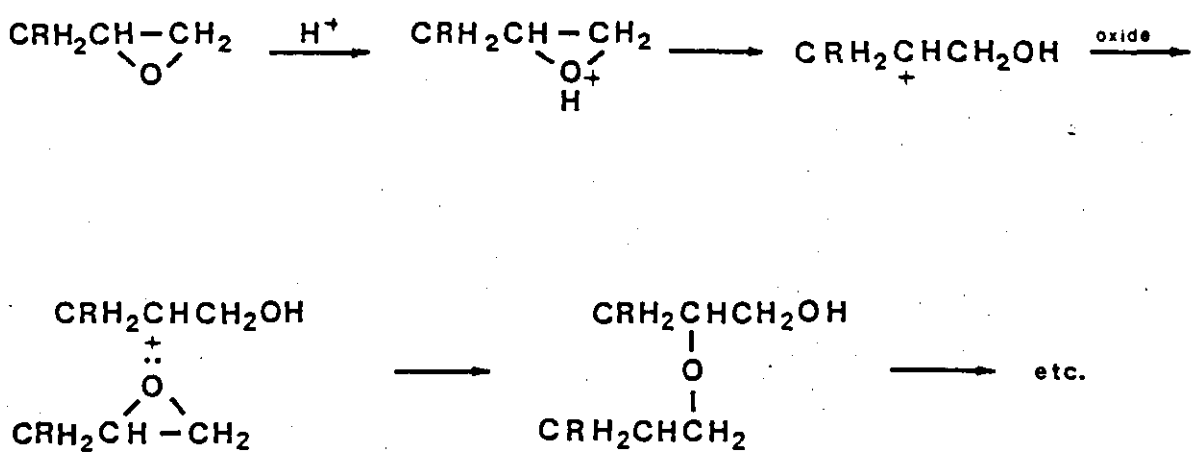

TABLE V-A-3

REACTION EQUATIONS FOR THE POLYMERIZATION WITH BASE

Initiation

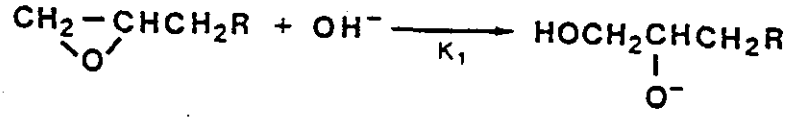

Propagation

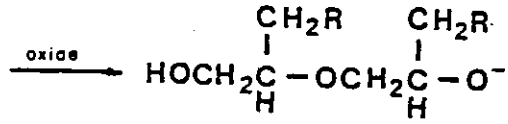

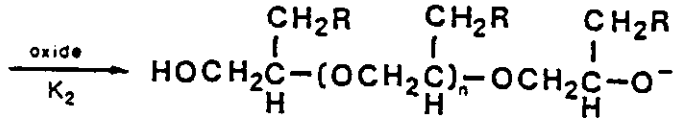

Termination

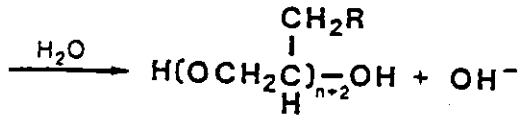

TABLE V-A-4

CURE REACTION WITH DIAMINE

Mechanism

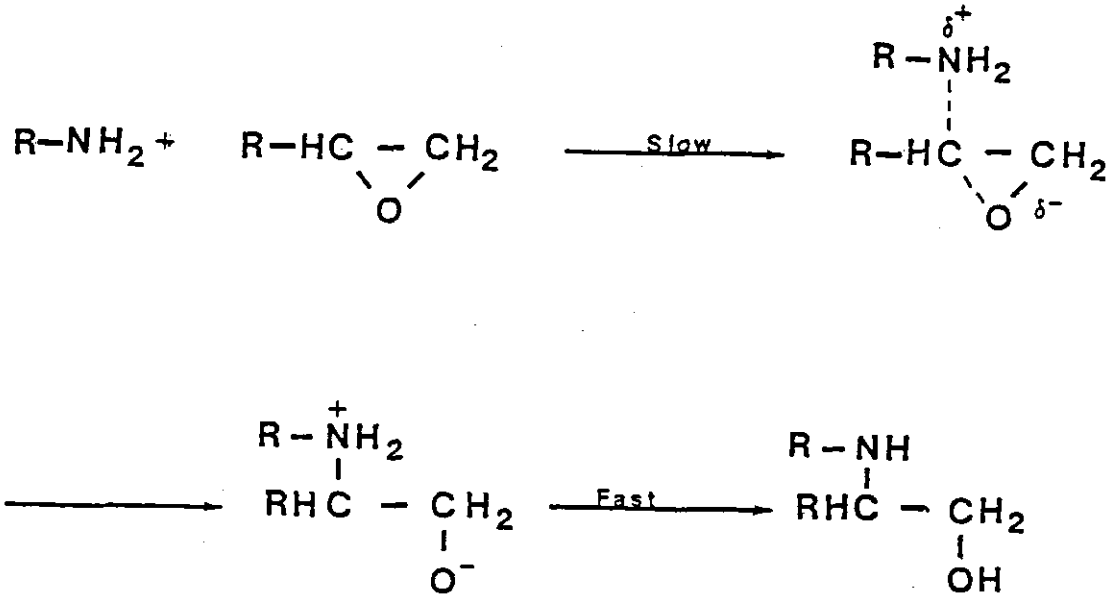

Reaction

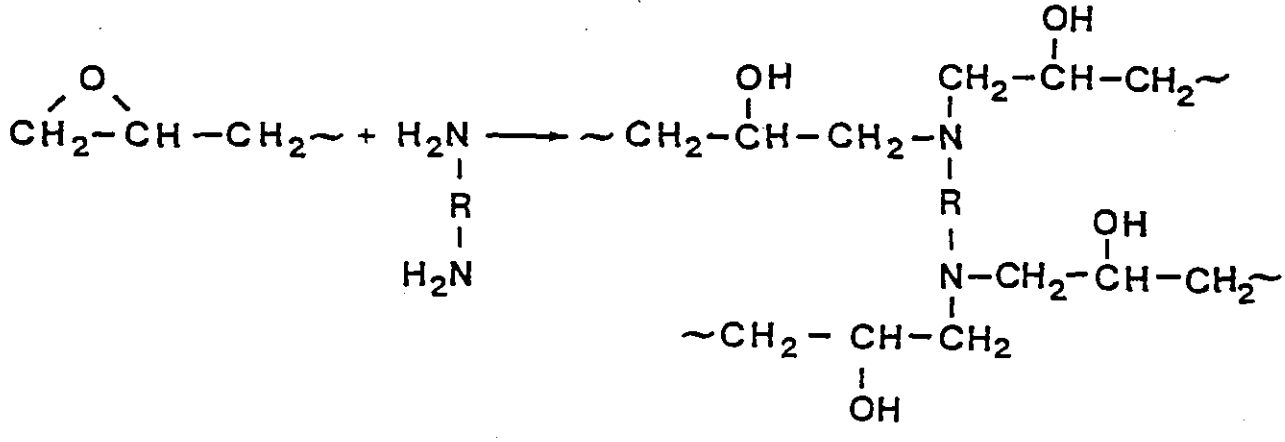

measurements on uncross-linked, partially cross-linked and fully cross-linked epoxy resins provide insight into basic mobility changes of the molecules. First, the value of the transition temperature gives the temperature range where microbronian motion starts. Then, knowledge of heat capacity changes at the glass transition yields an estimate of the number and type mobile units in the molecule. Coupled with information about the coefficients of expansion, compressibility and group and skeletal vibrations, this can provide a detailed understanding of the behavior of the epoxy resin molecule.

On this basis, we believe that study of changes in heat capacity with the advancement of cross-linking provides a means for characterizing polymeric networks.

Although there is a large body of literature concerning cross-linked epoxy resins, there appears to be no data available on heat capacities of these epoxy materials as such. Studies which have been made are limited to reactions which occur when these formulations are cross-linked to mechanical, thermal and other applications.

c. Glass Transition and the Hysteresis Phenomenon

The glass transition, T_g, is time dependent. The rate at which a liquid is cooled determines the position of T_g and, thus, the physical properties of the glass formed. A full thermal analysis must consider both the cooling rate (or the thermal history in case of more involved thermal pretreatment) and the heating rate through the transition region. The different cooling and heating rates may cause a hysteresis

effect. Fast cooling and then slow heating of the amorphous solid through its glass transition region should cause an exothermic hysteresis, while slow cooling and then fast heating results in an endothermic hysteresis[11]. Both are indicated in Figures V-A-1 and 2, respectively. The endothermic hysteresis is usually more easily produced and analyzed quantitatively. The hysteresis enthalpy, ΔH_h, is the area under the hysteresis peak such that a cyclic integral over cooling and heating curves ($\oint C_p dT$) is zero and satisfies the first law of thermodynamics.

In cross-linked systems the hysteresis peak seems to decrease with increasing cross-link density for the same thermal treatment. Decreasing of the hysteresis peak has been found in polystyrene with increasing divinyl benzene cross-link density[12]. Similarly, no hysteresis was noted for certain epoxy matrices[13]. A question to be resolved is if, in effect, for these samples the glass transition region is temperature independent within the chosen time scale or if the often-observed broadening of the transition region makes experimental observation of the hysteresis impossible.

The width of the glass transition region is usually stated in terms of either the difference between the end and beginning of the glass transition (T_E and T_B), ΔT_2, or between the extrapolated end and beginning (T_2 and T_1), ΔT_1. Figure V-A-3 illustrates the characteristic temperatures of the glass transition region, including T_g the point of half-

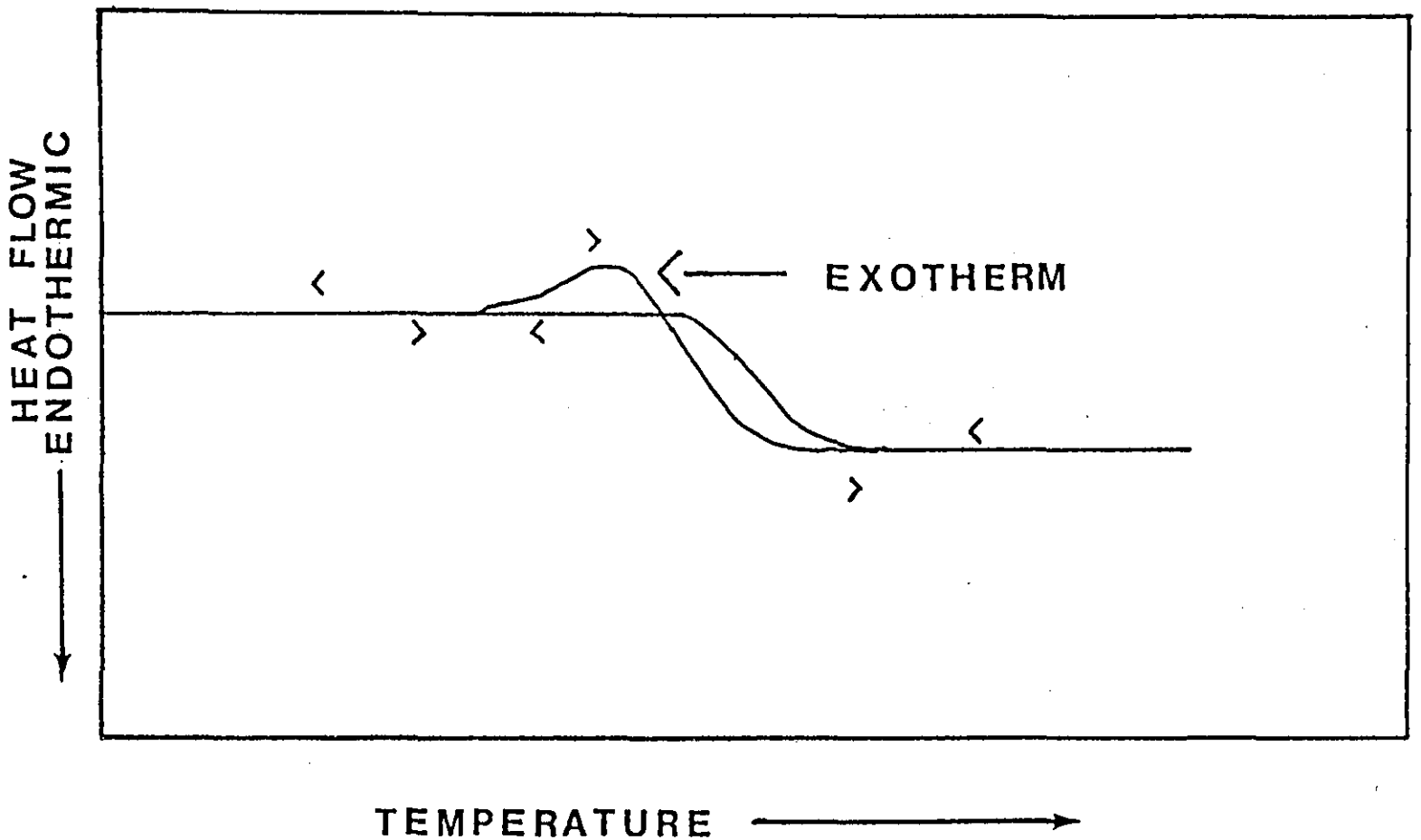

Figure V-A-1. Exothermic Hysteresis (schematic).

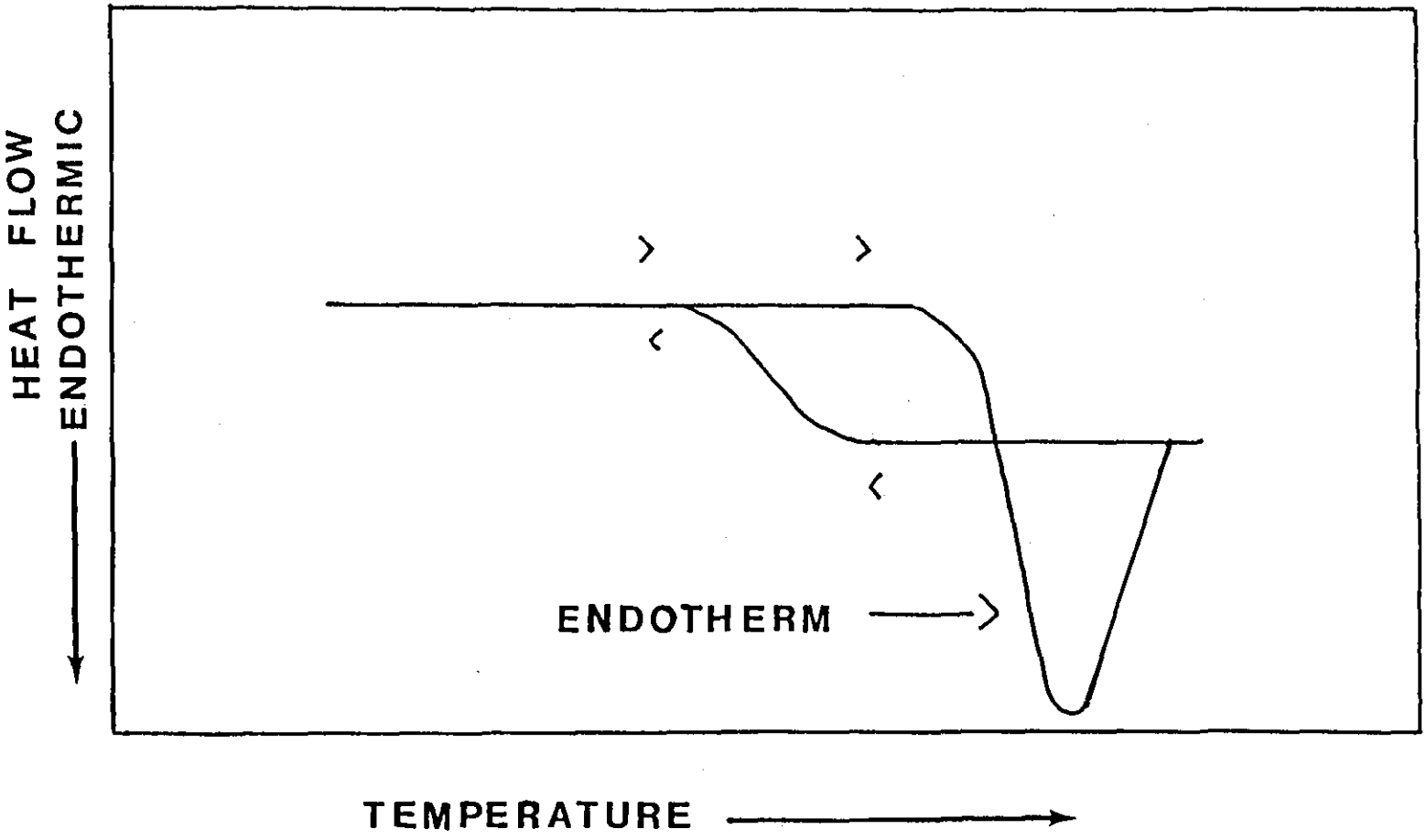

Figure V-A-2. Endothermic Hysteresis (schematic).

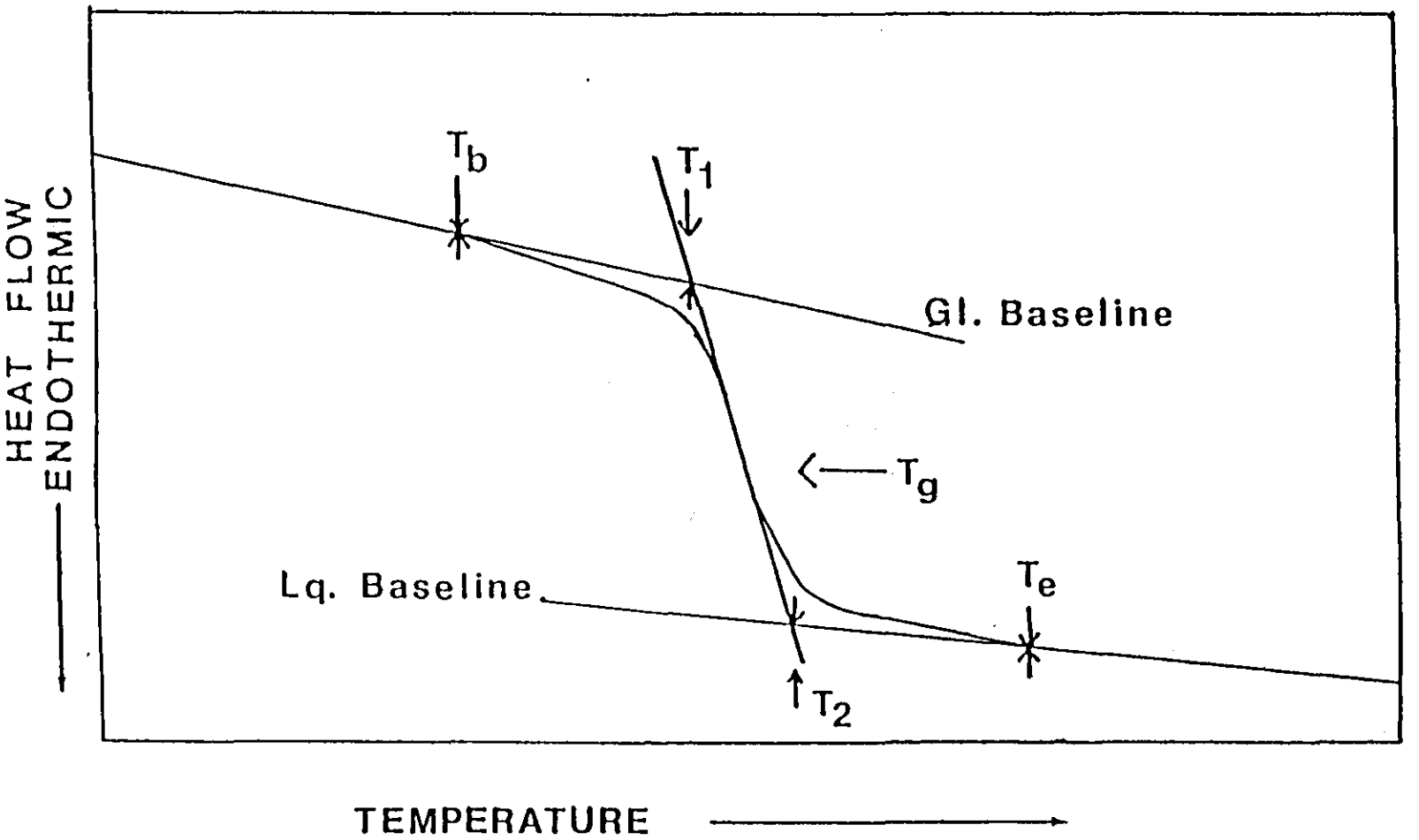

Figure V-A-3. Characteristic Temperatures in the Glass Transition Region.

vitrification. The end and the beginning of the glass transition region are usually least accurate, but indicate the often substantial broadening of the glass transition which affects the performance of the material. In this study, ΔT_1 will be used for the measurement of the broadness of the glass transition region with occasional reference to the wider range, $T_E - T_B$.

2. Status

It is the purpose of this work to gain knowledge of the glassy materials used as matrices in composites and to study the homogeneity resulting from the curing process. We intend to link the glass transition quantitatively with the presence of a given material. During the last report period, this led to the study of the hysteresis phenomenon at various cure states. The hysteresis was found to be strongly affected by cross-linking. Further testing of these novel approaches is planned using equipment and techniques developed in RPI's ATHAS (Advanced Thermal Analysis) laboratory.

As will be described in the next section, the data in question will require higher sensitivity calorimetry than is currently available. In preparation for this work, we developed a better means of measuring heat capacity, leading, in some cases, to a precision of ±0.1 percent. A report of this work has been prepared for publication in the Journal of Thermal Analysis.

This project has had the partial support of postdoctoral fellows Grebowicz, Suzuki and Menczel, and research assistant Mr. Judovits. The project was initiated on May 1, 1983 by Mr. Gjaja, and a full report of the work by Gjaja will be forthcoming shortly as a doctoral thesis. Dr. Grebowicz and Mr. Judovits will continue the work.

3. Progress During Report Period

Epoxy resins containing various amounts of hardener (TGDDM/DDS system) were cured in a muffle furnace at 473 K for seven hours. The glass transition temperature, T_g, versus weight minus percent of hardener in the epoxy resin were measured (see Figure V-A-4). A limit was rapidly reached in T_g at only two percent hardener. Thus, the glass transition of the fully cured epoxy-amine matrix seems not much different from the epoxide-epoxide cure.

To study this catalyst-free curing further, the T_g versus cure-time for the epoxide-epoxide reaction was also studied. MY 720 was cured by itself in an oil bath at 473 K for different lengths of time (Figure V-A-5). The T_g was found to increase exponentially with the cure time, and a maximum T_g of about 450 K was reached after eleven hours. The reaction was found to be inhibited by running the sample under argon.

The decrease of the hysteresis with increasing cross-link-density was investigated on divinyl benzene cross-linked polystyrene to get quantitative information on the structure.

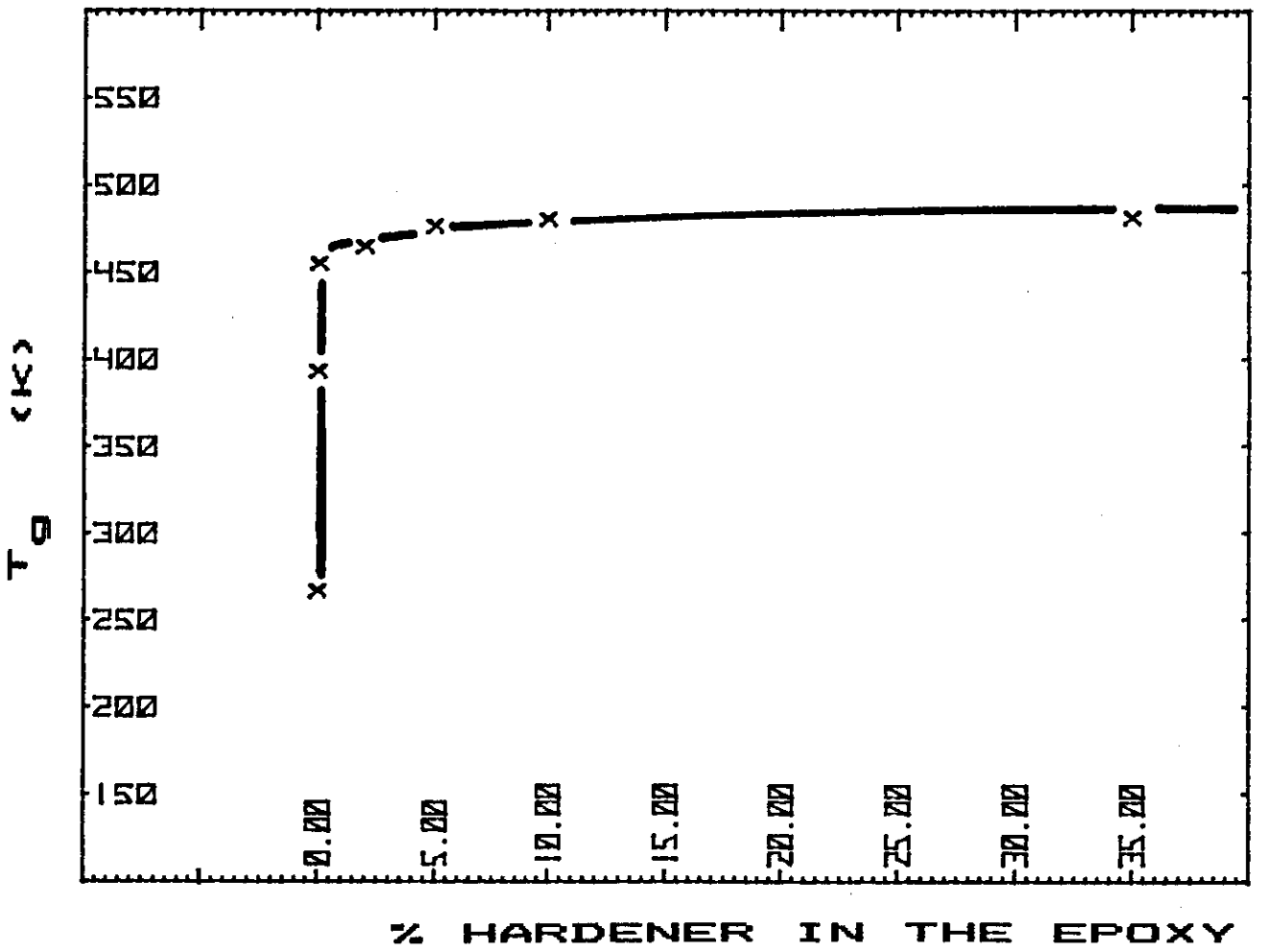

Figure V-A-4. Glass Transition Temperatures as a Function of Hardener Concentration. (curing of TGDDM/DDS for 7 hours at 473° K)

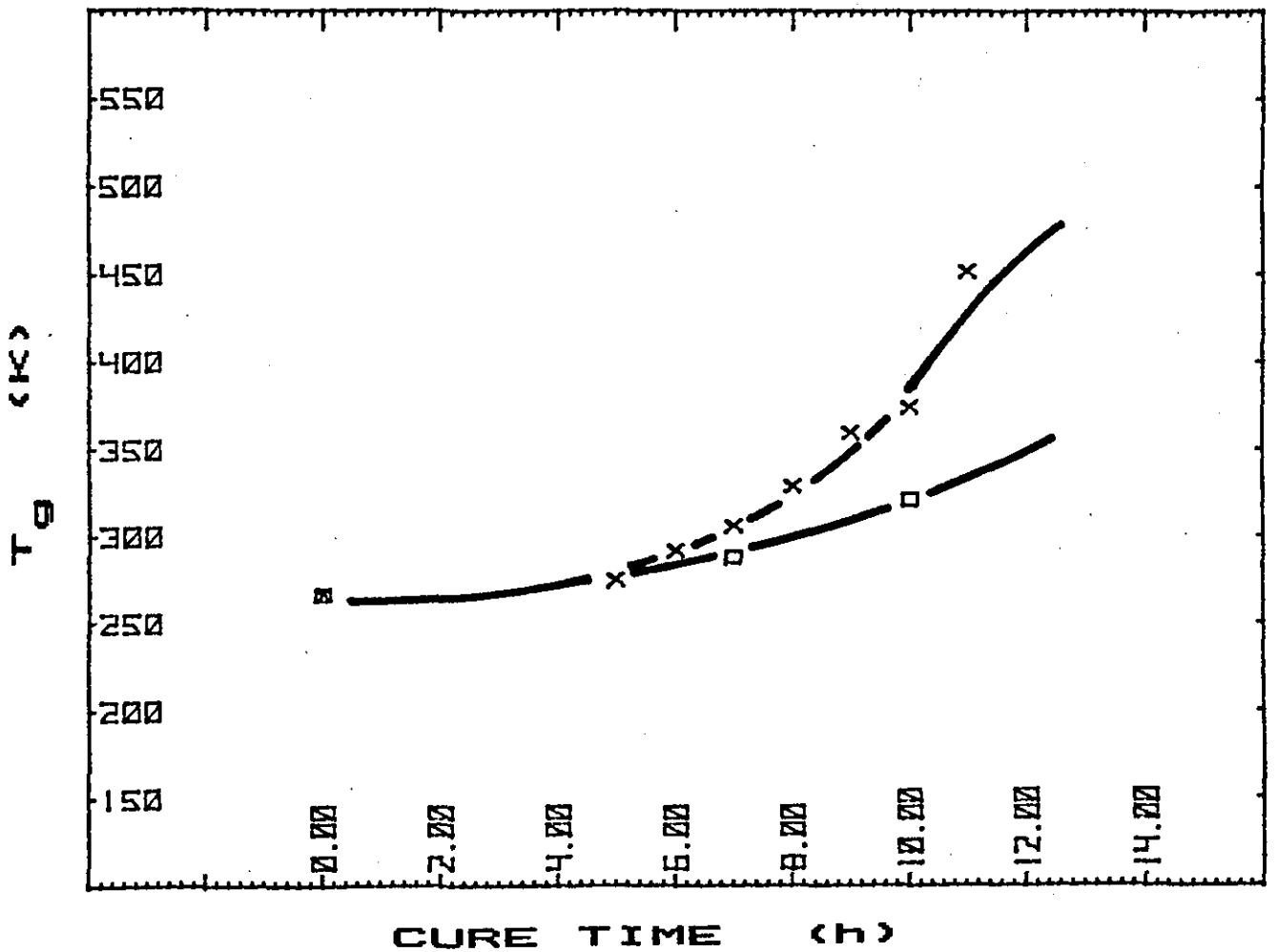

Figure V-A-5. Cure-Time Dependence of T_g of TGDDM (MY 720) Without Hardener at 473° K. (Squares indicate inhibited reaction under argon.)

A relationship between the broadness of the glass transition region, ΔT, and the disappearance of the hysteresis peak, ΔH_h, was noted (see Figure V-A-6). A similar behavior was found for MY 720 cured without catalyst (see Figure V-A-7). In general, with increasing cross-link density, T_g was found to increase, the glass transition region was found to broaden, and the hysteresis peak was found to dampen (see Figures V-A-8 and 9). At very high cross-link densities, however, the trend seems to reverse itself to some degree. That is, with increasing cross-linking at high cross-link densities, though T_g still increases, the glass transition region begins to narrow and the hysteresis peak increases again (see Figure V-A-7 and also the squares in Figure V-A-9).

With increased cross-link-density an increase in T_g is usually noted[15]. However, a plot of T_g versus percent-by-weight of DVB revealed for the first time a minimum of about two percent DVB (see Figure V-A-10). This decrease in T_g should be investigated further. It could be due to a plastization effect of the not-fully-reacted monomer[12]. Possibly only one end of the DVB reacted at low DVB concentration so that instead of a pure cross-linking effect, which would raise T_g, a branching effect would occur which might decrease T_g. Both these trivial reasons are countered by the extrapolation of the low cross-link density curve to zero concentration which is considerably higher than the normally accepted T_g of polystyrene (T_g = 373 K). This work connects with

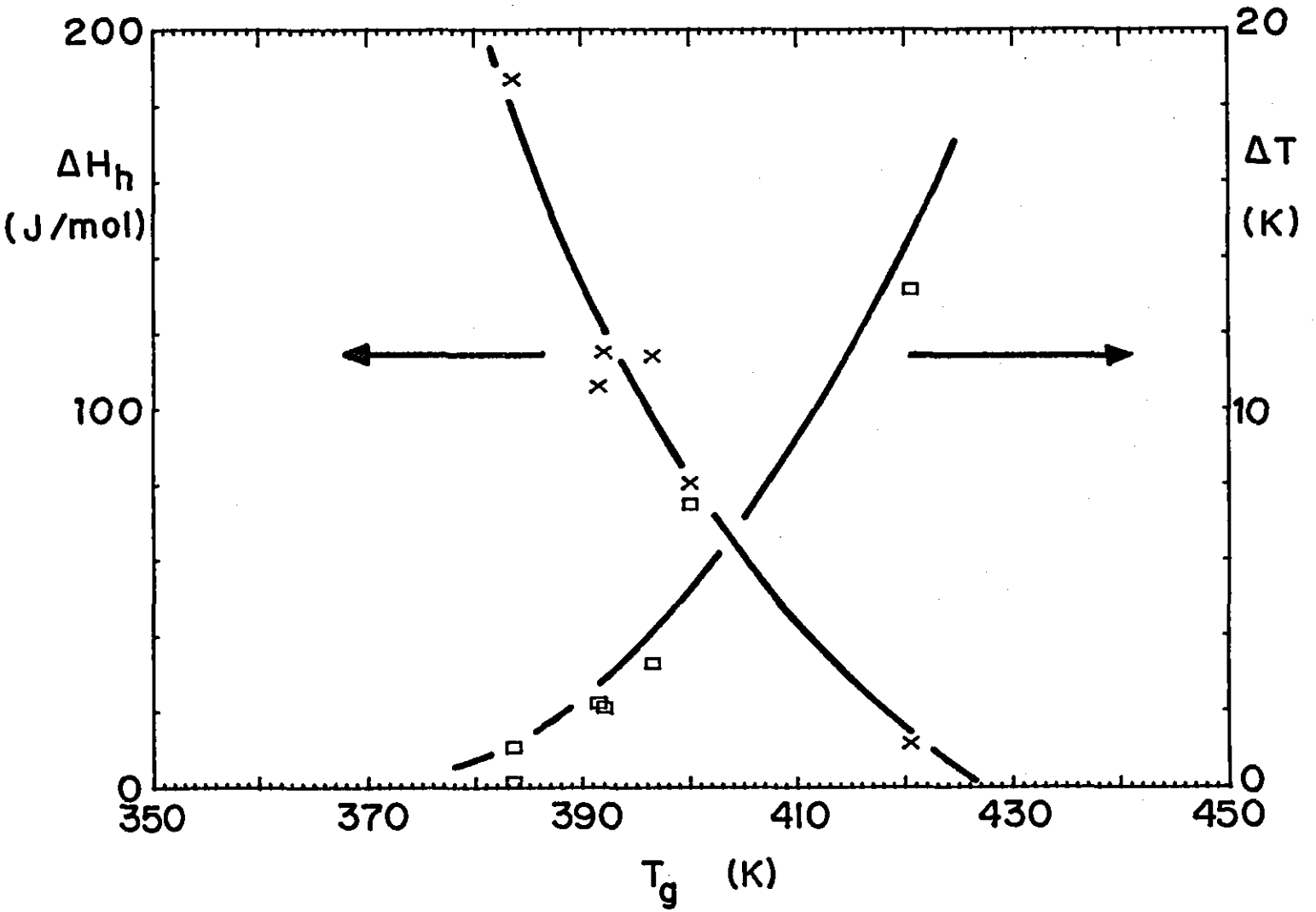

Figure V-A-6. Change of the Glass Transition Hysteresis Peak Area, ΔH_h, and the Breadth of the Glass Transition Region, ΔT, as a Function of Glass Transition, T_g, for Cross-Linked Polystyrene. (cooling rate of 0.5° K/min, heating rate 20° K/min)

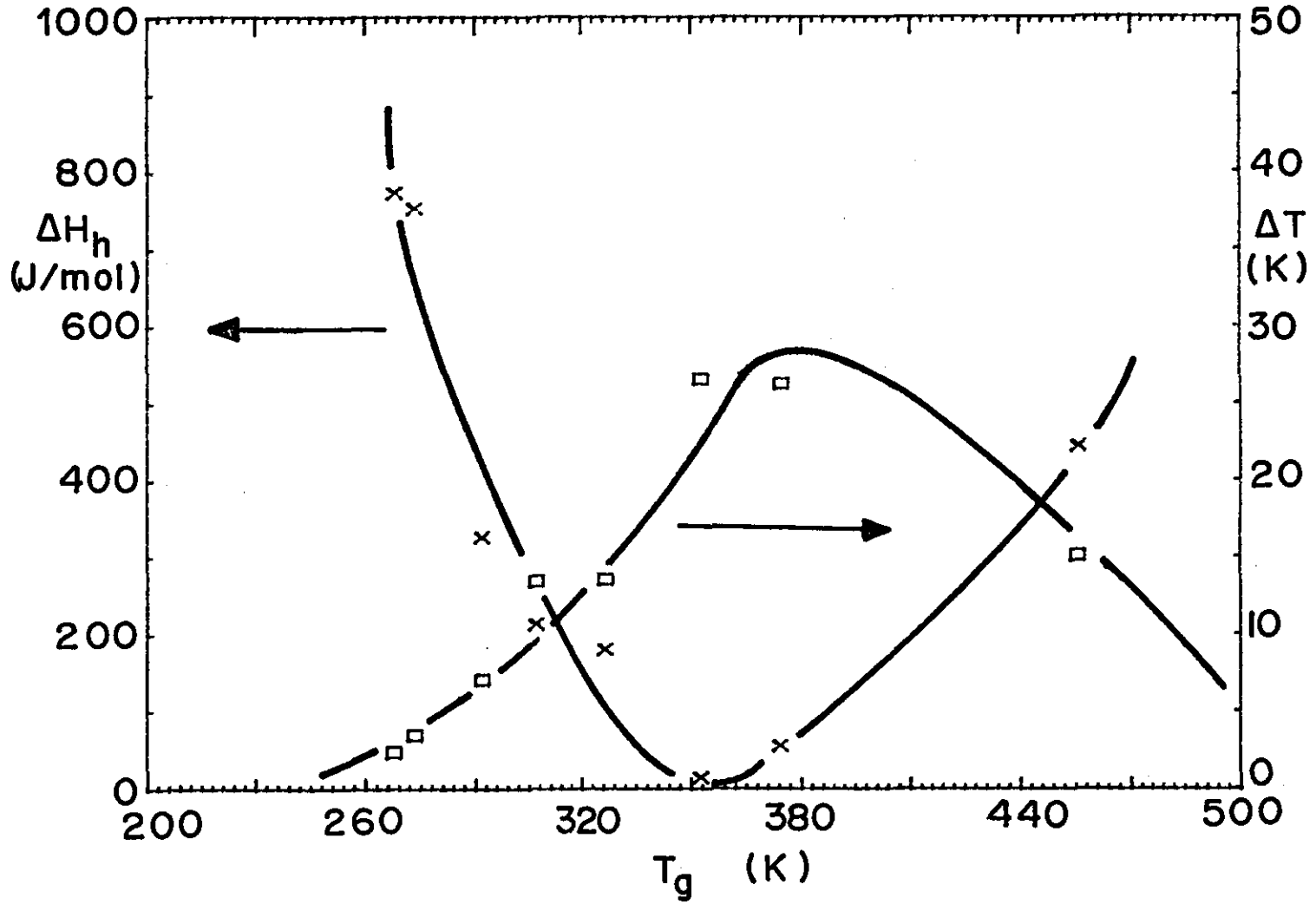

Figure V-A-7. Change of the Glass Transition Hysteresis Peak Area, ΔH_h, and the Breadth of the Glass Transition Region, ΔT, as a Function of Glass Transition, T_g, for the Samples Described in Figure V-A-5 (MY 720). (cooling rate 0.5° K/min, heating rate 20° K/min)

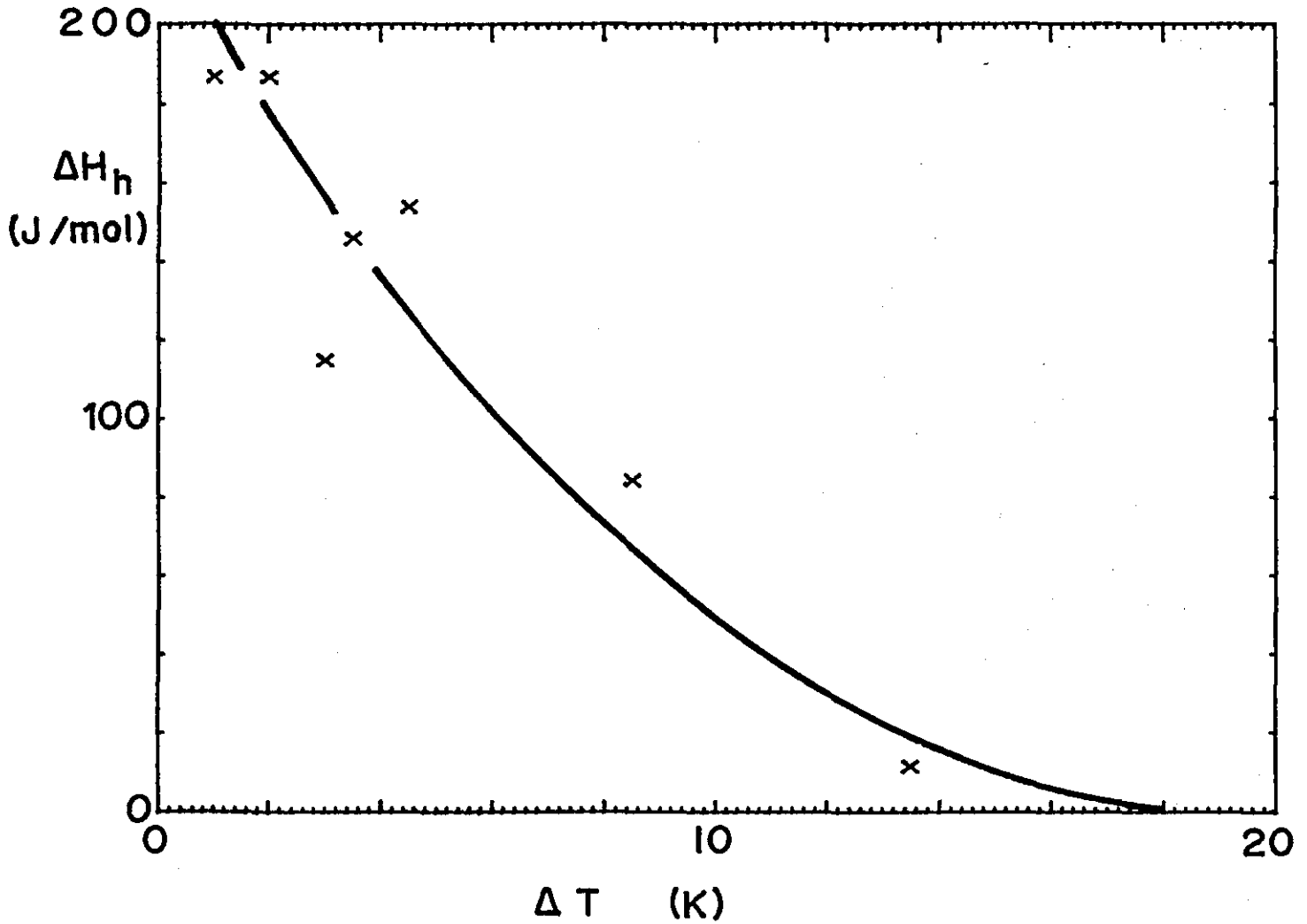

Figure V-A-8. Breadth of the Glass Transition, ΔT, Versus Hysteresis Peak Area (cross-linked polystyrenes, see Figure V-A-6)

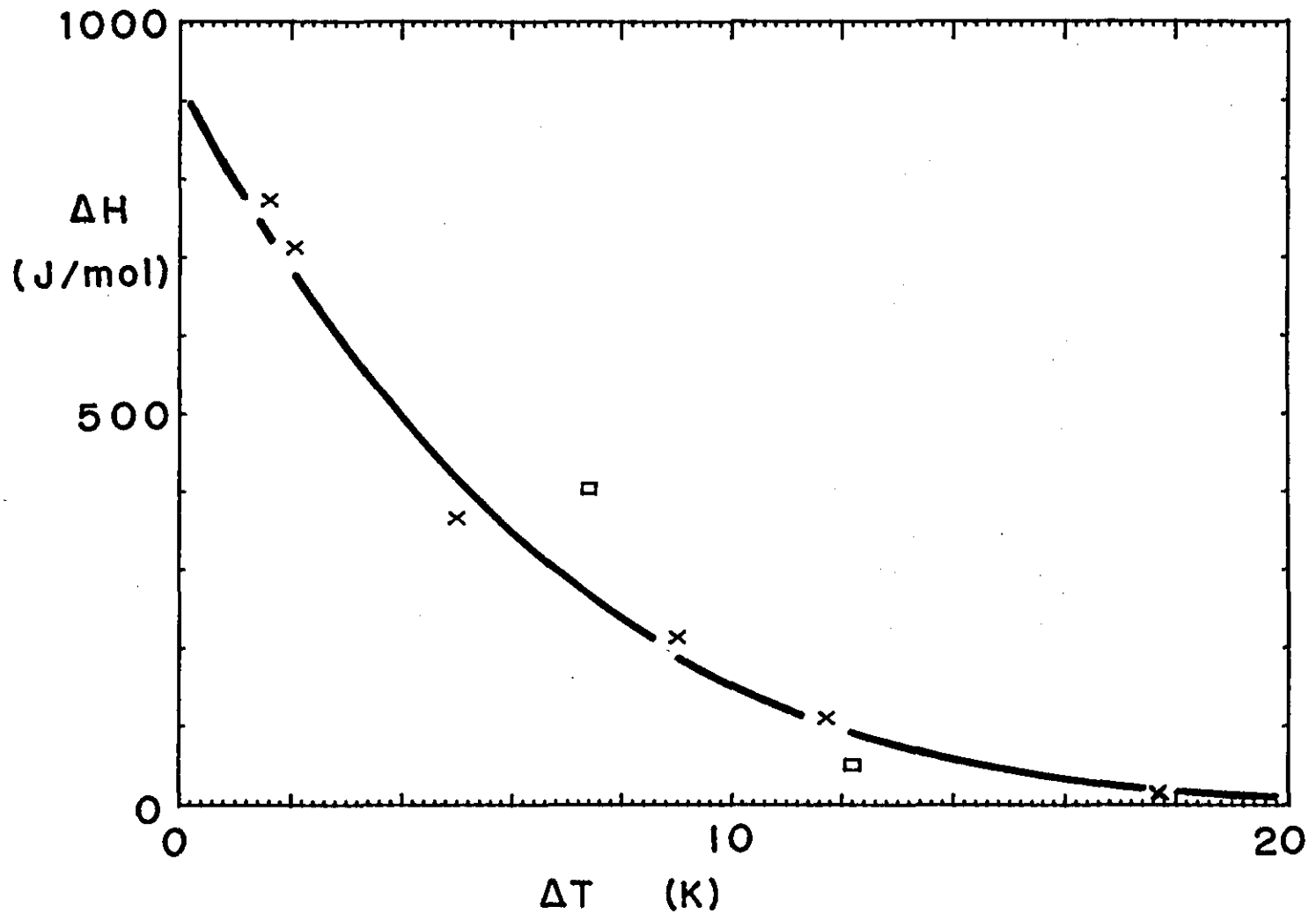

Figure V-A-9. Breadth of the Glass Transition, ΔT, Versus Hysteresis Peak Area (TGDDM [MY 720], see Figures V-A-5 and 7)

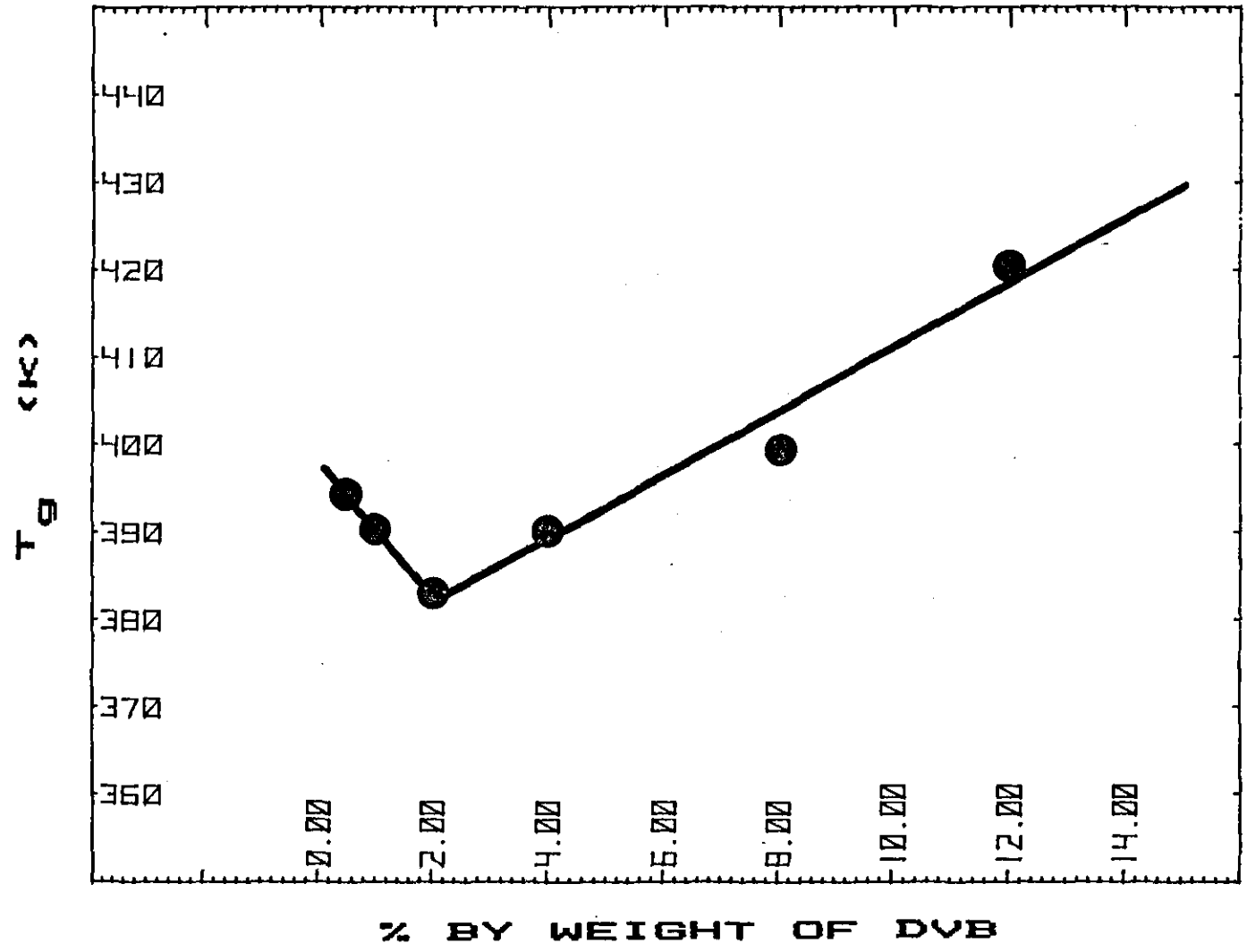

Figure V-A-10. Glass Transition Temperatures, T_g, Versus Degree of Cross-Linking. (expressed as concentration of divinyl benzene)

irregularities found in the analysis of a broad range of PS samples analyzed in our laboratory for the IUPAC thermal analysis working group.

4. Plans for Upcoming Period

The work on changes of T_g with cross-linking will be continued. Our initial attempt to link the glass transition quantitatively with the presence of a given material for the TGDDM/DDS matrix was complicated by the epoxide-epoxide reaction masking the T_g increase of the fully cured epoxide-amine matrix. Since the epoxide-epoxide cured samples are more brittle, we will explore how to limit this reaction. Initial attempts have proven successful (curing under an inert atmosphere).

After a method has been found to inhibit the epoxide-epoxide reaction, the T_g versus hardener characteristics for the TGDDM/DDS epoxide-diamine reaction can be studied.

Finally, the investigations of the decrease of the hysteresis effect and its relationship to the broadness of the glass transition will be continued. We will try to simulate various microscopic and macroscopic models of hysteresis to separate broadening effects from hysteresis.

Although the original goal of this research has moved somewhat into the future, we have gained a better understanding of cross-linked systems and hope to contribute, after solving some of the more fundamental problems, to the applied research with correspondingly better preparation.

5. References

1. Buckingham, J., "Dictionary of Organic Compounds", 5th Edition, Chapman and Hall, NY, 1982.

2. Mohajer, Y., E. Yurgitis, G. Wilkes and J. McGraph, "Physical Aging Studies of Epoxy Resins with Emphasis on Graphite Fiber-Epoxy Composites", Proceedings of the Critical Review: Techniques for the Characterization of Composite Materials, Army Materials and Mechanics Research Center, Watertown, MA 02172, 1982.

3. Kong, E. S. W., "Physical Aging and Its Effect on the Mechanical and Physical Properties of Graphite/Epoxy Composites", Organic Coatings and Applied Polymer Science Proceedings, Vol. 46, 1981, p. 568.

4. Mones, E. T. and R. J. Morgan, "FTIR Studies of the Chemical Structure of High Performance Composite Matrices", ACS Polymer Preprints, Vol. 22, 1981, p. 249.

5. Walkup, C. M., R. J. Morgan and T. H. Hoheisel, "Systematic Differential Scanning Calorimetry Studies of the Cure of Carbon Fiber-Epoxy Composite Prepregs", ACS Polymer Preprints, Vol. 25, 1984, p. 95.

6. "Epoxy Resins and Hardeners", Ciba-Geigy Corp., 1981.

7. Morgan R. J., J. E. O'Neal and D. B. Miller, "The Structure, Modes of Deformation and Failure, and Mechanical Properties of Diaminodiphenyl Sulphone-Cured Tetraglycidyl 4,4'-Diaminodiphenyl Methane Epoxy", J. of Materials Sci., Vol. 14, 1979. p. 109.

8. Brönsted, J. N., M. Kilpatrick and M. Kilpatrick", "Kinetic Studies on Ethylene Oxides", J. Am. Chem. Soc., Vol. 51, 1929, p. 428.

9. Stone, F. W. and J. J. Stratta, "1,2-Epoxide Polymers", Encyclopedia of Polymer Science and Technology, H. F. Mark, N. G. Gaylord and N. M. Bikales editors, Interscience, NY, 1967.

10. St. Pierre, L. E., "Polymers from 1,2-Epoxides: I. Chemistry", Polyethers Part I. Polyalkylene Oxide and Other Polyethers", N. G. Gaylord editor, Interscience, NY, 1963.

11. Wunderlich, B., audio course on "Thermal Analysis", Rensselaer Polytechnic Institute, Troy, NY, 1981.

12. Glans, J. H. and D. T. Turner, "Glass Transition Elevation of Polystyrene by Crosslinks", Polymer, Vol. 22, 1981, p. 1540.

13. Observation by L. Judovits during this report period.

14. Badram, B. M., A. A. Yehid and E. M. Abdel-Bary, "The Modification of Epoxidized Linseed Oil with Aromatic Amines", European Polymer Journal, Vol. 13, 1977, p. 155.

15. Ens, J. B. and J. K. Gillham, "The Time-Temperature-Transformation (TTT) Cure Diagram: Modelling the Cure Behavior of Thermosets", Organic Coatings and Applied Polymer Science Proceedings, Vol. 47, 1982, p. 575.

V-B ACCURATE MEASUREMENT OF HEAT CAPACITY BY DIFFERENTIAL SCANNING CALORIMETRY

Senior Investigator: B. Wunderlich

1. Introduction

Experience with high quality heat capacity measurement by differential scanning calorimetry is summarized and illustrated, pointing out three major causes of error:

a) incompatible thermal histories of the sample, reference and blank runs;

b) unstable initial and final isotherms;

c) incompatible differences between initial and final isotherm amplitudes for sample, reference and blank runs.

Considering these problems, it is shown for the case of polyoxymethylene that accuracies in heat capacity of ±0.1 percent may be possible.

2. Status

Improving the measurement of heat capacity by differential scanning calorimetry (DSC) is one of the goals in RPI's laboratory for Advanced Thermal Analysis (ATHAS). In the past we tested standards for temperature, heat of fusion and heat capacity[1]*. Comparisons between various DSC's were made at high and low temperature ranges[2]. Computerization was introduced early and compared to standard measurements[3]. More recently, this computerization was improved

*Numbers in brackets in this section refer to the references which are listed on page 144.

to sixteen bit data acquisition[4], which led over the past year to the discovery of some limitations in precision of heat capacity measurements. These limitations are described here, together with recommendations for avoiding these problems. The measurements were made with a Perkin-Elmer DSC-2, but the same effects were seen qualitatively on other instruments (Perkin-Elmer DSC-4, Du Pont 990, Mettler 2,000). We believe the effect is inherent in differential scanning calorimetry.

In the temperature range above 10° K, adiabatic calorimetry was, for a long time, the main technique for precision heat capacity[5]. Precision of ±0.1 percent could, with some care, be achieved routinely. The main problem in adiabatic calorimetry is minimizing and calibrating residual heat losses. One good practice[6] is to place the whole calorimeter laboratory into a room of constant temperature (±0.5° K) to eliminate changes in temperature gradients from within the calorimeter to outside it. Differential scanning calorimetry[7] has become precise enough to make acceptable measurements of heat capacity since about 1965[8]. The much larger problem of heat losses in twin calorimetry was bypassed by drastically reducing sample mass and increasing measuring speed. By now many of the other limiting factors of scanning calorimetry, such as data acquisition, sample handling and heat flow, have been improved sufficiently that a precision of ±0.1 percent by DSC is possible. The remaining

problem seems to be the handling of transient temperature gradients.

3. Progress During Report Period

This report deals with problems arising in attempting to measure the heat capacity of liquid polyoxymethylene[9] over as wide a temperature range as deomposition and crystallization permits. It includes the work of postdoctoral fellow H. Suzuki. Figure V-B-1 provides one illustration. Two successive runs, under identical measuring conditions, without reloading or repositioning the sample and at the same heating rate, gave the results shown. After sufficient work to indicate that no change in the sample itself had occurred, we had to conclude that instrument effects caused curve A to be in error.

a. Instrumentation

A Perkin-Elmer DSC-2 was used for all measurements. The prior Hewlett-Packard calculator used with this instrument[3] was replaced with a LMS-1000-DSC data station[10]. A block diagram and data handling flow diagrams of this system have been given in Reference [4]. The data station consists of a Z-80 based microcomputer with 64 k-bytes of random access memory and dual eight-inch floppy disk drives. A multichannel, 16-bit analog-to-digital converter with differential inputs is used for data assimilation. Data collection is interrupt-driven, using the DSC programming pulse. There are

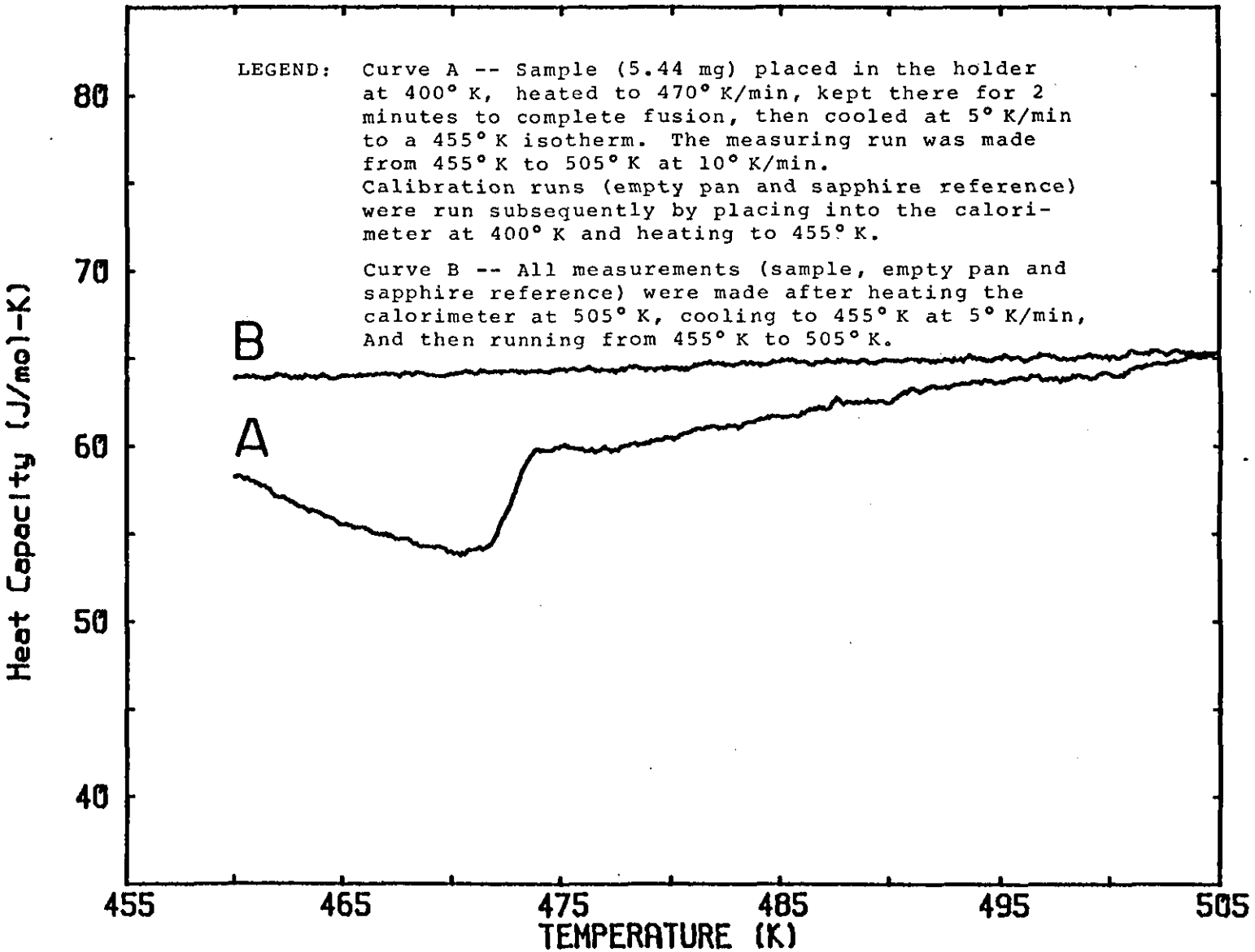

Figure V-B-1. Heat Capacity of Polyoxymethylene as a Function of Temperature

at present thirty data points recorded per degree kelvin. Typical heat capacity runs make use of fifteen to thirty milligrams samples. Aluminum pans of similar mass (±0.1 mg) are used for reference and sample. The standard heating rate is 10° K/min. All runs are made in a dry nitrogen atmosphere with the calorimeter block being thermostatted at about 200° K with a mechanical refrigeration unit. The calorimeter is shielded from the room environment, which is thermostatted to ±1° K, by the standard dry-box attachment of the Perkin-Elmer.

b. Results

A large series of DSC-runs (about 100) were made and analyzed with respect to their thermal history.

Study of the runs leading to Figure V-B-1 may serve as an example for a large series of similar experiments. It revealed the three major problems to be discussed:

a) A sudden change in the (measured) heat flow ("exotherm") occurs whenever the calorimeter is kept at a temperature above the initial isotherm for a time before measurement. (The effect decreases with increasing temperature difference from the isotherm.)

b) The heat flow under isothermal condition depends on the prior thermal history (for times much longer than the obvious approach to steady state).

c) Serious errors in heat capacity can result from coupling sample, reference and blank runs of different thermal history (due to different pen amplitudes).

As a first analysis of the "exotherm", the heat flow curves of the sample runs in Figure V-B-1 are shown in Figure V-B-2. It is clear from curve A that the sudden deviation ("exotherm") in heat capacity is due to the deviation in heat flow of the sample run in the vicinity of the temperature of the prior two-minute isotherm (470° K). The observation of such an "exotherm" is not restricted to a particular polyoxymethylene sample. The same heat flow pattern can be seen even in a reference (sapphire) run and a blank (empty pan) run as along as a similar thermal history is given prior to the measuring run. Figure V-B-3 depicts examples of the "exotherm" observed in sapphire runs. The thermal histories given are similar to those for run A of Figure V-B-2. A sudden change in heat flow can be seen just above 470° K, the temperature at which the calorimeter was kept for two minutes prior to the measurement run. Furthermore, this figure illustrates the time effects on the "exotherm". That is, before making a run from 450° K to 500° K, the calorimeter was held at the 450° K isotherm for five different periods of time from 3 minutes to 10.5 hours. Since the general feature of the "exotherm" can be seen in all heat-flow curves, it is understood that the prior thermal history does affect the actual heat flow, irrespective of the time the calorimeter is held at the initial temperature of a run, for times as long as ten hours. The reasons why a prior thermal history of the calorimeter remains influential for such a long time,

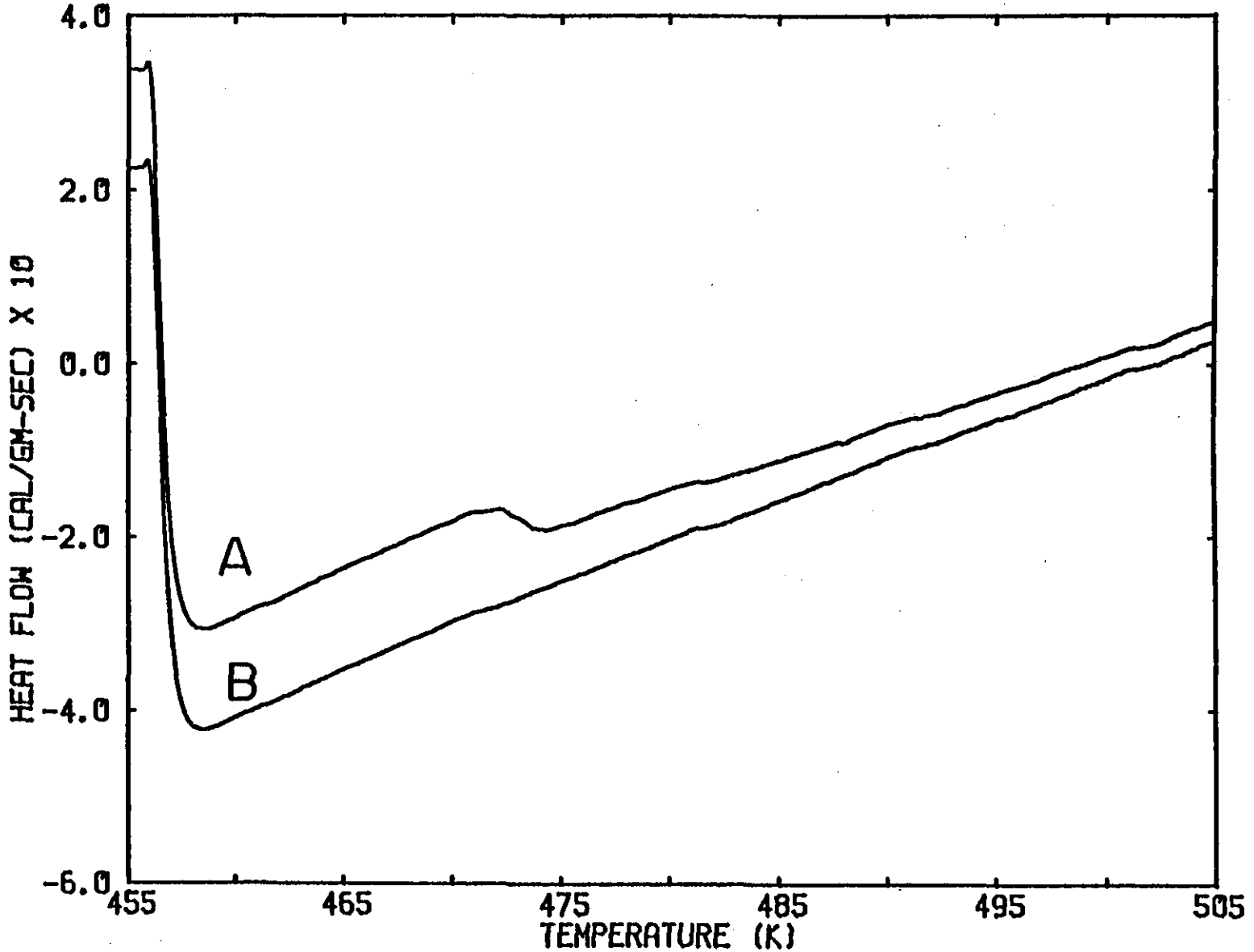

Figure V-B-2. Heat Flow Curves of Sample Runs A and B Described in Figure V-B-1

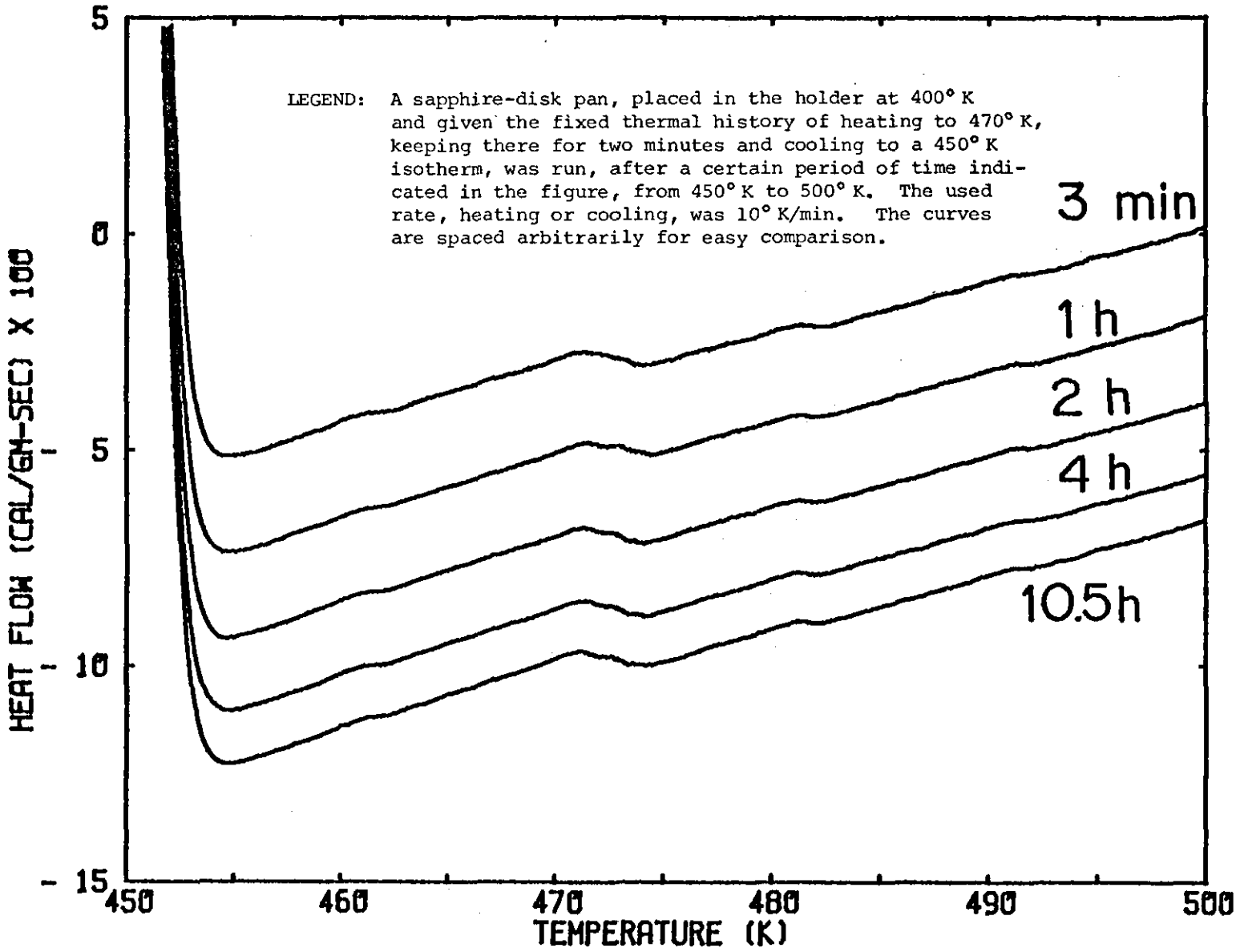

Figure V-B-3. Heat Flow Curves Observed on a Sapphire Reference

going beyond times needed to decay temperature gradients, is not clear at present. This is one of the instrumentation problems which operators must realize and avoid for quality heat capacity measurement. Other similar experiments showed, as a matter of course, that the effect decreased with increasing the temperature difference between the prior isotherm (for the case shown in Figure V-B-1, 470° K) and the initial temperature of a measuring run.

A problem to be discussed next concerns the different isotherm positions at the initial temperature, when that temperature is approached from different temperatures. This effect is obvious from Figure V-B-2 where different intercepts with the ordinate are seen for curves A and B. For a detailed discussion, computer readings of the isotherm positions of all runs used for the experiments of Figure V-B-1 are listed in columns 2 and 5 of Table V-B-1. Readings at 455° K for the runs, SA A and SA B correspond to the ordinate intercepts in Figure V-B-2, the difference of which amounts to 1.1 chart paper divisions. Such a difference in isotherm position occurs even when the initial temperature is approached in the same direction, but on cooling from different temperatures, i.e., 470° K and 505° K in runs SA A and SA B, respectively. More significant differences in the isotherm positions at 455° K can be seen for the runs BL and RE, when opposite directions of approach to the initial temperature are applied in the runs A and B. The different

TABLE V-B-1

COMPUTER READINGS OF PEN AMPLITUDES IN RUNS SHOWN IN FIGURE V-B-1

Run \ Temperature		(Init.) 455° K	470° K	476° K	(Final) 505° K
BL	A	2960	2322	2601	5539
			(1412)	(1442)	[2579]
	B	1988	1997	2382	5500
			(1045)	(1081)	[3512]
RE	A	2722	-5897	-5694	5258
			(9380)	(9481)	[2536]
	B	1766	-6230	-5920	5171
			(9018)	(9116)	[3404]
SA	A	2062	-1068	-1059	4832
			(3961)	(4284)	[2770]
	B	1319	-1780	-1441	4600
			(4083)	(4138)	[3281]

BL, RE and SA are blank, reference and sample runs, respectively.

Values in parentheses are absolute values of pen amplitudes (amplitude minus baseline, interpolated between initial and final isotherms).

Values in square brackets are differences between initial and final isotherms.

For run conditions, see legend to Figure V-B-1.

One chart division (2 mm) - 655 in computer units when the DSC settings are as follows: gain = 100, range = 0.5 m cal/s and recorder range = 200 mV.

isotherm positions observed after the attainment of steady state did not change with time over periods of more than ten hours. In contrast, it is seen from column 5 of Table V-B-1 that the differences in isotherm positions at the final temperatures of corresponding runs are negligibly small. This means that the slope of the line connecting initial and final isotherm positions changes with different approaches to the initial isotherm temperature. Hence, this affects the actual pen amplitude and, accordingly, the value of the heat capacity. In order to examine the possible error in heat capacity, computer readings of the pen amplitude at two intermediate temperatures, 470° K and 476° K, are listed in Table V-B-1 in columns 3 and 4, respectively.

The absolute values of the pen amplitudes (in parentheses) in Table V-B-1 should be invariant for runs A and B. Yet, they are not. For example, in the runs of RE A and RE B, the absolute values of the pen amplitude at 470° K are 9380 and 9018, respectively. This difference of four percent is caused by the different isotherm positions at 455° K in runs A and B. Assuming identical weights of the aluminum pans used, the heat capacity of the sample is proportional to (SA-BL/(RE-BL), where SA, BL and RE stand for the respective absolute pen amplitudes of sample, blank and reference. At 470° K this computation yields 0.3199 for runs A and 0.3810 for runs B. Accordingly, the heat capacity obtained from runs A is seen to be sixteen percent less than that

from runs B. Similarly, at 476° K, runs A yield a heat capacity value seven percent smaller than do runs B. These differences in heat capacity are those which have already been noted in Figure V-B-1. Their magnitude is aggravated by the relatively small sample mass used for the present illustration. The volume of the sample pan would permit a sample four times larger, and that would cut the errors to one-quarter the values shown, but still much too large for precision heat capacity.

In addition to the three major problems just discussed, there exist two additional minor effects. One of them is the roughness of the recording, as can be seen in Figure V-B-1. Those data were recorded when condensation was present on the surface of the DSC head. Since the curves become much smoother after defrosting and cleaning, it can be said that condensation introduces noise into the recording. The other effect is illustrated in Figure V-B-4. On slow runs, a discontinuous adjustment of the average temperature appears in the heat-flow curve every 10° K. At heating rates of 10° K/min or faster, the steps in the heat-flow curve are practically lost. The steps remain the same at all range settings.

c. Conclusions

From the above findings and considerations, one may set up a guide to better DSC experiments: prior to runs, fixed, identical thermal histories must be decided upon for sample, reference and blank runs. Preferably, we suggest heating to

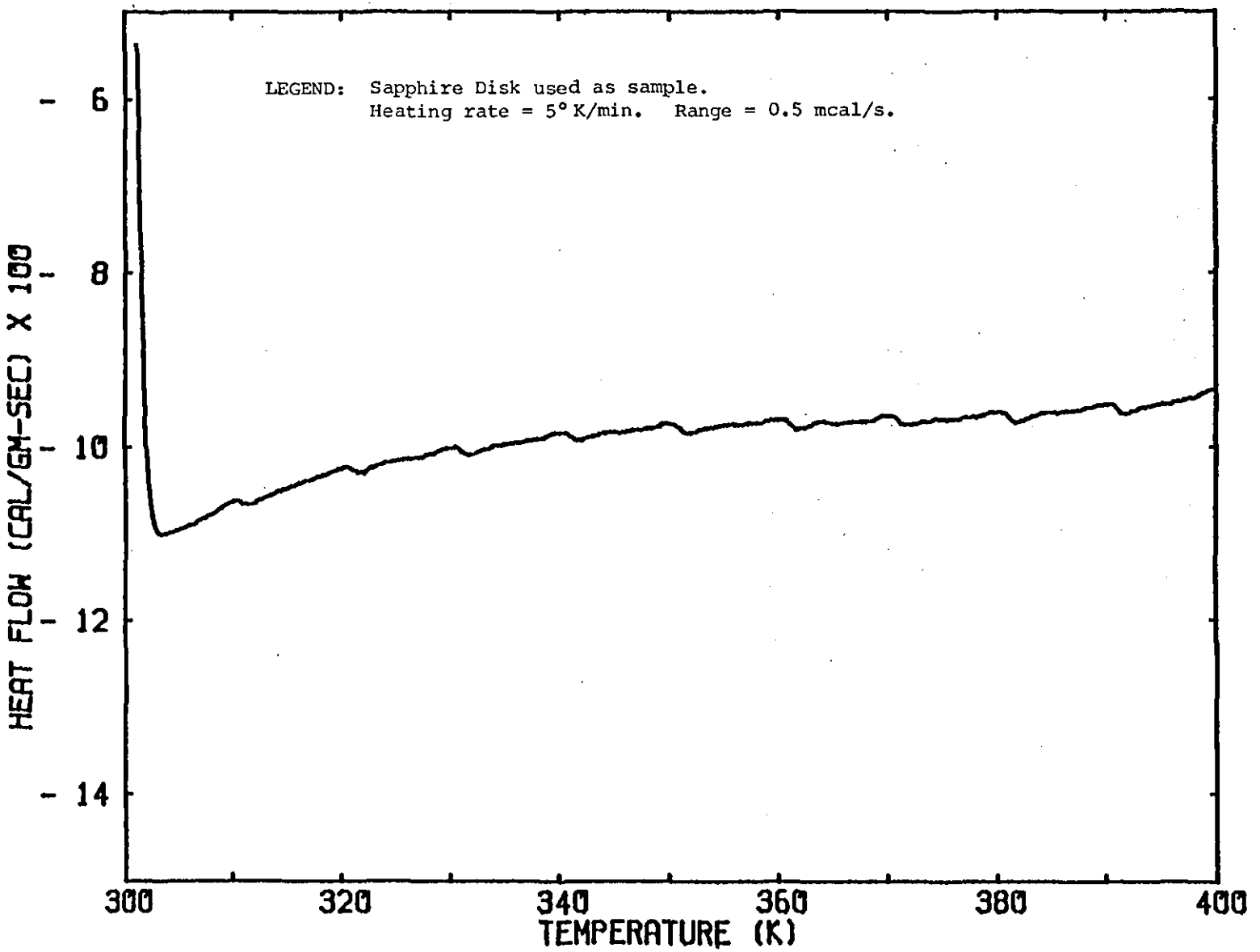

Figure V-B-4. Plot of Heat Flow Versus Temperature

the final temperature of a run, to erase any prior history and then cooling to the initial isotherm at a given rate. Even if this precaution is taken, all results may not be usable due to other inherent, well-known problems encountered in attempting to achieve reproducibility among runs (pan and lid positioning, gas flow, condensation, sample shifting, radiation changes by surface contamination, etc.). Only without reloading and repositioning a pan does one achieve repeated runs of almost perfect reproducibility. Strictly speaking, the same experimental conditions cannot be kept for blank, reference and sample runs. What must be managed is to minimize the changes in experimental conditions and to assess the quality of the obtained data from the following three point procedure. The first point is a check of whether three different runs have the same thermal history. If they have, they may be called compatible. The second point requires the check of initial and final isotherm stability. The third point involves a comparison of the actually achieved differences between the initial and final isotherm amplitudes, at least for reference and sample runs, but preferably for all three runs. Only if all three checks are positive can runs be considered of good quality. Generally, the baseline always tilts to some extent. This slope should remain constant during a given set of experiments.

As a final example, data on molten polyoxymethylene are presented. This polymer can be heated up to 543° K at rates

of 40° K/min only once, since on prolonged exposure to high temperatures it is subject to significant deomposition. Figure V-B-5 shows three sets of heat-capacities calculated for one sample run, H14D1, coupled with different blank and reference runs. The isotherm amplitudes of all runs are listed in Table V-B-2, and the run conditions are described in the footnote of the table. Curve A in Figure V-B-5 shows the results obtained from the incompatible set of runs H14D1, RE3 and BL3 (the latter two runs have a different thermal history). The result - namely, that the heat capacity A of the melt polyoxymethylene is almost independent of temperature - must be in error. Curves B and C, practically indistinguishable in the figure, are obtained by coupling the sample run H14D1 with RE5 and BL1 and with RE1 and BL1, respectively. All these runs are compatible with H14D1 and, needless to say, have stable isotherms. The run BL5 was not adopted, because its difference in isotherm amplitudes is too large, for unknown reasons. It is seen from column 5 that the difference in isotherm position of RE5 is closer to that of H14D1 than RE1. It can be seen from Figure V-B-5, however, that the observed ten percent difference in slope of the reference run is not sufficient to yield a noticeable difference in heat capacity.

The data obtained under such maximized conditions, which may require multiple baseline and reference runs, may push the precision of heat capacity runs to ±0.1 percent. This

TABLE V-B-2

COMPUTER READINGS OF THE ISOTHERM AMPLITUDES OF THE RUNS SHOWN IN FIGURE V-B-5

Run \ Temperature		(Init.) 457° K	(Final) 543° K	Difference ° K
BL	1	191.4	546.2	354.8
	3	30.2	527.6	497.4
	5	139.8	666.4	526.6
RE	1	143.0	472.2	329.2
	3	12.4	464.4	452.0
	5	127.6	425.2	297.6
H14D1		100.0	401.0	301.0

In all runs except BL 3 and RE 3, the pans were loaded into the holder at 400° K at 10° K/min. In runs of BL 3 and RE 3, the pan was cooled from 543° K to 457° K at 10° K/min prior to each run. Run conditions are the following: Heating rate = 40° K/min, range = 0.5 mcal/sec, range on the recorder = 500 mV, gain = 10. On these settings, one chart division $\underline{\sim}$ 170 in computer units.

H14D1 is the name of a sample run of polyoxymethylene.

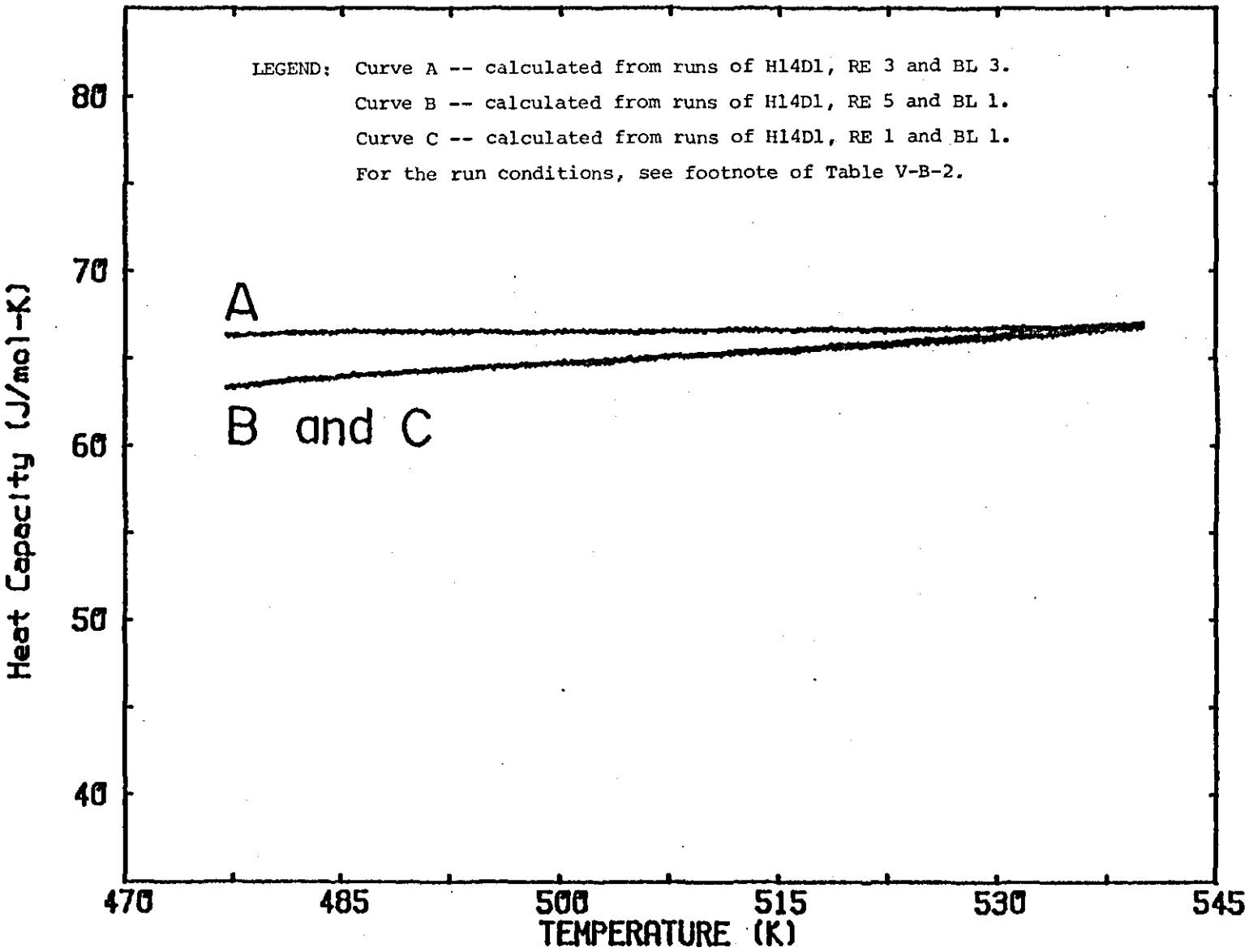

Figure V-B-5. Heat Capacity of Polyoxymethylene Melt as a Function of Temperature

extreme care and large amount of calibration suggests a need for advances in instrumentation which, in the past ten years, may have been neglected in favor of the development of computerization.

4. Plans for Upcoming Period

This report concludes the research activities associated with heat capacity measurement using DSC. The techniques developed here will now be used to ascertain the unformity of cure through the thickness of epoxy matrix composite laminates.

5. References

1. Wunderlich, B. and R. C. Bopp, "Journal of Thermal Analysis, Vol. 6, 1974, p. 335. (See also Chapter VIII in A. Weissberger and B. W. Possiter, "Physical Methods of Chemistry", Vol. 1, Part V, J. Wiley and Sons, New York, 1971.)
2. Mehta, A., R. C. Bopp, U. Gaur and B. Wunderlich, "Journal of Thermal Analysis", Vol. 13, 1978, p. 197. Wunderlich, B. and U. Gaur, Advances of Chemistry No. 203, C. D. Craver, ed., "Polymer Characterization", American Chemical Society, Washington, D.C., 1983, p. 95.
3. Gaur, U., A. Mehta and B. Wunderlich, "Journal of Thermal Analysis", Vol. 13, 1978, p. 71.
4. Lau, S.-F., H. Suzuki and B. Wunderlich, "Journal of Polymer Science", Polymer Phys. Edition, Vol. 22, 1984, p. xxx.
5. Hemminger, H. and G. Hoehne, "Grundlagen der Kalorimetry", Verlag Chemie, Weinheim, New York, NY, 1979 (English translation - 1983).
6. White, W. P., "The Modern Calorimeter", Chem. Catalog Co., New York, 1928.
7. Watson, E. S., M. J. O'Neill, J. Justin and N. Brenner, "Analytic Chemistry", Vol. 36, 1964, p. 1233.

8. Wunderlich, B., "Journal of Physical Chemistry", Vol. 69, 1965, p. 2078.

9. Suzuki, H. and Wunderlich, B., to be published.

10. Laboratory Microsystems, Inc., 106 Third Street, P. O. Box 336, Troy, NY 12181, (518)274-1990.

6. Current Publications or Presentations by Professor Wunderlich on this Subject

"The Measurement of High Quality Heat Capacity by Differential Scanning Calorimetry", with H. Suzuki.

To appear in the Journal of Thermal Analysis.

To be presented at the North American Analysis Society Meeting in Philadelphia, PA, September 1984.

V-C INITIAL SAILPLANE PROJECT: THE RP-1

Senior Investigators: F. P. Bundy
R.J. Diefendorf
H. Hagerup

On September 15, 1983 the annual static loading tests were made on the assembled wing/fuselage structure. Simple wing bending and wing bending/torsion tests up to about four G's were made, using sand bag loading on the inverted aircraft. Bending and torsion deflections were measured and compared to those obtained in previous years' tests. It appears that the structure is retaining its original strength and stiffness very well.

This aircraft has been disassembled and stored on the loft of the Composite Materials Shop Area in the Jonsson Engineering Center under ambient, indoor conditions of temperature and humidity. It will be given its annual strength and stiffness tests again about August or September, 1984.

V-D SECOND SAILPLANE PROJECT: THE RP-2

Senior Investigators: F. P. Bundy
R. J. Diefendorf
H. Hagerup

1. Status

In the previous report the results and analysis of the static strength proof tests of the sing/fuselage assembly were presented. The configuration tested was that of the glider with rebuilt wing, after failure in an earlier test, and redesigned carry-through and fuselage load-transfer structure. Except for excessive forward wing-bending deflections, which caused about a 3/16th-inch pull-out of the aft wing pins from their fuselage receptacles when loaded to about six G's, the modified and rebuilt airframe showed very good strength and stiffness characteristics. The redesigned and reconstructed wing beam carry-through, which transfers bending moments via two major shear pins oriented with their axes fore and aft through the webs of the port and starboard wing spar-roots, withstood the 6-G tests very well.

2. Progress During Report Period

During the present reporting period progress has been made on the design fabrication and installation of a tension carry-through linkage between the aft parts of the port and starboard wings to resist forward bending deflection. In addition, towhook/release mechanisms, landing gear and wheel

brake assembly, compound curved sandwich composite fuselage shells and an enclosed trailer to house and transport the completed disassembled aircraft, have all undergone various stages of design, fabrication, installation and testing.

Using the female molds constructed during previous report periods, two sets of left and right fuselage half-shells were fabricated. The first set was composite sandwich with the layers being, from outside to inside; medium Kevlar cloth, graphite cloth, medium Kevlar cloth, Divinycell foam, glass fiber cloth. This layering resulted in a shell with reasonably good overall contours but with several undesirable irregularities. A second set was made which utilized different layering and better vacuum bagging techniques. The layering, outside to inside, was as follows: ±45° glass cloth, ±45° Kevlar cloth, 0-90° Kevlar cloth, 1/8" Divinycell foam, ±45° Kevlar cloth. This produced a shell with very few minor surface imperfections, very good strength and stiffness, and a very satisfactory total weight of only eleven pounds.

An aft wing tension carry-through linkage was designed which was intended to (i) be consistent with the existing fuselage frame and wing structures; (ii) provide adequate tension strength, (iii) provide easy access for pinning and unpinning during assembly or disassembly of the sailplane and (iv) be consistent with clearances available during storage in the trailer. A full-size test model of the portions of the aft/inboard part of the wing which are involved was

made with the appropriate linkage fastenings to the wing skins and ribs. This model was load tested in the Instron machine and found to be fully adequate. This system is now being installed in the wings and fuselage. The stay-pin access is gained by opening the split flap of the wing to the full sixty-degree position.

The towhook/release mechanisms have been fabricated, installed and tested for the magnitudes and directions of tow cable tensions specified by the FAA. These tests verified the capability of the fuselage structure to transmit towline force to the wing roots, as in actual flight; and of the release mechanism to release the towline when under full load in the various specified directions.

The fuselage/landing gear system was statically tested for the FAA-specified capabilities of four-G up, two-G aft and 2/3-G sidewise. The system passed these tests without indication of any problems.

The fuselage/tail boom/empennage structure was given the specified FAA strength tests by rigidly mounting the structure by the four wing pin sockets and applying sand bag loading to the empennage airfoils up to the twelve pounds per square foot (psf) appropriate to the top speed allowed by the flight envelope for this aircraft. When the vertical stabilizer/rudder was so loaded the assembly was subjected to combined bending and torsion. This test was also survived successfully. For the horizontal stabilizer/elevator test, the

sandbag loading was symmetrical, left and right, so that only bending was involved. The structure passed this test, too, without any evidence of weakness.

An invitation was made by the Soaring Society of America (SSA) to RPI to exhibit the RP-2 glider at its annual convention, March 1-4, 1984, at Hartford, Connecticut. We accepted, and, thus, it became necessary to complete an enclosed trailer to transport the sailplane on the highways. A trailer was constructed during January and February of 1984 as a monocoque rectangular box with appropriate running gear, hitch, lights and internal fixtures to hold the glider component parts securely during transport. This trailer is now available for convenient and secure storage and transport of the sailplane.

At the SSA Convention, the RP-2 was among more than twenty other aircraft of sailplane and powered-sailplane categories exhibited. The RP-2 attracted considerable interest on the part of many dozens of attendees. At the technical lecture sessions, a paper was presented (by invitation) on the RPI Composite Materials Glider Projects by Dr. F. P. Bundy. It was received with lively interest by people such as Paul McCready (the Gossamer Condor man-powered airplane), Dick Johnson (eight times U. S. National Sailplane Champion and well-known aeronautical engineer) and Paul Schweizer (retired former President of Schweizer Aircraft Corporation).

3. Plans for Upcoming Period

Work will now be directed toward completion of the sailplane to flight-readiness condition. The various tasks remaining are:

a) Completion of the cockpit controls (rudder pedal system, control stick trim mechanism, flap notch selector),

b) application of the fuselage shells,

c) fabrication of the cockpit rim and canopy frame to fit it,

d) complete installation of the aft wing tension linkage,

e) installation and fitting out of the instrument panel and

f) filling, smoothing and painting.

Before any flight testing is started some additional tests will have to be performed. One will be the application of a full six-G simple bending load to the wing-fuselage structure, which will incorporate the tension carry-through near the aft wing pins. Another test will involve a combined wing bend-twist loading, simulating conditions at the bottom-right corner of the flight envelope (96 mph, -3.8 G's, -7000 lb/in torque). The weight and center of gravity location for the completed aircraft must then be measured prior to flight testing.

Finally, when the aircraft is completed, static-tested, weighed and balanced, flight tests will be conducted at

Saratoga County Airport by automobile tow, winch tow and/or airplane tow.

4. Current Publications or Presentations by Professor Bundy on this Subject

"Composite Material Glider Program at RPI"
Presented at Soaring Society of America Convention, Hartford, CT, March 1-4, 1984.

PART VI
TECHNICAL INTERCHANGE

Interchange of technical information is provided through technical meetings, both on- and off-campus. A central listing of upcoming meetings is compiled, maintained and distributed periodically, in order to assure that a Rensselaer faculty/staff member can participate. The calendar for this reporting period is shown in Table VI-1. Table VI-2 shows the meetings attended by composites program faculty/staff/students from RPI during the reporting period. Some on-campus meetings, with special speakers particularly relevant to composites, are listed in Table VI-3. A list of composites-related visits by RPI faculty/staff/students, to relevant organizations along with the purpose of each visit, is presented in Table VI-4.

The diversity of the research conducted within this program has increased over the last several years. To insure information transfer, once-a-week luncheon programs have been held among the faculty and graduate students involved (listed in Part VII - Personnel - of this report). These meetings are held during the academic year and are known as "Brown Bag Lunches" (BBL's), since attendees bring their own. Each BBL allows an opportunity for graduate students and faculty to briefly present plans for, problems encountered in and recent results from their individual projects. These seminars also are occasions for brief reports on the content of off-campus meetings attended by any of the faculty/staff participants (as listed in Tables VI-2 and VI-4 of this report) and for brief administrative reports, usually on the

TABLE VI-1

CALENDAR OF COMPOSITES-RELATED MEETINGS

(September 30, 1983 through April 30, 1984

1983

10/17-19	Aircraft Design Systems and Operations Meeting, Fort Worth, TX. Sponsored by AIAA/AHS.
10/17-19	Society of Rheology Meeting, Knoxville, TN.
10/24-26	Computers in Aerospace IV, Hartford, CT. Sponsored by AIAA.
10/24-26	9th Annual Mechanics of Composites Review, Dayton, OH. Sponsored by AFOSR.
11/6-10	Recent Advances in Experimental Characterization of Composites, Salt Lake City, UT. Sponsored by SESA.
11/7-10	4th International Conference on Metal Matrix Composite Materials, Bratislava, Czechloslavakia.
11/13-18	Symposium on Impact of New Computing Systems on Computational Mechanics, Boston, MA. Sponsored by ASME.
12/5-9	International Conference on Carbon Fibers, San José dos Compos, Brazil.

1984

1/9-11	Experimental Mechanics of Fiber Reinforced Composite Materials, San Diego, CA. Sponsored by SESA.
1/9-12	22nd Aerospace Sciences Meeting, Reno, NV. Sponsored by AIAA.
1/9-13	Gordon Research Conference on Polymers, Santa Barbara, CA.
1/16-20	Gordon Research Conference on Composites, Santa Barbara, CA.
2/20-22	Asilomar Conference on Polymers, Asilomar, CA.
2/27-29	Vibration Damping Workshop, Applications to Aerospace Structures, Long Beach, CA. Sponsored by Flight Dynamics Lab., AF Wright Aero. Lab.
3/14	Soaring Society of America, Hartford, CT.
3/8-13	American Chemical Society, Detroit, MI.
3/26-30	American Physical Society, St. Louis, MO.
4/3-5	International Conference on Limits in Fiber Reinforced Composites, Liverpool, UK. Sponsored by RAES-PRI.
4/3-5	29th National Symposium and Exhibition on Materials and Processes, Reno, NV. Sponsored by SAMPE.
4/6	3rd International Conference on Computing in Civil Engineering, San Diego, CA.

TABLE VI-2

COMPOSITES-RELATED TECHNICAL MEETINGS ATTENDED OFF-CAMPUS

(September 30, 1983 through April 30, 1984)

1983

10/17-19 Society of Rheology Meeting (Prof. Sternstein), Knoxville, TN.

Professor Sternstein presented the paper: "Mechanical Characterization of Composites".

10/24-26 9th Annual Mechanics of Composites Review (Prof. Bauchau and Prof. Sternstein), Dayton, OH.

Professor Sternstein presented the paper: "Overview of Composites Research".

11/7-10 4th Intl. Conference on Metal Matrix Composite Materials (Prof. Diefendorf), Bratislava, Czechoslovakia.

Professor Diefendorf presented the papers: "Consumer Applications of Carbon Fiber Composites", "Transverse Composite and Fiber Properties".

12/5-9 Intl. Conference on Carbon Fibers (Prof. Diefendorf), San José dos Compos, Brazil.

Professor Diefendorf presented the papers: "A Comparison of High Modulus Fibers", "Non-Aerospace Applications of Composite Materials".

1984

1/16-20 Gordon Conference on Composites (Prof. Sternstein), Santa Barbara, CA.

Professor Sternstein presented the paper: "Viscoelastic Characterization of Neat Resins and Composites".

2/20-22 Asilomar Conference on Polymers (Prof. Sternstein), Asilomar, CA.

Professor Sternstein presented the paper: "Mechanical Properties of Composites".

3/1-4 Soaring Society of America (Prof. Bundy), Hartford, CT.

Professor Bundy presented the paper: "Composite Materials Glider Program at RPI.

TABLE VI-2 continued

1984

3/8-13	American Chemical Society Meeting (Prof. Diefendorf)(Prof. Wunderlich with Drs. Suzuki and Grebowicz), Detroit, MI. Professor Diefendorf presented the paper: "Carbon Fibers".
3/26-30	American Physical Society (Prof. Wunderlich with Drs. Suzuki and Grebowicz), St. Louis, MO. Presented reports on RPI's general heat capacity work.
4/6	3rd Intl. Conference on Computing in Civil Engineering (Prof. Shephard), San Diego, CA. Professor Shephard presented the paper: "Finite Element Modelling Developments at RPI".

TABLE VI-3

COMPOSITES-RELATED MEETINGS/TALKS HELD AT RPI

(September 30, 1983 through April 30, 1984)

Topic	Date	Speaker(s)
	1983	
"Fundamental Studies of Acoustic Emission - The Role of Theory in the Design of Experiments"	10/25	Dr. Nelson Hsu National Bureau of Standards, Washington, D.C.
	1984	
"Boundary Element Method Applications to Small and Large Deformation Viscoplasticity"	2/14	Professor S. Mukherjee Dept. of Theoretical and Applied Mechanics, Cornell University, Ithaca, NY
Discussion of proposed research into manufacturing methods for advanced composites	2/16	Dr. H. Burte and Dr. V. Russo, USAF Materials Laboratory, WPAFB, Dayton, OH
"Thermomechanical Analysis of the Compression-Molding Process for Chopped Fiber Composites"	2/28	Dr. D. Caulk Engineering Mechanics Department, General Motors Research Labs.
"Plasticity and Cracking in Composite Laminates"	3/2	Dr. G. J. Dvorak Dept. of Civil Engineering, University of Utah, Provo, UT
"Asymptotics and Mechanics"	3/22	Dr. J. D. Cole Dept. of Mathematics, Rensselaer Polytechnic Institute, Troy, NY
"Thermoelasticity of Twinning"	3/23	Prof. J. L. Ericksen Depts. of Mathematics and Mechanics, University of Minnesota, Minneapolis, MN
"Mechanics of Crystalline Plasticity"	4/4	Dr. A. Needleman Prof. of Engineering, Brown University, Providence, RI

TABLE VI-4

COMPOSITES-RELATED VISITS TO RELEVANT ORGANIZATIONS

by RPI Faculty/Staff/Students

(September 30, 1983 through April 30, 1984)

Visited	Date	By	Purpose
	1983		
Fort Lewis and AMMRC, Fort Lewis, WA	10/20	Prof. R. J. Diefendorf	Presented a talk: "Composite Structures for Army Applications"
Saratoga Springs, NY	11/5	Prof. R. J. Diefendorf	Conducted GE Modern Engineering Course; "Composite Materials"
Lockheed-Georgia Co., Marietta, GA	11/15	Prof. R. G. Loewy	A review of company progress in composite technologies
NASA Langley Research Center, Langley, VA	12/6	Prof. R. G. Loewy	Attended USAF SAB Meeting on "The Health of Aeronautics"
	1984		
NASA and DOD, Austin, TX	1/15-19	Prof. R. J. Diefendorf	Presented a Summary of Materials Panel: "Materials 2000"
NASA and DOD, Washington, DC	3/1	Prof. R. J. Diefendorf	Same as above
USAF Office of Scientific Research, Bolling AFB, VA	3/15	Prof. R. G. Loewy	Discussion of RPI research in composites structural analysis
GE Research and Development Center, Schenectady, NY	4/17	Prof. R. J. Diefendorf	Presented a talk: "RP Sailplane Project"
Naval Surface Weapons Center, White Oaks, CA	4/24-25	Prof. R. J. Diefendorf	Presented an Aluminum/Carbon Composite Workshop: "Carbon Fiber Structures and Properties"

part of one of the Co-Principal Investigators. Off-campus visitors, at RPI during a BBL day, are often invited to "sit in". Table VI-5 lists a calendar of internal, oral progress reports as they were given at BBL's during this reporting period.

An integral part of the program management is an on-site review of research plans and progress, conducted under the aegis of the technical monitors at NASA and AFOSR. Such a program review was conducted at RPI on December 19 and 20, 1983. The agenda for this review is shown in Table VI-6, and the attendees from AFOSR; NASA headquarters, Langley Research Center and Lewis Research Center; and industry (members of the program's Industrial Technical Advisory Panel) are shown in Table VI-7.

TABLE VI-5

COMPOSITE MATERIALS AND STRUCTURES PROGRAM

BROWN BAG LUNCH (BBL) SCHEDULE

(September 30, 1983 through April 30, 1984)

Date	Topic	Responsible Faculty
1983		
9/30	Administrative Report	R. Loewy
	Fabrication Technology Experiments	F. Bundy H. Hagerup V. Paedelt
	Static Test Review	H. Scarton
10/7	Administrative Report	J. Diefendorf
	Resin-Fiber Interface Research	J. Diefendorf
	Composites Fatigue Research	E. Krempl
10/14	Administrative Report	J. Diefendorf
	Matrix Characterization and Environmental Effects	S. Sternstein
	Generic Structural Components	D. Goetschel
10/21	Administrative Report	J. Diefendorf
	Computer Aided Design and Analysis	M. Shephard
	Fabrication Technology Experiments	F. Bundy H. Hagerup V. Paedelt
10/28	Administrative Report	R. Loewy
	Report on AGARD Meeting	R. Loewy
	Resin-Fiber Interface Research	J. Diefendorf
11/4	Administrative Report	R. Loewy
	Composite Fatigue Research	E. Krempl
	Report on Mechanics of Composites Review Meeting	S. Sternstein
11/11	Administrative Report	R. Loewy
	Generic Structural Components	D. Goetschel
	Computer Aided Design and Analysis	M. Shephard

TABLE VI-5 continued

Date	Topic	Responsible Faculty
1983		
11/18	Administrative Report	R. Loewy
	Fabrication Technology Experiments	F. Bundy H. Hagerup V. Paedelt
	Resin-Fiber Interface Research	J. Diefendorf
12/2	Administrative Report	R. Loewy
	Composites Fatigue Research	E. Krempl
	Matrix Characterization and Environmental Effects	S. Sternstein
12/9	Administrative Report	R. Loewy
	Generic Structural Components	D. Goetschel
	Computer Aided Design and Analysis	M. Shephard
1984		
1/20	Administrative Report	R. Loewy
	Computer Aided Design and Analysis	M. Shephard
	Free-Edge Failures of Laminates	T-L. Sham
1/27	Report on Gordon Conference	S. Sternstein
	Fabrication Technology Experiments	F. Bundy H. Hagerup V. Paedelt
2/3	Coupled Bending Torsion in Composite Plates	I-H. Yang
	Composite Fatigue Research	E. Krempl
2/10	Unbalanced Laminates	O. Bauchau
	Quantifying St.-Venant's Principle	D. Goetschel
2/17	Administrative Report	R. Loewy
	Resin-Fiber Interface Research	J. Diefendorf
	Computer Aided Design and Analysis	M. Shephard

TABLE VI-5 continued

Date	Topic	Responsible Faculty
1984		
2/24	Fabrication Technology Experiments	F. Bundy H. Hagerup V. Paedelt
	Composite Fatigue Research	E. Krempl
3/2	Free-Edge Failures of Laminates	T-L. Sham
	Matrix Characterization	S. Sternstein
3/9	Administrative Report	R. Loewy
	Unbalanced Laminates	O. Bauchau
	Quantifying St.-Venant's Principle	D. Goetschel
3/23	Resin-Fiber Interface Research	J. Diefendorf
	Computer Aided Design and Research	M. Shephard
3/30	Free-Edge Failures of Laminates	T-L. Sham
	Matrix Characterization and Environmental Effects	S. Sternstein
4/6	Fabrication Technology Experiments	F. Bundy H. Hagerup V. Paedelt
	Composite Fatigue Research	E. Krempl
4/13	Administrative Report	R. Loewy
	Report on AGARD Meeting	R. Loewy
	Unbalanced Laminates	O. Bauchau
4/20	Quantifying St.-Venant's Principle	D. Goetschel
	Resin-Fiber Interface Research	J. Diefendorf
4/27	Computer Aided Design and Analysis	M. Shephard
	Free-Edge Failure of Laminates	T-L. Sham

TABLE VI-6

NASA/AFOSR COMPOSITE MATERIALS AND STRUCTURES PROGRAM ON-SITE VISIT

December 19 and 20, 1983

Rensselaer Polytechnic Institute: AGENDA

Monday, December 19 -- JEC 3117

8:30	Welcome and Program Overview	R. Loewy
9:15	Fibers and Interfaces	R. Diefendorf
10:00	Matrix Dominated Properties	S. Sternstein
10:45	Break	
11:00	Characterization of Thermosets	B. Wunderlich
11:45	Discussion	
12:00	Lunch (Visitors and Presenters)	
1:00	Fatigue in Composites	
	Axial-Torsion in Tubes	E. Krempl
1:25	Uniaxial Tension at Negative R-Ratios	D. Elzey*
1:50	Tension-Shear in Tapered Straps	R. Loewy
2:15	End-Effect Analysis	D. Goetschel
3:00	Break	
3:15	Fabrication Processes	F. Bundy
3:30	Lab Tour	
	Interactive Computer Graphics	M. Shephard
	Mechanics of Materials	E. Krempl
	Materials Characterization	S. Sternstein
	Thermal Analysis	B. Wunderlich
	Fabrication and Testing	V. Paedelt
4:45	Discussion	
5:00	Adjourn	
6:30	Dinner (Visitors and Presenters)	

*Graduate Student

TABLE VI-6 continued

Tuesday, December 20

8:30	Finite Element Studies of Fracture	M. Shephard
9:15	Delamination Failures at Edges	S. Sham
10:00	Break	
10:15	Mechanical Connections in Composite Shafts	S. Anderson*
11:00	Warping Effects in Unbalanced Laminates	O. Bauchau
11:45	Future Plans	R. Loewy
12:00	Lunch (Visitors and Presenters)	
1:00	Simultaneous Meetings	
	NASA/AFOSR (Executive Session)	
	Industrial Technical Adbisory Com./RPI	
2:00	NASA/AFOSR Program Guidance	Dr. Vosteen Dr. Amos
3:00	Adjourn	

*Graduate Student

TABLE VI-7

NASA/AFOSR COMPOSITE MATERIALS AND STRUCTURES PROGRAM ON-SITE VISIT

December 19 and 20, 1983

ATTENDEES

Dr. Anthony K. Amos	AFOSR
Dr. Christos C. Chamis	NASA - Lewis
Mr. Samuel Dastin	Grumman Aerospace
Mr. John T. Quinlivan	Boeing
Mr. Karl V. Stenberg	McDonnell Aircraft Co.
Dr. Louis F. Vosteen	NASA - Headquarters
Mr. Max E. Waddoups	General Dynamics

PART VII

PERSONNEL

AUTHOR INDEX

PERSONNEL

Co-Principal Investigators

Ansell, George S., Ph.D.	Dean, School of Engineering
Loewy, Robert G., Ph.D.	Institute Professor
Wiberley, Stephen E., Ph.D.	Professor of Chemistry

Senior Investigators

Bauchau, O., Ph.D. (Structural dynamics, advanced composites)*	Assistant Professor of Aeronautical Engineering
Bundy, F. P., Ph.D. (Physical chemistry and structures testing)*	Research Professor of Materials Engineering
Diefendorf[i], R. J., Ph.D. (Fabrication, resin matrix, fiber behavior, interfaces)*	Professor of Materials Engineering
Feeser[i], L. J., Ph.D. (Computer applications and graphics, computer-aided design, optimization)*	Professor of Civil Engineering Associate Dean, School of Engineering
Goetschel, D. B., Ph.D. (Structural analysis design and testing)*	Assistant Professor of Mechanical Engineering
Hagerup, H. J., Ph.D. (Aerodynamics, configuration, pilot accomodation, flight testing)*	Associate Professor of Aeroneering Engineering
Krempl, E., Dr.Ing. (Fatigue studies, failure criteria)*	Professor of Mechanics and Director of Cyclic Strain Laboratory
Sham, T-L., Ph.D. (Fracture mechanics, composites)*	Assistant Professor of Mechanical Engineering

*Fields of Speciality

[i]Member of Budget Committee together with Co-Principal Investigators

Shephard, M. S., Ph.D. (Computer graphics, finite element methods)*	Associate Director, Center for Interactive Computer Graphics and Assistant Professor of Civil Engineering
Sternstein[i], S. S., Ph.D. (Failure analysis, matrix behavior, moisture effects)*	William Weightman Walker Professor of Polymer Engineering
Wunderlich, B., Ph.D. (Processing science, constituent material characteristics)*	Professor of Chemistry

Research Staff

Manager & Master Technician, Composites Laboratory

Paedelt, Volker

Research Associates

Grebowicz, Janusz, Ph.D
Menczel, Joseph, Ph.D.
Suzuki, Hidematsu, Ph.D.

Graduate Assistants

An Deuk, M.S.
Burd, Gary, B.S.
Chen, Kuong-jung, M.S.
Coffenberry, Brian, B.S.
Gjaja, Niko, M.S.
Hu, Tsay-hsin, M.E.
Judovits, Lawrence, M.S.
Liu, Shiann-hsing, M.S.
Shick, Douglas, M.S.
Singh, Sachchida, M.S.
Srinivasan, Krishna, B.Tech.
Uzoh, Cyprian, B.S.
Weidner, Theodore, B.S.
Yang, Chung-Ming (Philip), M.S.
Yehia, Nabil, M.S.
Yerry, Mark, M.E.
Yurgartis, Steven, M.S.

Undergraduate Assistants - Seniors

Caligiuri, Joseph
Casabella, Susan
Halicki, Paul
Iorizzo, Carol
Keavney, Thomas
Lewis, Scott
Lopez, Matthew
Schmitt, William
Williams, Thomas

*Fields of Specialty

[i]Member of Budget Committee together with Co-Principal Investigators

Undergraduate Assistants - Juniors

Basel, Roger
Botwinik, Sharon
Cimino, Paul
De La Fuente, Horacio
Drake, James
Father, Richard
Henderson, Robert
Hansen, Michael
Karkow, Jon
Kirker, Phillip
O'Connell, James
Rajewski, David
Sawyer, Christina
Sohn, Kyu Yeon
Tse, Suet Ting
Witt, Jay

Undergraduate Assistants - Sophmores

Desmarais, Michael
Egbert, Mark
Kashynski, Stephen
Morris, Scott

AUTHOR INDEX

	Page(s)
Bauchau, O.	89
Bundy, F. P.	147 149
Diefendorf, R. J.	11 147 149
Goetschel, D. B.	67
Hagerup, H. J.	147 149
Krempl, E.	195
Sham, T. L.	63
Shephard, M. S.	39
Sternstein, S. S.	35
Wunderlich, B.	103 127